UNIVERSITÀ
DEGLI STUDI
DI PADOVA

Università degli Studi di Padova

Dipartimento di Scienze Biomediche

CORSO DI DOTTORATO DI RICERCA IN SCIENZE BIOMEDICHE SPERIMENTALI

CICLO XXXIV

The regulation of protein synthesis and function in muscle plasticity and disease

Coordinatore: Ch.mo Prof. Fabio Di Lisa

Supervisore: Ch.mo Prof. Bert Blaauw

Co-Supervisore: Dr. Leonardo Nogara

Dottorando: Ana Georgia Dumitras

INDEX

SUMMARY **5**

RIASSUNTO **8**

1. INTRODUCTION **11**

1.1. Skeletal muscle structure and function **11**

1.2. Mechanochemistry of actomyosin cross-bridge cycle **15**

1.3. Fibre type composition **17**

1.4. Skeletal muscle hypertrophy **18**

1.5. Skeletal muscle atrophy **19**

1.5.1. The ubiquitin-proteasome system 19

1.5.2. The autophagy-lysosome system 21

1.6. Different approaches for studying protein synthesis **23**

1.6.1. Isotope traces to measure protein turnover 23

1.6.2. SunSET: a novel non-isotopic technique 24

1.6.3. Metabolic labelling of newly synthesized proteins with uncanonical amino acids 26

2. Aim of the work **32**

3. MATERIALS AND METHODS **34**

3.1. Animal handling and generation of constitutive muscle-specific MetRS mice and AKT-MetRS mice **34**

3.1.1. Generation of muscle-specific MetRS mice 34

3.1.2. Generation of muscle-specific MetRS-AKT mice.....35

3.1.3. Generation of inducible muscle-specific Raptor ko mice 36

3.1.4. Generation of MetRS-Balb/C animals 36

3.1.5. Generation of MetRS/MDX animals.....37

3.1.6. Genotyping of muscle-specific transgenic mice.....37

3.2. Virus Injection 40

3.3. In vivo muscle force measurements 41

3.4. Measurement of *in vivo* protein synthesis.....41

3.5. FDB single fibre isolation.....41

3.6. Histological analysis and immunofluorescence stainings 42

3.6.1. Hematoxylin & Eosin staining (H&E).....42

3.6.2. Periodic Acid-Schiff staining (PAS) 43

3.6.3. SDH staining 43

3.6.4. Immunofluorescence analysis.....44

3.6.5. Neural Cell Adhesion Molecule (NCAM) staining.....44

3.6.6. Myosin staining 45

3.6.7. FUNCAT (Cryosections).....45

3.6.8. FUNCAT (single FDB fibres).....45

3.6.9. FUNCAT-PLA.....46

3.6.10. Whole-mount EDL and SOLEUS preparation. 47

3.7. Immunoblotting.....47

3.7.1. Protein gel electrophoresis 47

3.7.2. Protein transfer on nitrocellulose membrane 48

3.7.3. Incubation with antibodies 48

3.7.4. BONCAT 49

3.7.5. Myosin Heavy chain electrophoresis 50

3.7.6. Quantification of Immunoblotting 50

3.8. Gene expression analysis 51

3.8.1. RNA extraction 51

3.8.2. Reverse Transcription 51

3.8.3. Real-Time PCR reaction 51

3.8.4. Quantification of the PCR products 52

3.8.5. Primer pair design 53

3.9. Statistical analysis 53

4. RESULTS 54

4.1. MetRS expression and ANL incorporation 54

4.2. Generation of muscle-specific MetRS mouse line 54

4.3. ANL incorporation is efficient in all skeletal muscles examined. 55

4.4. Long time ANL labelling does not affect muscle histology or force 60

4.5. MetRS-AKT transgenic mice as hypertrophy model 63

4.6. Proteomics analysis of MetRS and MetRS-AKT animals 66

4.7. Localization of ANL-containing proteins 68

4.8. Overload hypertrophy leads to increased labelling of muscle fibres near the myotendinous junction 71

4.9. Protein synthesis in different fibre types 74

4.10. Analysis of muscle proteome in catabolic conditions: starvation.....75

4.11. Analysis of muscle proteome in catabolic conditions: chemical denervation.....78

4.12. Muscle-specific labelled proteins are present in sciatic nerves.86

4.13. Rapamycin, a mTORC1 inhibitor, decreases protein labelling...88

4.14. Analysis of labelled proteins in HSA-Cre-MetRS Raptor ko mice.....90

4.15. Analysis of muscle proteome in pathological conditions: Duchenne muscular dystrophy.....92

4.16. Analysis of muscle proteome in pathological conditions: cancer cachexia.....94

5. DISCUSSION.....97

6. Bibliography.....104

SUMMARY

Skeletal muscle accounts for almost 40% of the total body mass[1]. Besides its role in locomotion, it is the organ with the largest amino acid storage in the human body, and its metabolism influences whole-body homeostasis. Since skeletal muscle plasticity and metabolism change in response to physiological and pathological conditions, it is crucial to investigate the molecular mechanisms regulating muscle mass.

Here we want to dissect the identity and localization of nascent skeletal muscle proteome in vivo. For this purpose, we used transgenic mice expressing a mutant methionyl-tRNA synthetase together with a green fluorescent protein. Due to its expanded amino acid binding site, the mutated tRNA synthetase can incorporate a synthetic analogue of methionine, azidonorleucine (ANL), into a nascent polypeptide chain. The polypeptide chain containing ANL can be tagged using click chemistry and then identified through Western Blotting (BONCAT) or visualized on cryosections (FUNCAT).

This approach's novelty consists of crossing MetRS mice with transgenic mice expressing Cre recombinase under the Mlc1f skeletal muscle-specific promoter. In this way, we can mark proteins synthesized only by skeletal muscle fibres.

We successfully generated the Cre-MetRS mouse line expressing the mutated methionyl tRNA and established the amount of labelled proteins we can visualize with FUNCAT or identify with BONCAT. Different pulses of intraperitoneal injections suggested that both time and ANL dosage influence labelled proteins levels. To increase the labelling, we changed the administration route supplying ANL in drinking water. Force productions measurements and histological analysis showed that incorporating ANL into newly synthesized peptides does not influence the proteins' physiological role. The proteins are correctly folded and reach their intracellular target. They can be localized coupling click reactions to a proximity ligation assay for proteins of interest. We chose to localize actin and dystrophin because of their abundance in muscle fibres, and as expected, PLA showed the membrane localization of dystrophin compared to actin.

Furthermore, we monitored protein synthesis during skeletal muscle hypertrophy and atrophy. We used AKT-MetRS animals and observed that the higher protein synthesis mediated by mTORC1 increases the amount of myofibrillar protein labelling. On the other hand, overload increases protein synthesis via the Hippo pathway.

How atrophic stimuli influence skeletal muscle labelling was also checked both during starvation and chemical denervation. In both models, we observed a selective reduction in fibre labelling. Combining myosins stainings with FUNCAT, we observed that nutrient deprivation leads to a fibre-type dependent reduction in labelled proteins. Surprisingly, this striking correlation was no longer maintained in chemical denervated mouse models of atrophy. This time, the amount of labelled proteins seems to depend on whether the muscle is in a denervated or reinnervated status.

Our results proved that the *in vivo* labelling of MetRS transgenic mice allows for a sensitive visualization and localization of newly synthesized skeletal muscle proteins. However, skeletal muscle is a highly metabolic, endocrine tissue that influences all the other structures around. For that reason, we wanted to test whether labelled proteins that originated within the muscle are being transferred into sciatic nerves, thus demonstrating inter-tissues communication. We collected sciatic nerves of chemically denervated animals and performed western blot analysis on these samples. The presence of ANL-incorporating peptides, revealed by western blotting analysis, indicated a potential role of skeletal muscle proteins in the homeostasis of sciatic nerve tissue.

The sensibility of the technique allows many applications, especially on pathological conditions where there is either a fibre type transition or fibre type-specific loss. We back-crossed Mlc-1f CRE-MetRS animals into a Balb/C background to analyze muscle proteins changing in response to cancer cachexia. These preliminary studies confirm muscle protein synthesis rate changes in a fibre-type depended manner. Moreover, we crossed the Cre-MetRS mouse line also with the *MDX* mouse model for *Duchenne muscular dystrophy (DMD)* and

visualized in more details protein synthesis rates in different fibres, changing as a consequence of muscle fibre damage, fibrosis and regeneration. Finally, RAPTOR KO MetRS animals presented a lower amount of labelled proteins at NMJ level when rapamycin was administered in vivo, suggesting a correlation between mTORC1-mediated protein synthesis and the stability of NMJ.

RIASSUNTO

Il muscolo scheletrico ha una massa equivalente al 40 % della massa totale corporea e rappresenta l'organo più voluminoso. Considerando che il muscolo scheletrico rappresenta la più grande riserva proteica dell'organismo, le sue funzioni non si limitano solo alla locomozione ma includono anche la regolazione metabolica. La sua plasticità e metabolismo cambiano in risposta a stimoli fisiologici e patologici pertanto diventa cruciale lo studio dei meccanismi molecolari che regolano la sua massa e come tali meccanismi vengano up o down-regolati.

Questa tesi riguarda quindi l'identità e la localizzazione delle proteine sintetizzate dal muscolo scheletrico sottoposto a diversi stimoli. A tal proposito, abbiamo utilizzato un modello murino transgenico che esprime la metionil-tRNA sintetasi mutante insieme alla proteina “”GFP”. Una singola mutazione nella sequenza genica della metionil-tRNA sintetasi nativa ingrandisce il sito di legame amminoacidico rendendo il mutante capace di incorporare un aminoacido non canonico, l'azidonorleucina invece della naturale metionina. Le catene polipeptidiche che contengono l'azidonorleucina possono essere marcate mediante una serie di reazioni chimiche classificate come “click” e successivamente identificate mediante WB (BONCAT) e visualizzate su sezioni trasversali di muscolo (FUNCAT). La novità di questo approccio consiste nell'incrociare la linea transgenica murina che esprime il mutante con animali che esprimono la Cre ricombinasi sotto il controllo di un promotore muscolo-specifico. Il risultato è un animale che sintetizza le proteine contenenti l'amminoacido modificato esclusivamente nel muscolo scheletrico rendendo possibile uno studio muscolo-specifico del proteoma murino.

Dopo aver generato la linea Cre-MetRS, abbiamo stabilito la quantità di proteine che si possono identificare mediante FUNCAT o BONCAT. Da esperimenti basati su iniezioni intraperitoneali di ANL in animali transgenici, è emersa una proporzionalità tra la quantità e il tempo di somministrazione di ANL e il livello delle proteine marcate. Pertanto per aumentare quanto più possibile il livello di proteine marcate, abbiamo cambiato la via di somministrazione da intraperitoneale ad orale. Prove di forza ed esami istologici non hanno mostrato segni di tossicità suggerendo che l'incorporazione dell'ANL nelle proteine sintetizzate *ex novo* non

influenza il ruolo fisiologico di tali proteine. Le proteine sintetizzate e correttamente ripiegate riescono a raggiungere i propri target intracellulari e possono essere localizzate accoppiando alla reazione click un saggio chiamato “proximity ligation assay” (PLA). La click-PLA, scegliendo come proteine target l’actina e la distrofina, ha infatti mostrato che la peculiare localizzazione sarcoplasmatica della distrofina è diversa da quella citoplasmatica dell’actina.

Considerando che la presenza di stimoli ipertrofici ed atrofici influenza il proteoma muscolare, abbiamo deciso di monitorare la sintesi proteica in alcuni modelli murini di crescita e di perdita muscolare. Abbiamo quindi marcato le proteine di un modello murino transgenico chiamato AKT-MetRS e abbiamo osservato un aumento nel contenuto di proteine miofibrillari in muscoli a contrazione lenta come il soleo. L’altro stimolo ipertrofico usato, il sovraccarico dell’EDL, ha portato a risultati differenti suggerendo un aumento nelle sintesi proteica mediata dalla proteina YAP e dalla sua localizzazione nucleare e non più da mTORC1.

Nei due modelli murini di atrofia che abbiamo scelto, il digiuno e la denervazione chimica, abbiamo osservato, una riduzione selettiva nella quantità delle proteine marcate. Per confermare tale risultato abbiamo combinato FUNCAT e immunofluorescenza per le diverse isoforme della miosina e abbiamo notato una riduzione della marcatura delle proteine nelle fibre a contrazione veloce.

Questa stretta correlazione tra tipo di fibra e sintesi proteica è venuta meno analizzando muscoli denervati. In tale condizione, la marcatura di particolari fibre sembra dipendere di più dallo stimolo elettrico e meno dal tipo di fibra.

I precedenti risultati hanno mostrato quanto sensibile sia la visualizzazione e la localizzazione delle proteine muscolari, tuttavia il metabolismo del muscolo scheletrico influenza tutti i tessuti nel corpo spesso mediante proteine rilasciate in circolo e trasportate all’organo target. Abbiamo quindi cercato di vedere se proteine sintetizzate all’ interno della fibra muscolare possano essere ritrovate in altri tessuti come i nervi sciatici dimostrando la continua comunicazione che esiste tra questi due tessuti.

Analisi BONCAT di nervi sciatici prelevati da animali MetRS hanno rivelato la presenza in tali tessuti di proteine marcate che possono, quindi, influenzarne l’omeostasi.

La versatilità di questa tecnica non si limita tuttavia solo allo stato fisiologico del tessuto scheletrico ma anche, e specialmente, in condizioni patologiche, dove c'è una transizione e una perdita selettiva di un determinato tipo di fibre.
Abbiamo quindi incrociato il modello murino Mlc-1f CRE-MetRS con un background di tipo Balb/C, suscettibile all'induzione di tumori. Questi studi preliminari hanno confermato che la perdita di massa muscolare interessa principalmente le fibre veloci. Il modello Cre-MetRS applicato nello studio delle distrofie muscolari ha invece mostrato come la sintesi proteica cambia in risposta alla necrosi e alla rigenerazione del muscolo scheletrico dovute alla perdita di distrofina funzionale. Infine, abbiamo osservato una diminuzione nella quantità delle proteine marcate a livello neuromuscolare somministrando rapamicina ad animali RAPTOR KO MetRS. Tale risultato suggerisce una correlazione tra la sintesi proteica e la stabilità della giunzione neuromuscolare mediata da mTORC1.

1. INTRODUCTION

1.1. Skeletal muscle structure and function

Skeletal muscle is a highly organized structure responsible for all voluntary movements. Adult skeletal muscle tissue arises from the fusion of mononuclear myoblasts to form a multinucleated syncytium that ensures a coordinated response to somatic nervous system input.

Skeletal muscle fibres are elongated, cylindrical and multinucleated cells. These fibres are protected by a layer of connective tissue called endomysium and bundled into fascicles. Each fascicle is formed from tens to hundreds of bundled muscle fibres, protected by another protective layer formed by collagen, called perimysium. Perimysium allows nerves and blood vessels to enter the muscle.

Another layer of connective tissue called epimysium covers the entire muscle. Connective tissue protects skeletal muscle cells and allows them to withstand the forces of contraction[1] **(Figure 1).**

Skeletal muscle fibres are very large compared to other cells. They have diameters up to 100 um and lengths up to 3 cm and contain cellular organelles such as mitochondria and endoplasmic reticulum specialized for muscle contraction. For example, the smooth endoplasmic reticulum is called the sarcoplasmic reticulum, and it stores, releases and retrieves calcium ions. The muscle fibre plasma membrane is called the sarcolemma, and its cytoplasm is called sarcoplasm. Sarcoplasm contains cylindrical structures composed of contractile proteins called myofibrils. Myofibrils are composed of sarcomeres, the smallest functional unit of skeletal muscle fibre responsible for the contraction.

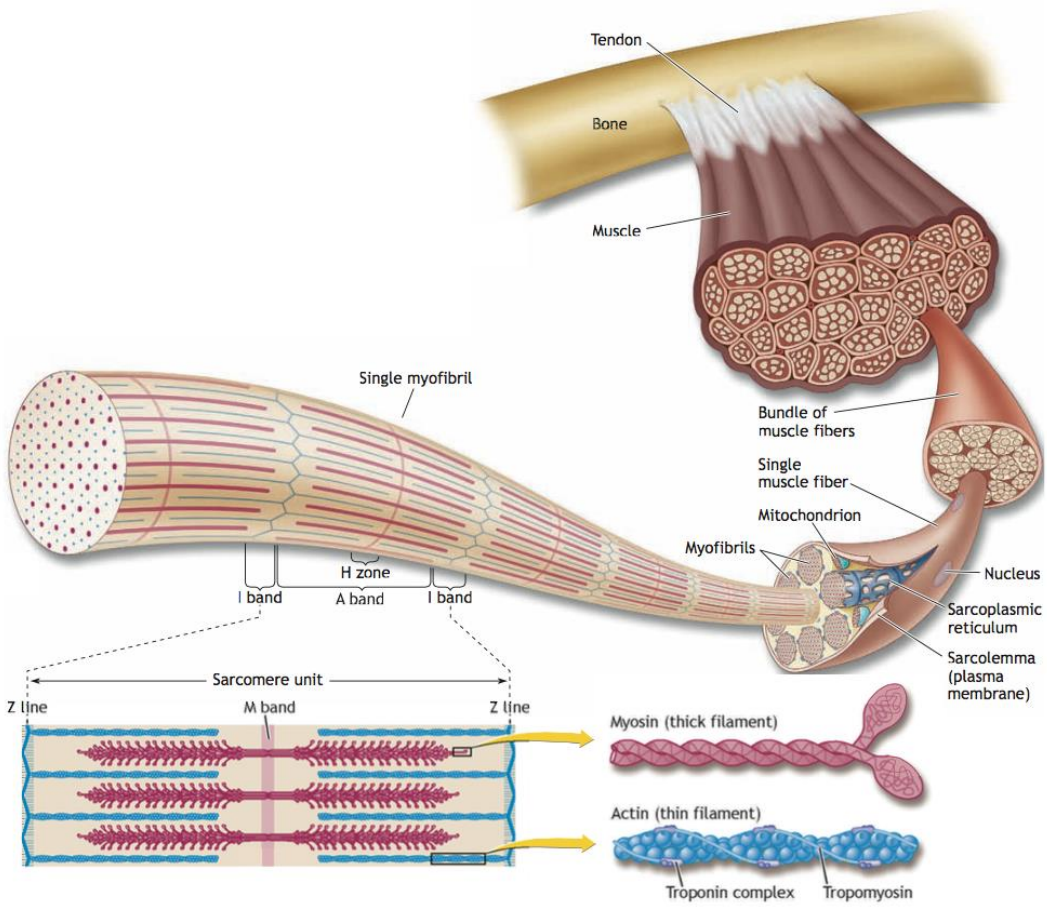

Figure 1: Muscle structure, macroscopic to microscopic (Source McArdle, 2010)

The sarcomere is the region of a myofibril contained between two cytoskeletal structures called Z-lines. The important striated appearance of skeletal muscle fibre, observed through a light microscope, is due to alternate isotropic (light) and anisotropic (dark) bands perpendicular to the axis of the fibre. The dark band A is located in the middle of the sarcomere, whereas the I band lies between A bands of two consecutive sarcomeres. A band contains another paler region, called H-zone halved by M-line, that defines the middle of the sarcomere. In addition, I bands are bisected by the Z line, and the sarcomere is the area between two Z lines **(Figure 2).**

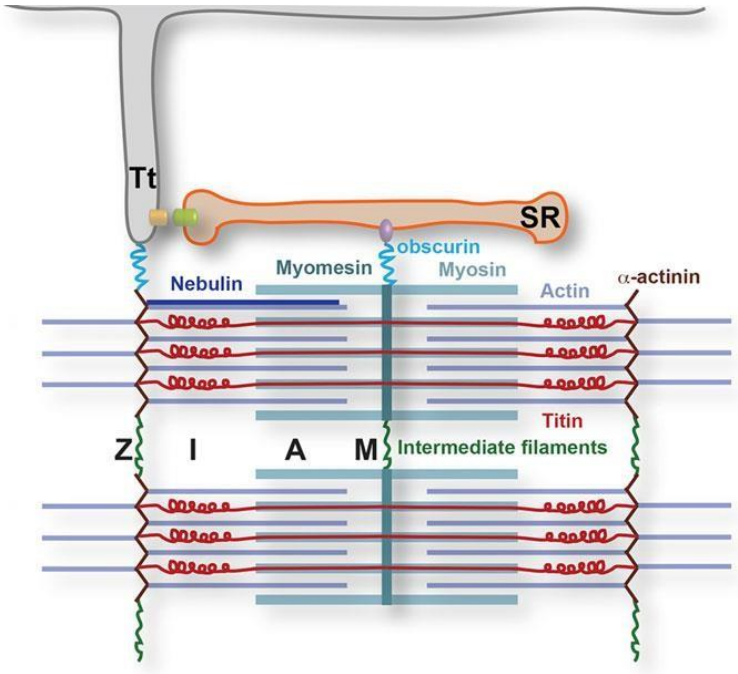

Figure 2: The Sarcomere structure[2]

This morphology is caused by the regular disposition of thick and thin filaments composed of proteins involved in muscle contraction. Thick filaments are composed of myosin and occupy the A band in the middle of the sarcomere. They are anchored elastically to the Z line through stringy proteins called titin.

On the other hand, thin filaments are composed of actin anchored to a specific zone in the Z line known as α-actinin. They constitute a half I band and reach the H zone limit, going through the A band's myosin filaments. Moreover, several proteins such as troponins and tropomyosins bind actin and myosin, modulating the contractile activity of the sarcomere. Myosin filaments are halved by the M line, which contains structural proteins such as myomesin and essential enzymes such as creatine kinase (involved in the regeneration of ATP). A cross-section through A bands shows the regular, almost crystalline, arrangement of overlapping thick and thin filaments surrounded by a hexagonal array of thin filaments surrounded at the end by a triangular arrangement of three thick filaments (**Figure 3**).

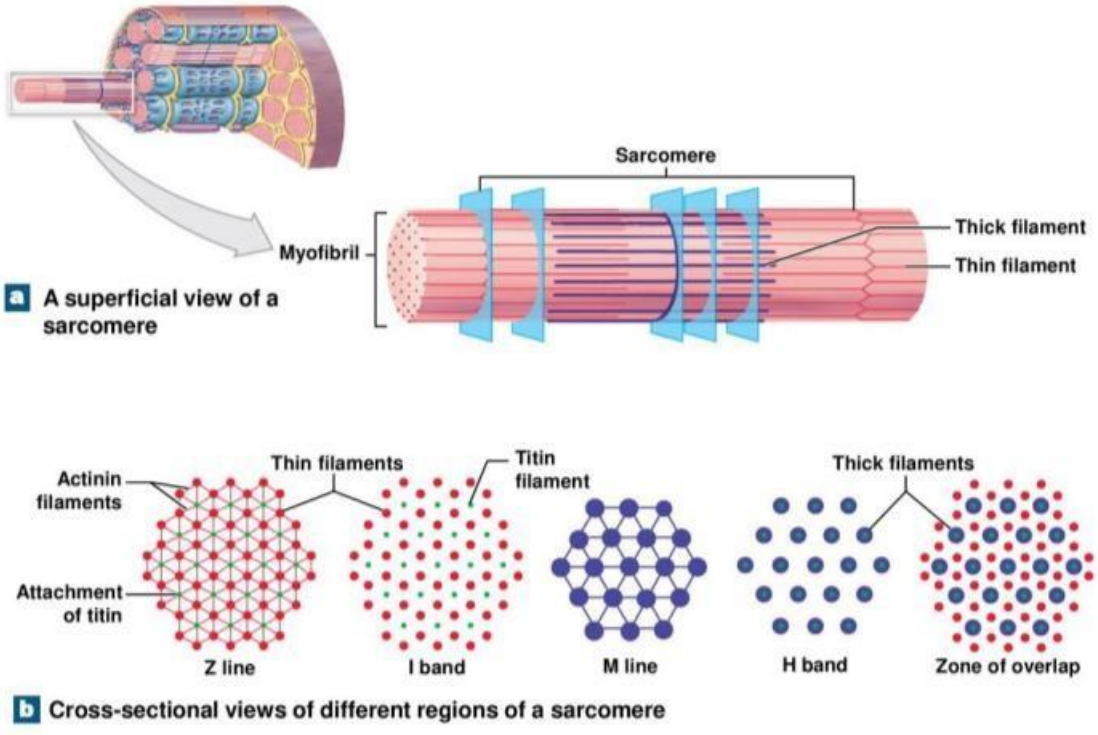

Figure 3: Organization of skeletal muscle (Fundamentals of anatomy and physiology eleventh edition, Pearson)

The motor neuron, whose cell body is located in the spinal cord, directly projects its axons to muscles. This way, they carry the signals from the spinal cord to the muscle effector. When an action potential reaches the presynaptic membrane in the axon terminal, voltage-sensitive calcium channels open, and the influx of calcium causes the synaptic vesicles to fuse with the presynaptic nerve membrane. The content of the vesicles, in particular, acetylcholine, is released into the synaptic cleft and diffuses to its acetylcholine receptors (AchR) on the postsynaptic membrane. The binding of acetylcholine to the postsynaptic receptor causes a depolarization of the muscle fibre membrane. The highly folded muscle membrane is rich in Na+ channels and allows the depolarization to propagate along the fibre's surface and T tubular membranes (extending the surface membrane). Each transverse tubule has two terminal cisternae on either side. The three assume a triade conformation with numerous calcium voltage-gated channels known as DHPR (they bind drugs belonging to the diidropiridine family). These channels are in touch with *Ryanodine*

receptors (RyRs), voltage-gated channels located on the terminal cisternae membrane. This structure forms a bridge between the transversal tubules and the terminal cisternae membrane in the sarcoplasmic reticulum.

The depolarization carried out in-depth through the transverse tubules leads to a change in the conformational shape of dihydropyridine receptors located in the triads; consequently, there is the opening of the ryanodine receptors in the terminal sacs. Calcium stored in the SR is released through ryanodine receptors into the narrow gap between the SR and T tubular membranes and binds to troponin C on the thin filaments ***(Figure 4)***. This binding causes a change in troponin C conformation that moves away from tropomyosin. When actin-binding sites for myosin are exposed, the cross-bridge cycle is activated, and force develops, allowing contraction to happen[3].

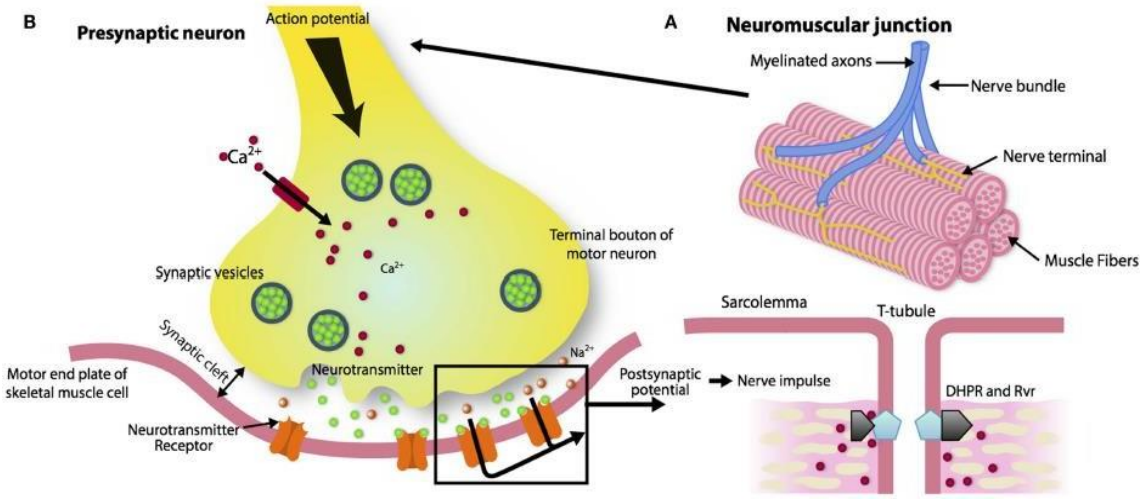

Figure 4: The architecture of a neuromuscular junction (NMJ). (A, B) NMJ is composed of three elements: presynaptic (motor nerve terminal), intrasynaptic (synaptic basal lamina), and postsynaptic component (muscle fibre and muscle membrane)[4].

1.2. Mechanochemistry of actomyosin cross-bridge cycle

The muscle ability to generate force and movement depends on the interactions of the contractile machinery—myosin in thick filaments and actin in thin filaments—and energy provided by ATP. Each actin molecule contains a binding site for myosin. Each myosin molecule's tail lies along the thick filament's axis, and two globular heads extend out to the sides, forming cross-bridges.

During the cross-bridges cycle, the binding of an ATP molecule in the active site of the myosin head produces the dissociation of a myosin head from the actin filament. In this step, ATP is not hydrolyzed. It produces an allosteric modulation of the myosin head that weakens myosin binding to actin.

The energy released from ATP hydrolysis in ADP and inorganic phosphate induces a structural rearrangement, and the myosin's head binds weakly with actin forming a low-affinity actin-myosin complex. A conformational change in the head of a myosin leads to the formation of a high-affinity actin-myosin complex. During the first step of the power stroke, the dissociation of inorganic phosphate from the active site of myosin leads to myosin and actin filaments moving toward each other of 6-8 nm. In the second step of the power stroke, ADP dissociation causes a more pronounced folding in the converter region and the lever domain, producing an additional 3-4 nm movement. After the dissociation of ADP, myosin heads lacking in the energetic nucleotide are firmly bound to actin filaments, so another molecule of ATP must dissociate myosin from actin **(Figure 5)**[5,6]**.**

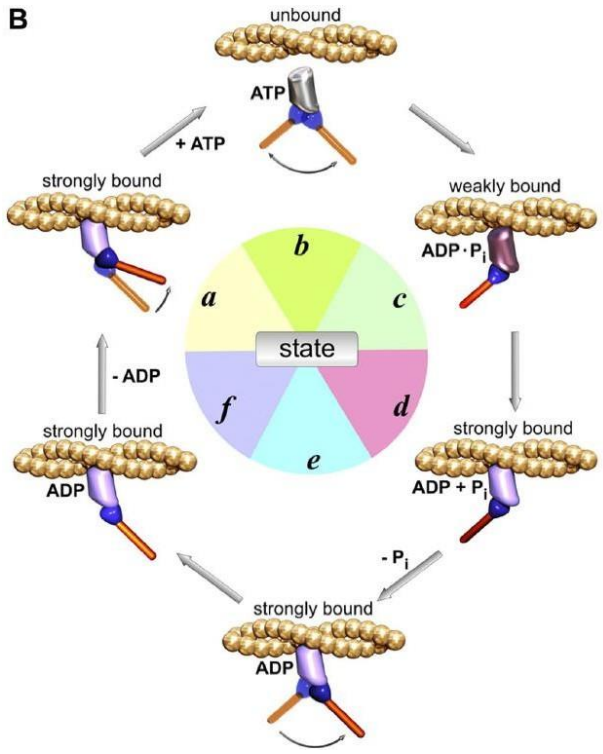

Figure 5: Schematic representation of the cross-bridge cycle[5].

1.3. Fibre type composition

The contractile ability of a muscle depends on its fibre type composition.

In 1873 Ranvier, physician and physiologist, recognized that different skeletal muscles have different contractile properties due to fibres innervation and various ways they are used[5].

Until 1970 the mammalian skeletal muscle was divided into two types: red or white muscle. White muscles were composed of fast-twitch fibres, specialized in phasic activity, and characterized by glycolytic metabolism. In comparison, red muscles were specialized in tonic activity and characterized by a higher myoglobin content and oxidative enzymes.

Later evidence from histochemical and physiological studies of motor units, ATPase histochemistry, and biochemical studies on oxidative and glycolytic enzymes suggested a more accurate classification comprising four different skeletal muscle fibre types. Fibre type I, also called slow oxidative, is more present in slow muscles such as the soleus. They usually have a high content of mitochondria since their primary source of energy is through aerobic metabolism. They have a very high resistance to fatigue and express a slow isoform of MyHC. On the other hand, fast fibres can be divided into three different types: 2A, 2B and 2X. Type 2A fibres are fatigue-resistant and have intense staining for SDH (succinate dehydrogenase activity). Type 2B are fast, fatigable fibres, SDH negative. The last type 2 fibres identified are called 2X. They have a similar twitch (contraction and half-relaxation time) to 2A and 2B but resistance to fatigue intermediate between 2A and 2B fibres. They also have a different isoform of myosin called 2X[7]. Muscle fibres classified on different myosin heavy chain isoforms are different in both energy production and ATP usage. Type 1 and 2B fibres use an oxidative metabolism, while 2X and 2B fibres rely on glycolytic metabolism. Moreover, there is also a difference in sarcomere contractile machinery based on different fast or slow tropomyosin isoforms[8].

The four different fibre types are differently distributed in different muscle types. The prevalence of a particular fibre type determines the function of a specific muscle. For example, postural muscles such as the *transversus abdominis* are mainly composed of slow fibres, while a higher content of fast fibres characterizes

the movement muscles[7].

1.4. Skeletal muscle hypertrophy

Hypertrophy is defined as the increase in an organ or tissue volume due to its component cell increase. The physiological condition of the growth of skeletal muscle mass depends both on cell turnover and protein turnover[9]. Cell turnover plays a significant role in the development of skeletal muscle in an embryo. In this stage, the activation and differentiation of satellite cells into adult myofibers ensure the formation of a functional contractile apparatus[10]. The activation of satellite cells can also occur during adulthood in response to injuries to form new myofibers, but most adult myofibers are in a postmitotic state[11]. Because adult muscle cells lack the ability to divide further, the physiological condition of growth in adult skeletal muscle depends on increased protein synthesis and decreased protein degradation[12].

Among muscle growth-promoting mechanisms, there is the IGF1- AKT signalling pathway. This is one of the best-characterized pathways and involves both a circulating isoform of IGF1 produced by the liver under the control of GH and an autocrine/paracrine production of IGF. IGF1 binds to its receptor, IGF1-R and activates PI3K generating phosphatidylinositol-3-4-5 triphosphate (PIP3). PIP3 recruits AKT to the plasma membrane by binding to its NH2-terminal pleckstrin homology domain. It is, then, phosphorylated by the two different kinases: PDK and mTOR-Rictor complex. In skeletal muscle, the activated form of Akt leads to rapid muscle hypertrophy, improved calcium handling and force production without changing fibre type[12].

AKT pathway regulates muscle hypertrophy and protein synthesis mainly by modulating the activation of mTORC1. Moreover, it also regulates protein degradation through FoxO signalling. Akt indirectly activates mTOR through the phosphorylation and inactivation of tuberous sclerosis complex 2, which inactivates the small G protein Rheb. Rheb, in turn, activates mTOR in its complex with Raptor, named mTORC1[13].

Myostatin/Smad signalling is the other pathway regulating protein synthesis in adult skeletal muscle. Myostatin, growth differentiation factor 8 (GDF-8), is a myokine

that acts as a negative regulator of protein synthesis and muscle mass. It binds to its receptors activin type II receptors resulting in the activation of transcription factors belonging to the SMAD family (SMAD 1 and 2). There was strong muscle hypertrophy in mice lacking the myostatin gene; however, this was not accompanied by a similar increase in muscle force. The specific tetanic tension was decreased when normalized for muscle size[14].

1.5. Skeletal muscle atrophy

Atrophy is defined as the reduction of cell, organ or tissue due to the decrease in number or cell size or component cells or both. An increase in protein breakdown over time leads to skeletal muscle atrophy. In adulthood, muscle mass loss seems to be caused by the reduction of adult skeletal muscle cells size. Myonuclear turnover does not change significantly in adulthood[15]. There is no evidence indeed that satellite cells blockage would trigger atrophy.

Muscle atrophy is a highly coordinated process based on two different systems: the autophagy-lysosome machinery and the ubiquitin-proteasome system. They are continuously implicated in the degradation of intracellular and extracellular proteins that need to be replaced, and their equilibrium is vital for tissue homeostasis[16].

1.5.1. The ubiquitin-proteasome system

In the ubiquitin-proteasome system, proteins that have to be degraded are targeted by multiple ubiquitin molecules. Ubiquitin is a protein of 76 amino acids, and its attachment to a target protein is an enzymatic post-translational modification that leads to its breakdown. The ubiquitinylation forms an isopeptide bond between the carboxyl group of the ubiquitin glycine and a lysine residue on the target protein. The process requires three enzymes: the ubiquitin-activating enzyme E1, the ubiquitin-conjugating enzyme E2 and ubiquitin ligases E3. The first step involves the activation of ubiquitin through the binding of its C-terminal to cysteine sulfhydryl group of E1 ubiquitin-activating enzymes in an ATP-dependent manner. During the second step, ubiquitin is transferred from the E1 cysteine to the E2 cysteine. The

third and ultimate step consists of the isopeptide bond formation between the target protein lysine and the C-terminal glycine of ubiquitin. This reaction is catalysed by ubiquitin ligases E3 (***Figure 6***). The attachment of a single molecule of ubiquitin triggers the attachment of many others, forming a polyubiquitin chain that the 26S proteasome can recognize[17]. The proteasome is the degrading machinery responsible for breaking down proteins into peptides. It is composed of a hollow region responsible for protein digestion and a 19S region responsible for protein recognition. 19S regulatory particle of the proteasome contains six homologous ATPases that bind proteins meant to be degraded.

After ATP hydrolysis, ubiquitin is removed, and proteins become unfolded and translocated into the 20S structure. In the end, the active sites of the proteasome degrade proteins in peptides which can then be further degraded into single amino acids by cytosolic endopeptidase and aminopeptidase and used in synthesizing new proteins[18].

Muscle atrophy is based on the over-expression of different atrogenes (genes involved in muscle atrophy). Among them, there are two important ubiquitin ligases E3: MAFbx/atrogin-1 and MuRF1 (muscle ring factor 1). Atrogin-1 is involved in the turnover of sarcomeric proteins such as myosins, desmin and vimentin, while MuRF1 controls the ubiquitination of troponin I, actin and myosin binding protein C. The two most important pathways regulating the expression of muscle ubiquitin ligases are Akt/PKB that phosphorylates FoxO (forkhead box O), causing its cytosolic localization and inactivation and NF-κB that activates MuRF1 through TNF-α[19]. Post-translation modifications of FoxO are not limited to phosphorylation. It is also reported that FoxO3 acetylation indeed limits his localization in the cytoplasm, downregulating atrogin-1 and causing its proteasomal degradation[19].

.

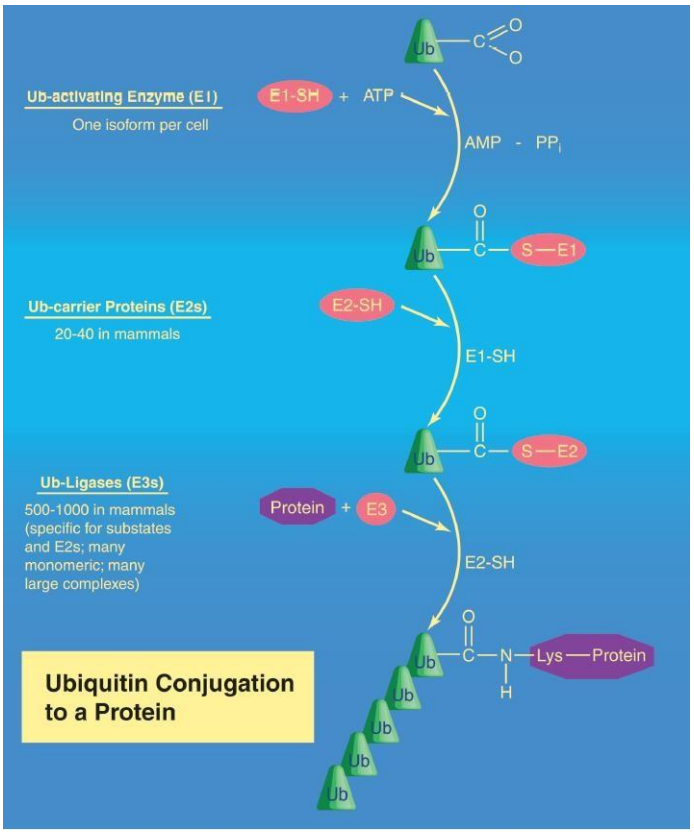

Figure 6: Ubiquitin conjugation to a protein [19]

1.5.2. The autophagy-lysosome system

The autophagy-lysosome system is the other catabolic pathway involved in protein breakdown. Unlike the ubiquitin-proteasome system responsible for myofibrillar and soluble protein degradation[16], autophagy-lysosome systems degrade cytoplasmic material ad organelles[20] and the resulting macromolecular constituents are recycled. Stressful conditions such as starvation, unfolded proteins accumulation, and pathogens infections trigger the delivery of organelles to lysosomal lumen using three different routes: macroautophagy, microautophagy and chaperone-mediated autophagy.

Macroautophagy is the main pathway through which damaged organelles and portions of cytoplasm are degraded. A double membrane cistern is formed around the organelles meant to be degraded called *phagophore* that will mature into an *autophagosome*. This first step involves proteins called "core autophagy machinery"[21], while ESCRT proteins (endosomal sorting complex required for

Transport) are primarily involved in phagophores maturation into autophagosomes[22]. Autophagosomes fuse with late endosomes or lysosomes determining the formation of amphisomes or autophagosomes that contain acidic lysosomal hydrolases. Lysosomal hydrolases degrade the contained material, and the degraded product is transported back to the cytoplasm, where it will be used for protein synthesis or energy production. The ultimate fusion step involves proteins belonging to the SNARE complex, tethering proteins that bring the two vesicles in close proximity[23]. Autolysosomes are then ready to become lysosomes again and undergo another round of fusion with autophagosomes **(Figure 7)**.

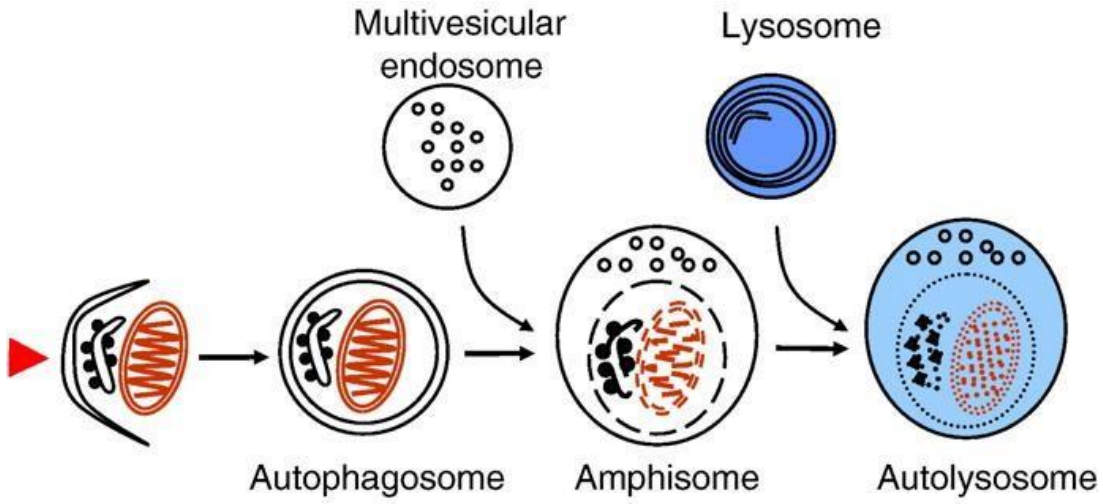

Figure 7: Autophagosome formation and maturation into autolysosomes[23].

Microautophagy is directly based on the engulfment of cytoplasmic material. This invagination leads to autophagic tubes formation by membrane composition changes that result in vesicles formation on the top of the tubes and their scission into the lumen[23].

The last autophagic route is the chaperone-mediated autophagy (CMA), involved in the lysosomal degradation of intracellular proteins. This autophagic pathway selectively recognizes these proteins through a recognition motif in their amino acid sequence. In particular, hsc70, a constitutive chaperone, binds to a pentapeptide motif in the target protein, then targeted to the surface of lysosomes[23].

The autophagy-lysosome system plays a crucial role in muscle atrophy. During starvation and denervation, autophagy-related genes are upregulated. Fasting upregulates two different members of the Atg8 family: LC3 and Gabarapl1, while denervation upregulated Beclin 1 and Atg8. Moreover, FoxO3 activates autophagy via upregulation of atrophy genes such as LC3 and Bnip in a proteasome independent way[13].

1.6. Different approaches for studying protein synthesis

Tissues turn over at different rates depending upon their role in the body. Some tissues, for example, splanchnic tissue, have a turnover rate of about 50%/day. When adult skeletal muscle is considered, the turnover rate is 1-1.5%/day[24].
Nutrition, exercise and hormones influence skeletal muscle proteome and consequently the activity of all the other organs. The intense metabolic activity of adult skeletal muscle and its large mass, which account for more than 50% of the total body mass, makes the knowledge of skeletal muscle protein synthesis fundamental. An efficient tool to study protein synthesis is essential to better understand changes in muscle composition and contractile properties.

1.6.1. Isotope traces to measure protein turnover

For almost eighty years, the tool of choice for studying protein synthesis was based on the administration of isotope tracers. Isotopes are species of an element that differ in mass because of the addition of one or more neutrons into the element nucleus. Two different type of isotopes were employed: radioactive isotopes such as ^{14}C, ^{3}H and stable isotopes such as ^{2}H, ^{13}C, ^{15}N, ^{18}O[25].
The first studies regarding the rate of protein synthesis in skeletal muscle were performed, introducing deuterium isotopes into compounds of interest. Proteins containing deuterium instead of hydrogen allowed the studies on dynamics, utilization and flux *in vivo*. The subsequent discovery and isolation of nitrogen and carbon isotopes allowed more specific studies based on aminoacidic tracers. For example, a specific amino acid, ^{13}C leucine or ^{15}N lysine, was

administered at a constant rate as a primed bolus to animals. The synthesis was directly proportional to the rate of disappearance of isotopic tracers from the arterial pool[26]. Moreover, the administration of [^{14}C]tyrosine allowed to study protein synthesis rates in phasic and tonic muscle, measuring the amount of radioactive tyrosine incorporated into soluble and myofibrillar protein. These results proved there is higher tracer incorporation into the soleus than in the EDL[27]. The discovery of liquid chromatography coupled to a mass spectrometer and the optimization of this technique increased the number of proteins identified by isotope administration. For quantitative proteomics purposes, the *in vivo* labelling with $^{13}C_6$-lysine increases the identified proteins. Based on SILAC food administration, the technique made it easier to label animals[28], even though still very expensive.

The administration of isotopes is the gold standard for proteomics analysis. However, the technique has some drawbacks. First of all, it is a costly technology due to the isotope availability. They are indeed challenging to extract because of their low natural abundance. When isotopic traces are considered, they can also be harmful due to the atomic instability of the elements. The only way to identify these proteins using WB and IHC tools is by autoradiography[29]. In the end, it does not allow monitoring protein synthesis at a single-cell level.

1.6.2. SunSET: a novel non-isotopic technique

Because isotope tracers techniques are time-consuming and very expensive, another non-isotopic technique was explored, which involved puromycin. Puromycin is an amino nucleoside antibiotic produced by the bacterium *Streptomyces alboniger*. It is a structural analogue tyrosyl-tRNA, so the P site in the ribosome can take it up. The difference between puromycin and the natural tyrosyl-tRNA is that puromycin has a non-hydrolysable amide moiety while tyrosyl-tRNA has a breakable ester one[30]. When the ribosome takes up puromycin, it prevents the formation of a peptide bond with the next aminoacyl-tRNA. This way, it leads to the release from the ribosome of the truncated peptides where there is still attached the antibiotic itself (***Figure 8***).

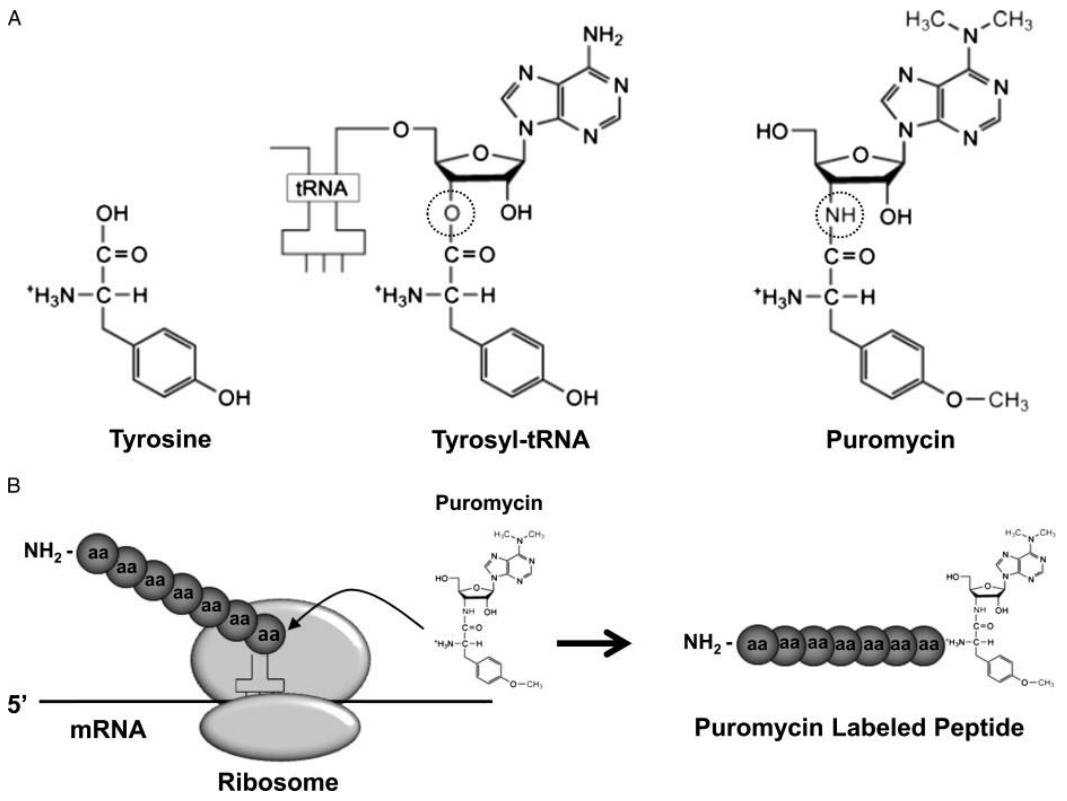

Figure 8: Puromycin action and mechanism of action

Truncated polypeptide chains can be identified using antibodies against puromycin. The most important advantage of this tool is the identification of newly synthesized proteins by standard laboratory techniques such as western blots. Another critical advantage of puromycin is the labelling visualization at a cellular level. It was indeed proved that muscle fibres differ from each other also at a protein synthesis level, besides the already known difference in contractile ability and energy consumption[30]. The application of this tool allowed the identification of proteins using western blot and their visualization with immunohistochemistry techniques. However, it did not allow for the localization of newly synthesized proteins since the translation is incomplete. Moreover, the compound itself is toxic because of ribosome blockage and accumulation of incomplete peptides, so it is not suitable for monitoring protein synthesis for more than 30 min[31].

Most importantly, isotope tracers or puromycin incorporation do not allow monitoring protein synthesis of a specific tissue. They are incorporated in the same manner in all cells. So, it is impossible to distinguish whether a specific protein is being synthesized by tissues of interest or by all associated structures. We generated a new approach to study protein synthesis, specifically in skeletal

muscle, to overcome these problems.

1.6.3. Metabolic labelling of newly synthesized proteins with uncanonical amino acids

A new tool for studying protein synthesis consists in expressing a mutant methionyl-tRNA that can be charged by uncanonical amino acids (amino acids that are not present in living systems) and consequently incorporate them into newly synthesized proteins.

The typically used uncanonical amino acids are derivatives of the natural methionine. In particular, azidohomoalanine (AHA), homopropargylglycine (HPG) and azidonorleucine (ANL) are suitable for this application due to their small chemical group that prevents perturbation into the protein folding[32]. (**Figure 9**).

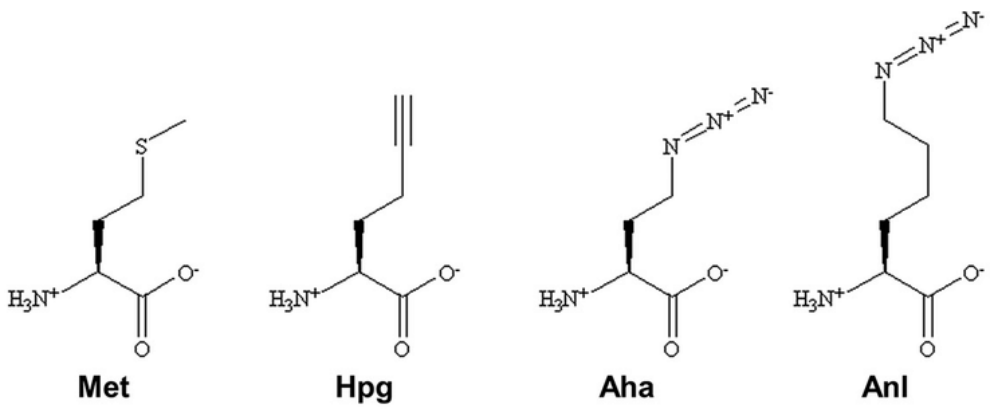

Figure 9: Uncanonical amino acids compared to the natural amino acid methionine.

Uncanonical amino acids have an azido group in the amino acid side chain instead of the typical thioether group present in a methionine side chain. The azido chain is critical because it can be coupled to alkynyl probes, using [3 + 2]- cycloaddition reactions, also called click chemistry (Figure 10). The reaction results in the formation of a covalent bond very stable in physiological conditions and biological solutions.

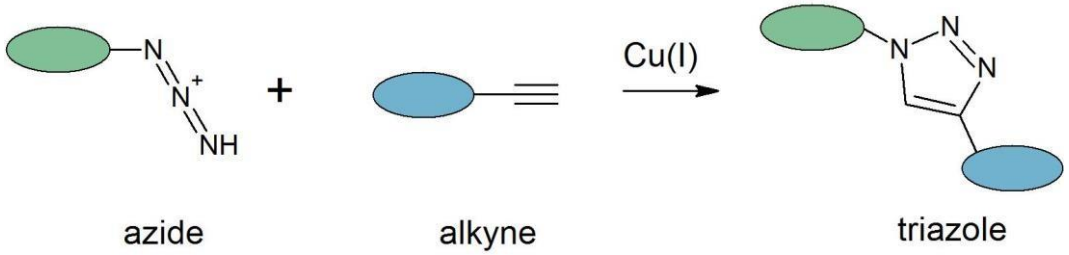

Figure 10: Schematic representation of the azide-alkyne cycloaddition

Since its discovery, this reaction has become very important for bioconjugative applications for three important reasons. First of all, in physiological conditions it is quantitative. It has a large thermodynamic driving force (>20 kcal/mol) to favour a single reaction product. Second, it is a very specific reaction since no azido group is usually present in living systems. Hence the coupling occurs only between the proteins containing azidonorleucine (instead of methionine) and dyes of choice. Third, the reaction is fast and irreversible in biocompatible solvents at room temperature[33].

Azidohomoalanine (AHA) and homopropargylglycine (HPG) can be charged onto the wild-type methionyl-tRNAs and, consequently, by endogenous methionyl-tRNA synthetases, they can be incorporated into newly synthesized proteins instead of the natural methionine exploiting the biological translational cell machinery. Once synthesized, proteins containing the amino acid with the azido group will fold properly. The most important advantage of this technique is that translation is completed (unlike puromycin), and newborn proteins can reach their intracellular target. After the incorporation, they can be both identified using chemiluminescent-alkyne and visualized using fluorescent-alkyne[34]. Proteins proper localization offers an advantage over the puromycin method where truncated proteins accumulates into the cytosol; however, the technique still lacks cell-type specificity.

To overcome this problem, a mutant methionyl-tRNA synthetase needs to be genetically engineered. The first studies were performed on bacteria. Three different forms of the *E.coli* methionyl-tRNA synthetase were used to incorporate the methionine surrogate L-azidonorleucine (ANL), allowing ANL to be incorporated into new proteins.

This labelling was restricted to N-terminal positions because it involved the initiator tRNA; thus it could not be applied to mammalian cells. The second step

was the identification of mutant aminoacyl-tRNA synthetase that would charge ANL into mammalian methionine tRNAs (**Figure 11**).

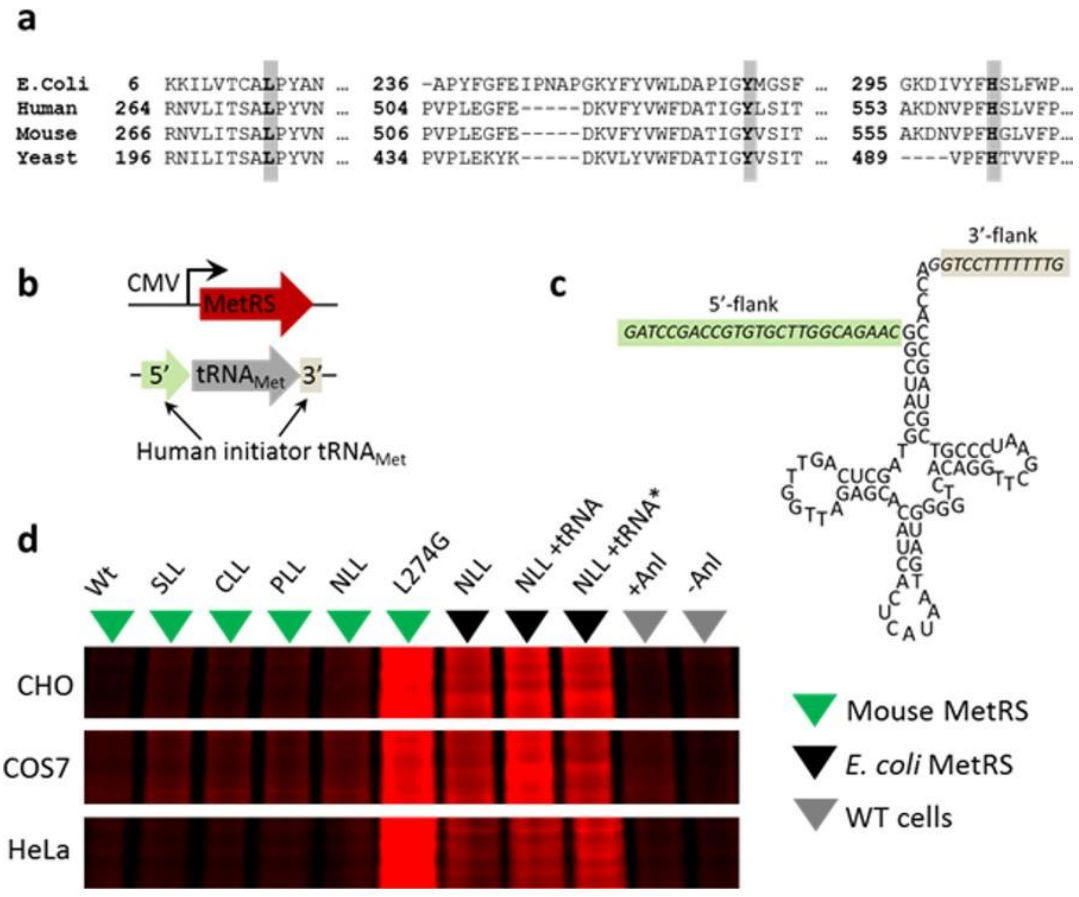

Figure 11: Different MetRS mutants examined[35]

Among all the different mutants tested, the one called L274GMmMetRS incorporated ANL successfully. A single-point mutation enlarged the amino acid binding site of the mutant methionyl-tRNA synthetases allowing it to activate both azidonorleucine and methionine (**Figure 12**). The Michaelis-Menten equation of azidonorleucine activation was also calculated, suggesting that the mutant methionyl-tRNA synthetase activates four-fold faster methionine than azidonorleucine at an equimolar concentration of the substrate[35].

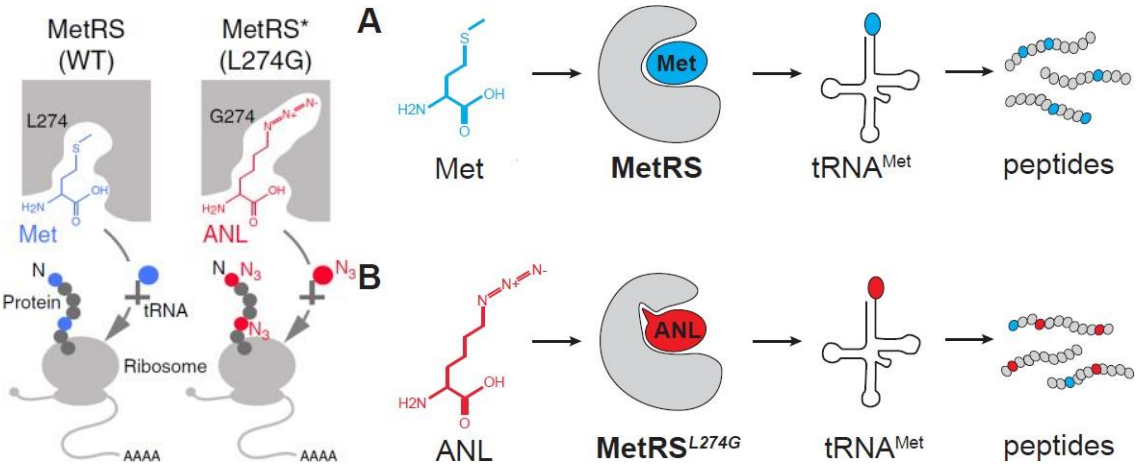

Figure 12: The difference between the wild-type methionyl tRNA synthetase **(A)** and the mutate one **(B)** with the enlarged amino acid binding site[36]

Mammalian cell proteins containing the surrogate ANL are visible using immunofluorescence techniques, and they can be enriched for mass-spectrometry analysis (**Figure 13**).

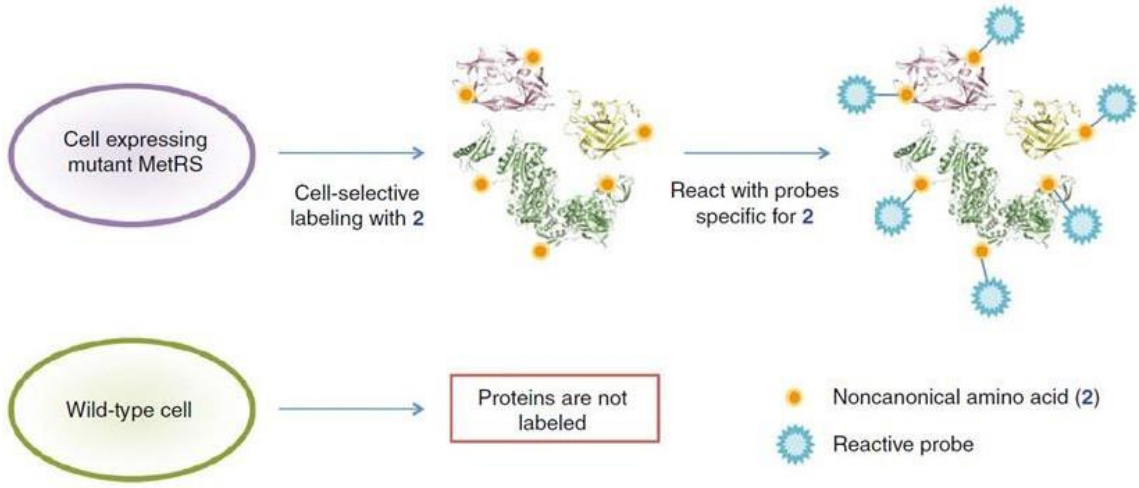

Figure 13: Cell-selective labelling of proteomes with azidonorleucine. Schematic representation of incorporation of azidonorleucine exclusively in cells expressing the mutated MetRS[37].

A further step can be done traducing this technique also *in vivo*. To do so, the MetRS transgenic mouse line was generated. These animals express the mutated methionyl-tRNA under the control of a tissue-specific Cre-recombinase. When the Cre is expressed under a particular cell type-specific promoter, it cuts away the

two LoxP flanking the stop sequence, allowing the mutant methionyl tRNA expression. (**Figure 14**).

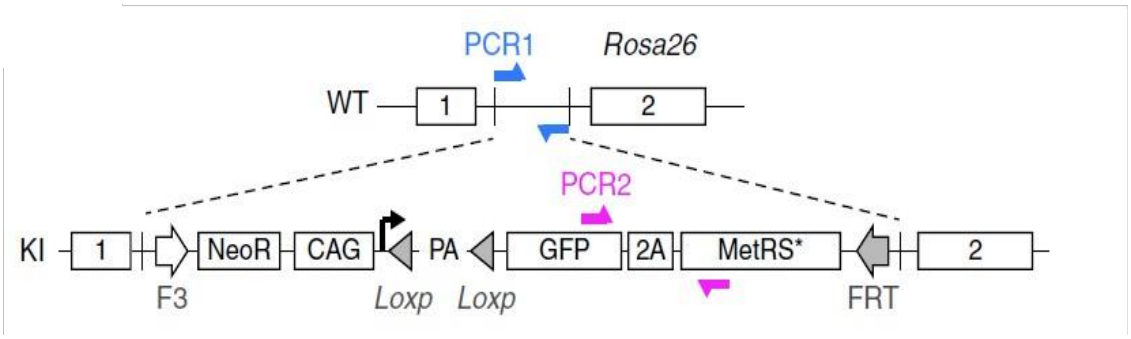

Figure 14: Graphic representing the wild-type and knock-in alleles in the R26-MetRS L274G mouse line[38].

For the first time, the technique was applied on neurons, inducing the expression of the mutated methionyl-tRNA in glutamatergic and GABAergic neurons along with the GFP protein. The two sequences were linked together by a peptide hydrolysed after the enzyme translation. This way, it was possible to see that the expression of the mutated methionyl-tRNA synthetase, ensured by the GFP, goes along with the correct incorporation of the uncanonical amino acid into proteins, visualized using fluorescent alkynes. The novelty of this technique is that, indeed, only proteins synthesized by the tissue of interest will be identified, while proteins from associated structure cells will not be labelled.

Consequently, it is possible to overcome one of the most important problems of the previous techniques: the lack of cell-type specificity. In other words, when wild-type animals are fed with methionine-containing food, they will incorporate methionine into the natural newly synthesized proteins. On the other hand, when azidonorleucine is administered to MetRS animals, they will incorporate ANL into nascent polypeptides giving, as a result, proteins that can be identified and visualized and that only originated from the tissue of interest (**figure 14**).

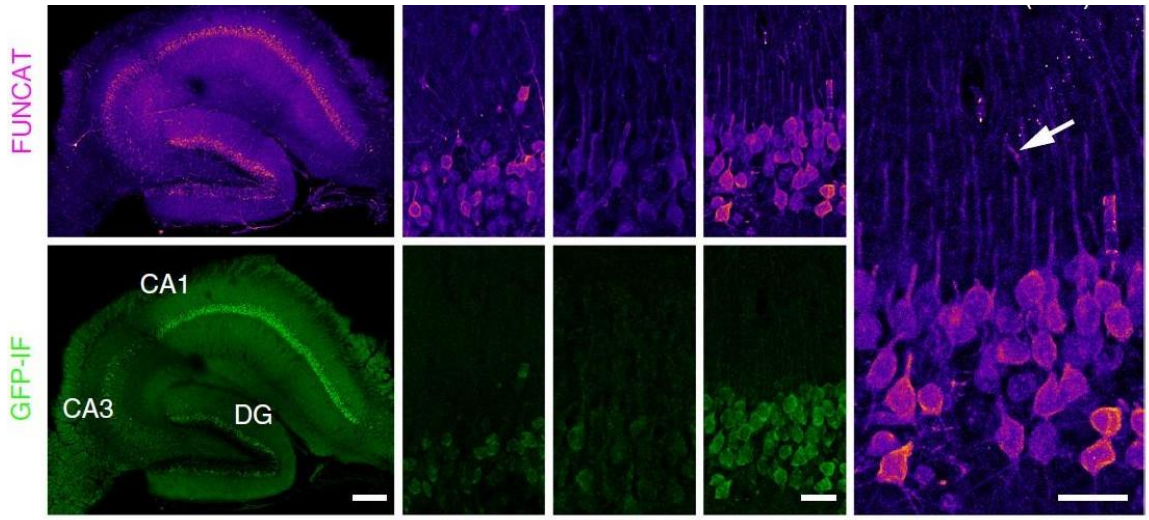

Figure 14: Labelled proteins of hippocampal regions can be visualized with FUNCAT (magenta). (In green) anti-GFP staining ensures the correct MetRS expression[39].

2. Aim of the work

Skeletal muscle accounts for approximately 45-50% of body mass and plays an essential role in locomotion, nutrient metabolism and energy consumption. It shows a high heterogenicity and plasticity and, thus, an incredible ability to change in response to physiological and pathological stimuli. Moreover, exercise has a beneficial effect in preventing many chronic diseases, thus suggesting an important ability in regulating the homeostasis of different tissues.

Since skeletal muscle plays a crucial role in maintaining body homeostasis, it is imperative to investigate the molecular mechanisms regulating muscle mass and understand how the proteome is regulated in the presence of a particular stimulus.

In the past, the methods of choice for measuring changes in protein synthesis has been either the use of radioactive/stable isotopes tracers or SUnSET. Even if the two techniques were very effective, they had drawbacks. Isotopes were very expensive, and there was a problem linked to their availability and disposability. On the other hand, puromycin estimates protein synthesis rate by stopping the synthesis itself and blocking ribosomes. A high number of incomplete peptides and the blocked ribosomes resulted in a toxic effect of puromycin, not allowing long-time labelling and potentially interfering with protein synthesis itself.

Moreover, it did not allow for the localization of nascent proteins as translation is not completed. Ultimately, none of these techniques allowed for the detection of newly synthesized proteins in a specific tissue. They used the natural translational apparatus of the cell incorporating the isotopic tracer indistinctively in all the tissues. To overcome these problems, new techniques to evaluate protein synthesis in skeletal muscle needs to be developed.

My PhD project regards the identity and localization of nascent skeletal muscle proteins *in vivo a*nd how muscle proteome influences other organs. For this purpose, we used a novel transgenic mouse expressing a mutant methionyl-

tRNA synthetase together with a green fluorescent protein only in skeletal muscle fibres.

This thesis is so composed of three different aims:

- The first thing we were focused on was the generation and the characterization of the Cre-MetRS mouse line expressing the mutated methionyl-tRNA synthetase in skeletal muscle fibres. We established the amount of labelled proteins we can visualize on IHC or identify with WB techniques, and we tested whether the introduction of ANL into nascent polypeptide chains was toxic.
- The second aim was to understand how to apply this technique to study muscle proteome in pathological conditions. In particular, we crossed the Cre-MetRS mouse line with an MDX mouse model for *Duchenne muscular dystrophy* (*DMD).* By using FUNCAT, we were able to visualize in more details protein synthesis rates in different fibres, changing as a consequence of muscle fibre damage, fibrosis and regeneration. Moreover, we successfully also visualized what happens to the proteome of starvation mouse models, cachectic muscles and chemically-denervated muscles suggesting a fibre type-dependence to atrophy.
- The third and ultimate goal regarded how skeletal muscle influences other organs mediating inter-tissue communication. Since the MetRS mouse line is muscle-specific, all labelled proteins detected in other tissues come from the muscle itself. The presence of labelled proteins in sciatic nerves confirms that muscle proteins partially mediate the continuous communication between these two tissues.

3. MATERIALS AND METHODS

3.1. Animal handling and generation of constitutive muscle-specific MetRS mice and AKT-MetRS mice

Animals were handled by specialized personnel under the control of inspectors of the Veterinary Service of the Local Sanitary Service (ASL 16 - Padova), the local officers of the Ministry of Health. All procedures are specified in the projects approved by the Italian Ministero Salute, Ufficio VI (authorization numbers 1060/2015PR). All tissues were removed at different time points and frozen in liquid nitrogen for further analysis.

3.1.1. Generation of muscle-specific MetRS mice

Constitutive muscle-specific MetRS mice have obtained crossing mice expressing Cre recombinase under the control of Mlc1f (myosin light chain 1 fast) fast promotor with animals expressing the mutated methionyl tRNA gene. When these animals are crossed with muscle-specific Cre recombinase, the two LoxP sites flanking a stop sequence are cut away, allowing the expression of the mutated methionyl tRNA along with a green fluorescent protein. Between the MetRS and GFP sequence, there is a sequence encoding for the foot-and-mouth disease virus 2A peptide sequence (***Figure 1***).

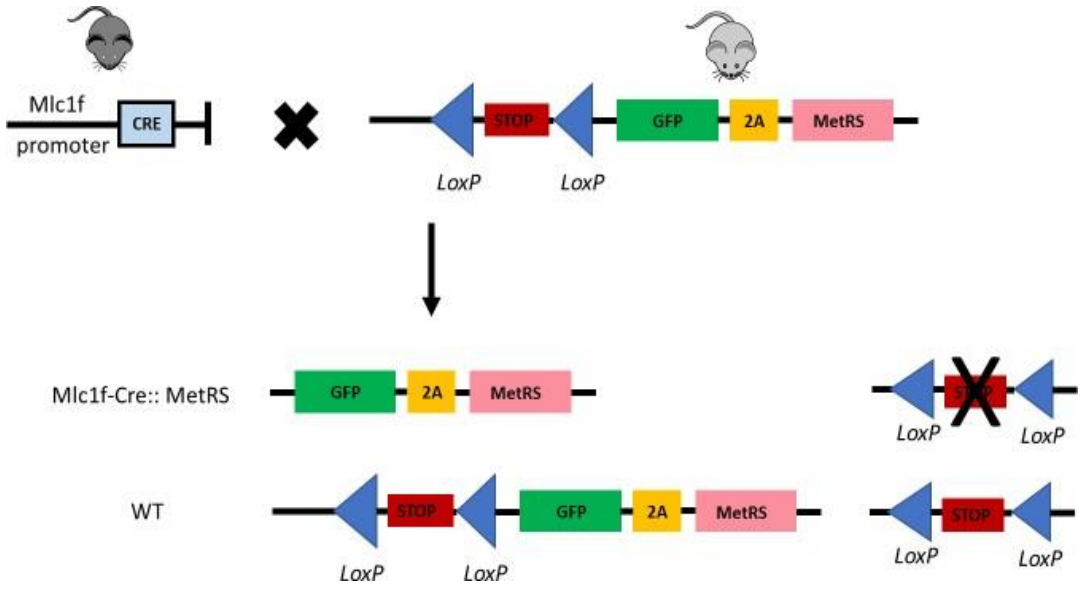

Fig.1: Schematic Representation of Mlc1f-Cre::MetRS knock-in mouse model

3.1.2. Generation of muscle-specific MetRS-AKT mice

Muscle-specific inducible AKT transgenic mouse line was obtained crossing a transgenic line expressing AKT-ER with Cre recombinase under the control of Mlc1f promoter. The sequence contains an src myristoylated signal fused to a modified estrogen receptor hormone-binding domain (silent AKT line). Cre recombinase cleaves the two lox P allowing the expression of AKT. Muscle-specific AKT animals were crossed with MetRS animals to obtain Mlc1f- Cre::MetRS::AKT animals. The synchronous cleavage on AKT and MetRS STOP sequences allows the expression of the mutated methionyl tRNA synthetase along with the AKT gene. To induce AKT transgenic expression, animals were injected with 1 mg of tamoxifen, i.p., every other day for one, two and three weeks. Tamoxifen binds the mutated estrogen receptor that induces AKT phosphorylation and activation. Control animals received vehicle i.p. injections (sunflower oil) for the same time (***Figure 2***).

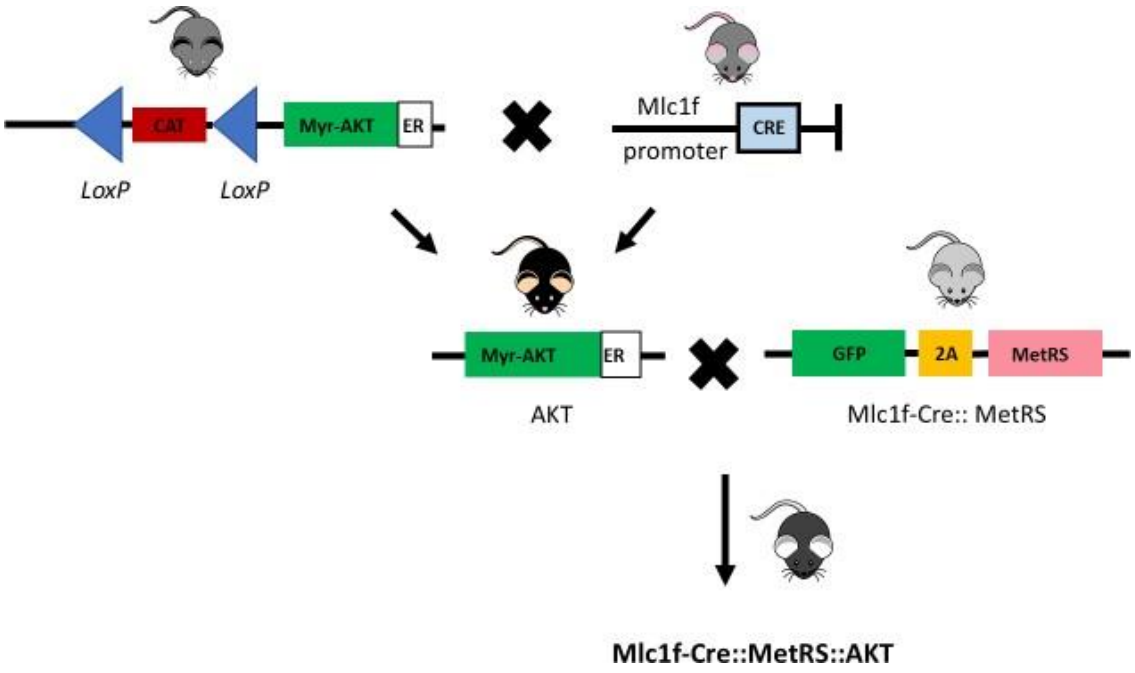

Fig.2: Schematic Representation of Mlc1f-Cre::MetRS::AKT knock-in mouse model.

3.1.3. Generation of inducible muscle-specific Raptor ko mice

Inducible muscle-specific Raptor knock-out mice have generated crossing mice expressing Raptor gene between two LoxP sites ($Raptor_{fl/fl}$) with mice carrying Cre recombinase fused to a mutated estrogen receptor (ER) domain under the control of human skeletal actin promoter. Tamoxifen-induced Cre LoxP recombination was activated by oral administration of tamoxifen-containing chow (Tam400/Cre-ER Harlan), which was administered for three weeks.

3.1.4. Generation of MetRS-Balb/C animals

Cre line under a muscle-specific promoter (Mlc1f) was crossed with floxed MetRS mouse line. This mouse line was back-crossed for two generations into a Balb/C background to generate a model where we can use C26 colon carcinoma cells to induce cachexia. Two-month-old mice were anaesthetized and injected subcutaneously with 5*10^5 C26 colon carcinoma cells.

3.1.5. Generation of MetRS/MDX animals

Mdx mice were purchased from Charles River and crossed with MetRS animals. A homozygous line for both transgenes was obtained. The *MDX* mutation was identified as a C-to-T transition resulting in a termination codon at position 2983 within exon 23 of the X chromosome's dystrophin muscular dystrophy gene (Dmd). Colony is maintained by sibling mating homozygous females with hemizygous males.

3.1.6. Genotyping of muscle-specific transgenic mice

DNA was extracted using a lysis buffer containing Tris-HCL 1M pH 7.5, Proteinase K 10mg/mL (Life Technologies) and $CaCl_2$ 1 mM. The samples were denatured by incubation for 1 hour at 57°C, and then proteinase K was inactivated at 99°C for 5 minutes. Mice were identified by analyzing the presence of Cre-recombinase and LoxP recombination of AKT and MetRS on genomic DNA by PCR.

The following primers were used for the PCR reaction to identify Cre recombinase:

Cre Forward: NSP-780: CACCAGCCAGCTATCAACTCG

Cre Reverse: NSP-979: TTACATTGGTCCAGCCACCAG

We prepared a 20µl total volume mix for each sample with:

Template DNA: 2µl

Primer NSP-780 (10µM): 0.2µl Primer

NSP-979 (10µM): 0.2µl

GoTaq Green master mix 2X (Promega): 10µl

Gibco water DNAase, RNAase free

Program:

step 1: 94° C for 3 minutes

step 2: 94° C for 45 seconds

step 3: 61° C for 30 seconds

step 4: 72° C 1 minute

step 5: go to step 2 for 40 times

We detected Cre-recombinase DNA (200 bp) with a 1% agarose gel.

The genotyping analysis of the Akt allele was performed by using the following primers:

Akt Forward: ACTATCCCGACCGCCTTACT

Akt Reverse: TAGCGGCTGATGTTGAACTG

We prepared a 11µl total volume mix for each sample with:

Template DNA: 1µl

Primer FW (10µM): 0.5µl

Primer RV (10µM): 0.5µl

GoTaq Green master mix 2X (Promega): 5µl

Water

Program:

step 1: 94° C for 5 minutes

step 2: 94° C for 45 seconds

step 3: 60° C for 30 seconds

step 4: 72° C for 1:45 minutes

step 5: go to step 2 for 29 times

step 6: 72°C for 10 minutes

We detected Akt DNA (300 bp) with a 1% agarose gel.

The genotyping analysis of MetRS allele was performed using the following primers:

Mutant Forward: 12614 ACCACTACCAGCAGAACACC

Mutant Reverse: 26209 GGCAGATTGCACTAGCAGAG

Wild-type Forward: 21306 CTGGCTTCTGAGGACCG

Wild-type Reverse: oIMR 9021 CCGAAAATCTGTGGGAAGTC

We prepared a 12ul total volume for each sample with

Template DNA: 1ul

Primer mutant FW (2.5uM): 0.6ul

Primer mutant RV (2.5uM): 0.6ul
Primer wild-type FW (2.5uM): 0.6ul
Primer wild-type RV (2.5uM): 0.6ul
GoTaq Green master mix 2X (Promega): 5µl
Water RNAase DNAase free Program:
step 1: 94° C for 2 minutes
step 2: 94° C for 20 seconds
step 3: 65° C for 15 seconds – 0.5 C per cycle decrease
step 4: 68° C for 10 sec
step 5: repeat steps 2-4 for 10 cycles (Touchdown)
step 6: 94° for 15 seconds
step 7: 60° for 15 seconds
step 8: 72° for 10 seconds
step 9: Repeat steps 6-8 for 28 cycles
step 10: 72° for 2 minutes
step 11: 12° hold

The genotyping analysis of the Raptor floxed allele was performed by using the following primers:
Raptor Forward: CTCAGTAGTGGTATGTGCTCAG
Raptor Reverse: GGGTACAGTATGTCAGCACAG
We prepared a 10µl total volume mix for each sample with:
Template DNA: 2µl Primer FW (20µM): 0.6µl Primer RV (20µM): 0.6µl
GoTaq Green master mix 2X (Promega): 5µl Water
Program:
step 1: 94° C for 3 minutes
step 2: 94° C for 30 seconds
step 3: 58° C for 30 seconds
step 4: 72° C for 30 seconds
step 5: go to step 2 for 35 times

step 6: 72°C for 2 minutes
We detected Raptor DNA (Mutant= 180 bp; heterozygote: 141 bp & 180 bp; wild-type: 141 bp) with a 2% agarose gel.
Three primers were used in mdx genotyping including a common forward primer, a wild-type allele-specific reverse primer and a mutant allele-specific reverse primer.

The genotyping analysis of *MDX* was performed by using the following primers:
Common fw (DL1577):
5'GCGCGAAACTCATCAAATATGCGTGTTAGTGT
Wild-type rw (DL1509):
5'GATACGCTGCTTTAATGCCTTTAGTCACTCAGATAGTTGAAGCCATTTTG
Mutant rw (DL1573):
5'CGGCCTGTCACTCAGATAGTTGAAGCCATTTTA
Step 1: 95° for 120 minutes
Step 2: 95° for 20 minutes
Step 3: 57.7° for 20 minutes
Step 4: 74° for 20 minutes
Step 5: go to step 2 for 4 times
Step 6: 95° for 20 minutes
Step 7: 63.7° for 20 minutes
Step 8: 72° for 60 minutes
Step 9: go to step 6 for 22 times
Step 10: 12° end

3.2. Virus Injection

Mice were anaesthetized, and Gastrocnemius muscles were injected with $2*10^{10}$ vg of AAV-9 for the Cre recombinase, which was brought to 30µl with sterile physiological solution.

3.3. In vivo muscle force measurements

Gastrocnemius muscle force was measured in living mice as previously described (Blaauw et al., 2008). Briefly, animals were anaesthetized, and contractile muscle performance was measured *in vivo* using a 305B muscle lever system (Aurora Scientific Inc.). The contraction was elicited by electrical stimulation of the sciatic nerve. Common peroneal nerve was cut, and the torque developed during isometric contractions was measured at stepwise increasing stimulation frequency, with pauses of at least 30 seconds between stimuli to avoid effects due to fatigue. The duration of the trains never exceeded 600ms. Force was normalized to the muscle mass as an estimate of specific force. Time to peak, half time to peak and relaxation time of the twitch were also measured. Animals were then sacrificed by cervical dislocation, and muscles were dissected, weighed and frozen.

3.4. Measurement of *in vivo* protein synthesis

In vivo protein synthesis was measured using Click chemistry techniques. Le labelling was obtained after azidonorleucine (ANL) administration to animals either dissolved in drinking water or injected intraperitoneally. For i.p injections, a concentration of 90mM ANL was dissolved into an aqueous solution and administered to animals once a day. For the drinking water administration, a concentration of 30mM ANL supplied with 0.7% maltose was used.

3.5. FDB single fibre isolation

Animals were sacrificed through cervical dislocation. FDB muscles were collected with tendons and digested in a tube with collagenase (3mg/ml GIBCO-Life Technologies) in DMEM (GIBCO-Life Technologies) for 1 hour and 30 minutes at 37° C. Meanwhile, coverslips were coated with 10% matrigel (Bdolah et al.) in Tyrode's buffer. After digestion, muscles were removed from collagenase, washed to inactivate the collagenase and dissected.

3.6. Histological analysis and immunofluorescence stainings

Collected muscles were directly frozen in liquid nitrogen. Then, muscles were cut in 10µm thick cryosections using Cryostat (Leica CM 1950) and used for further analysis. Images were collected with an epifluorescence Leica DM6B microscope.

3.6.1. Hematoxylin & Eosin staining (H&E)

Hematoxylin is a basic dye that binds to basophilic substrates, such as DNA and RNA contained in ribosomes and nuclei, thus staining them violet. Eosin colours eosinophilic structures, such as intracellular and extracellular proteins, staining them pink. For the staining, we used the Bio-Optica kit “Rapid Frozen sections H&E staining kit” performing the following protocol:

Material	Procedure
Hematoxylin	1 minute
Wash in tap water	5 dips
Buffer solution	5 dips
Wash in tap water	5 dips
Eosin Solution	30 seconds
Ethanol solution 95%:	5 dips
Ethanol solution 95%:	5 dips
Ethanol solution 100%	5 dips
Ethanol solution 100%	5 dips
Xylene	10 dips
Xylene	10 dips
Mount with EU Kitt (Sigma-Aldrich)	

3.6.2. Periodic Acid-Schiff staining (PAS)

PAS staining is a method to detect polysaccharides such as glycogen and glycoproteins. Periodic Acid oxidizes vicinal diols of these sugars, breaking up the bond between two adjacent carbons and creating a pair of aldehydes.
These aldehydes, then, react with Schiff reagent, giving a purple-magenta colour.
The following procedures were used:

Material	Procedure
Carnoy's solution	10 minutes
Wash in distilled water	5-6- times
Periodic Acid 0,5% (Merck)	5 minutes
Wash in distilled water	5-6- times
Schiff reagent (Merck)	15 minutes
Wash in running tap water	5 minutes
Mount with Elvanol	

Carnoy's solution is a fixative composed of 60% ethanol, 30% chloroform and 10% glacial acetic acid. Elvanol is a saturated solution of polyvinyl alcohol in Phosphate Buffered Saline (PBS), 20% glycerol and 1mM sodium azide.

3.6.3. SDH staining

Succinate dehydrogenase is an enzyme that forms complex II of the respiratory chain and is localized in the inner mitochondrial membrane. Colourimetric evaluation of the staining is used either to assess approximately the quantity and the distribution of mitochondria within muscle fibres or to evaluate the oxidative activity of the enzyme. The reaction gives a purple colouration in the oxidative fibres, whereas glycolytic ones appear white. The sections were incubated for 30 minutes at 37°C with SDH solution (0.2M sodium succinate) (Sigma-Aldrich), 0.2M phosphate buffer (Sigma) pH 7.4 and 50mg of nitro blue tetrazolium (NBT) (Sigma-Aldrich). After the incubation, sections were washed with distilled water five times and then mounted with Elvanol solution.

3.6.4. Immunofluorescence analysis

Muscle cryosections were fixed in 4% paraformaldehyde for 10 minutes, treated with 0,1% Triton in PBS for 2 minutes and blocked with blocking solution (0,5% Bovine Serum Albumin BSA, 10% goat serum in PBS) for
30 minutes RT. Samples were then incubated with primary antibodies in 0,5% BSA, 4% goat serum in PBS at 4°C overnight. Then the sections were washed with PBS three times for 5 minutes and incubated with secondary antibodies (dilution 1:200) and WGA (Wheat Germ Agglutinin- Invitrogen) to label plasma membrane, 1:100 in 0,5% BSA, 4% goat serum in PBS at 37°C for 1 hour. After the washes, slides were mounted with Elvanol.
The antibodies used for immunofluorescence:

- Dystrophin (abcam) 1:100; anti-rabbit-647-conjugated.
- GFP Booster Alexa Fluor® 488.
- Anti P-S6 (cell signaling) 1:800; anti-rabbit 594-conjugated 1:20.
- Anti-Dystrophin (abcam) 1:100; anti-rabbit 488-conjugated 1:200.
- BF- G6 embryonic myosin (DSHB) 1:50 anti mouse; anti-mouse 488-coniugated 1:100.

Dystrophin staining is then used to fibre CSA measurements using ImageJ software (National Institutes of Health). All data are expressed as the mean ± SEM (error bars). Comparisons were made by using a t-test, with $p<0.05$ being considered statistically significant.

3.6.5. Neural Cell Adhesion Molecule (NCAM) staining

NCAM is localized at NMJ level in a normal muscle, whereas it diffuses throughout myofibers when impairment in the communication nerve-muscle occurs. Therefore, NCAM staining is used as a sign of muscle denervation. Muscle cryosections were fixed with Methanol -20°C and incubated in blocking solution (10% goat serum in PBS) at room temperature (RT) for 1 hour.
Samples were then incubated with the primary antibody against NCAM (Millipore) (dilution 1:100 in 2% goat serum in PBS) at 4°C overnight.
Then the sections were washed with PBS three times for 5 minutes and incubated with the anti-rabbit-594-conjugated secondary antibody (dilution 1:200 in 2% goat

serum in PBS) at 37°C for 1 hour (Jackson ImmunoResearch). After washing and incubation with DAPI, which labels nuclei, slides were mounted with Elvanol solution.

3.6.6. Myosin staining

Muscles cryosections were blocked with mouse-on-mouse (MOM-Vector Laboratories) for 1 hour at RT. Then, primary antibodies were put (anti- BAD5, anti-SC71, anti BFF3) 1:100 (Hybridoma Bank) in BSA 1% for 1 hour at 37°C. After washes, secondary antibodies were added (DyLight 549-conjugated anti-mouse IgM, 488-conjugated anti-mouse IgG 1:200 and 405-conjugated anti-mouse IgG2b 1:100) in BSA 1% for 1 hour at 37°C. Then, samples were mounted with Elvanol.

3.6.7. FUNCAT (Cryosections)

After ANL labelling, animals were sacrificed, and muscles were dissected. Tissue cryosections were fixed in 4%(w/v) PFA for 10 min, then permeabilized in 1% (w/v) Triton x-100 for 3 min. FUNCAT reaction is performed overnight at 4°C using 1mM THPTA (Tris(3 hydroxypropyl triazolyl methyl)amine, Sigma, ref. 762342), 7mM $CuSO_4$, 100mM Tris pH8, 100mM Sodium ascorbate and 10uM alkyne probe (AF594-Alkyne, Jena bioscience ref. CLK-1297). After the click reaction, the slices were washed in PBS (3 x 5 min) and further washed in PBS-EDTA- Tween (EDTA 0.5Mm, Tween 0.05% (w/v)) to quench the reaction. DAPI was added in the end to visualize nuclei and Alexa Fluor® 488 WGA that binds to sialic acid and N-acetylglucosaminyl residues to visualize cell membranes.

3.6.8. FUNCAT (single FDB fibres)

After the ANL labelling, animals were sacrificed and muscles were dissected. Tissue fibres were dissociated from the entire muscle in DMEM. Then cultured on Matrigel overnight. The following day the single fibres were fixed in 4%(w/v) PFA for 20 min, then permeabilized in 1%(w/v) Triton X-100 for 30 min.
FUNCAT reaction is performed overnight at 4°C using 1mM THPTA (Tris(3

hydroxypropyl triazolyl methyl)amine, Sigma, ref. 762342), 7mM $CuSO_4$, 100mM Tris pH8, 100mM Sodium ascorbate and 10uM alkyne probe (AF594-Alkyne, Jena bioscience ref. CLK-1297). After click reaction, the slices were washed in PBS (3 x 5 min) and further washed in PBS-EDTA-Tween (EDTA 0.5Mm, Tween 0.05% (w/v)) to quench the click reaction. DAPI was added to visualize nuclei, and α-Bungarotoxin, Alexa Fluor 488 conjugate (1:1000), was added to localize the neuromuscular junction.

3.6.9. FUNCAT-PLA

Following ANL labelling, animals were sacrificed and muscles were dissected. Tissue cryosections were fixed in 4% (w/v) PFA for 10 min, then permeabilized in 1%(w/v) Triton x-100 for 3 min. Tissue cryosections were blocked in blocking buffer containing PBS, 10% goat serum, 5% sucrose, 2% fish skin gelatine, then incubated overnight with antibodies against the protein of interest (anti-actin sc-56459 1:100, anti-myosin BF-F3 1:100, anti-myosin sc71 1:100, anti- myosin BA-D5 1:50 or anti-dystrophin Abcam 15277 1:200) in a twofold dilution of the blocking buffer. The following day, FUNCAT reaction was performed overnight at 4°C using 1mM THPTA (Tris(3 hydroxypropyl triazolyl methyl)amine, Sigma, ref. 762342), 7mM $CuSO_4$, 100mM Tris pH 8, 100mM Sodium ascorbate and 250uM Acetylene-PEG_4-Biotin (Jena Bioscience). After click reaction, the slices were washed in PBS (3 x 5 min) and further washed in PBS-EDTA-Tween (EDTA 0.5Mm, Tween 0.05% (w/v)) to quench the click reaction. Tissue cryosections were then incubated overnight at 4°C with rabbit anti-biotin (Bethyl A150-109A 1:500), rabbit-anti-biotin monoclonal (Cell- signalling 5597 1:200) or mouse-anti-biotin monoclonal (sigma B7653, 1:500) in a 2-fold dilution of the blocking buffer. The last day PLA probes (Duolink in situ PLA Probe Anti-rabbit PLUS and anti-mouse MINUS) were applied in 1:5 dilution in the blocking buffer for 2 h at 37° C, washed several times with wash buffer A (0.1 M Tris, 0.15M NaCl, 0.05% Tween 20) and incubated for 30 min with the ligation reaction containing the circularization oligos and T4 ligase prepared according to the manufacturer's recommendation (Duolink Detection reagents Red, sigma DUO92008) in a prewarmed humidified chamber at 37°C for 100 min. Three or more washes stopped amplification in 0.2M Tris, 0.1M NaCl, pH 7,5 followed by washes in PBS, pH 7,4. Cryosections were further processed with

cell markers and DAPI nucleus stain.

3.6.10. Whole-mount EDL and SOLEUS preparation.

EDL was dissected and pinned down with small pins from tendon to tendon on a Sylgard dish. A solution of 4% paraformaldehyde was added until the muscle was utterly covered at room temperature for 20 minutes.
The muscle was then abundantly washed with PBS and transferred to +4° C until needed.
IHC protocol
Muscles were abundantly washed in PBS, then bundles were mechanically teased apart using a solution of 0.04% saponin, leaving them attached to tendons. They were transferred in a twelve-well plate and washed in PBS. Bundles of fibres were permeabilized with 1% triton for 30 min and blocked for 1 h at room temperature (10 % goat serum, 5% sucrose, 2% fish skin gelatin, 0,5% triton X- 100). Anti-Yap (proteintech 13584_1_AP) antibody was added 1:100 in a twofold dilution of the blocking buffer overnight at 4°C and suitable fluorescent secondary antibody was added 1:200 for 3.5 hours at room temperature.
Images were acquired with Leica TCS SP5 confocal microscope.

3.7. Immunoblotting

Cryosections of 20µm of TA muscles were lysed in 100µl of a buffer containing 50mM Tris pH 7.5, 150mM NaCl, 10mM MgCl2, 0.5mM DTT, 1mM EDTA, 10% glycerol, 2% SDS, 1% Triton X-100, Roche Complete Protease Inhibitor Cocktail and Roche Phospho-Stop Phosphatase Inhibitor Cocktail.
Lysates were incubated at 70°C for 10 minutes and centrifuged at 13.300 rpm for 15 minutes at 4°C. The concentration of supernatant protein was then measured using a BCA protein assay kit (Pierce) following the manufacturer's instructions.

3.7.1. Protein gel electrophoresis

Extracted proteins were solubilized in a buffer containing 5µl of 4X NuPAGER LDS

Sample Buffer (Life Technologies), 1µl of 20X DTT (Life Technologies) and water until reaching 20µl of volume. After 10 minutes of denaturation at 70°C, samples were loaded on SDS 4-12% or SDS 12 % precast polyacrylamide gels (Life Technologies), according to the molecular weight of the protein to be analyzed. The electrophoresis was run in 1x MES/MOPS or 1X Tris-Acetate Running buffer, respectively (Life Technologies), starting from a voltage of 90V until reaching 120V when samples entered the wells.

3.7.2. Protein transfer on nitrocellulose membrane

Proteins were now transferred from gels to nitrocellulose membranes. For the transfer, we used a Semi-dry method (Bio-Rad). Membrane and blotting paper (Bio-Rad) were equilibrated with Transfer Buffer, 20% Methanol and 1X Tris-Glycine (SERVA). Protein transfer was obtained by applying a current of 2mA/cm2, according to the dimension of the gel, for 1 hour at RT. To evaluate the efficiency of the transfer, proteins were stained with Red Ponceau 1X (Sigma-Aldrich). The staining was quickly reversed by washing with distilled water and TBST.

3.7.3. Incubation with antibodies

After the transfer of proteins into nitrocellulose membranes, the membranes were saturated with Blocking Buffer (5% no-fat milk powder or BSA solubilized in TBS 1X with 0,1% TWEEN) for 1 hour at RT and incubated over-night with different primary antibodies at 4°C listed in Table 3). Tris-buffer saline (TBS) is composed of 50mM Tris and 150mM NaCl in water, adjusted to pH 7.6.
Membranes were then washed three times with TBS 1X with 0,1% TWEEN at RT and incubated with secondary HRP-conjugated antibody for 1 hour at RT. Immunoreaction was revealed by Clarity Chemiluminescent substrate (Bio-Rad) and developed with ImageQuant LAS 4000 Mini (GE Healthcare).
Stripping solution was made with 25mM glycine and 1% SDS, pH 2.

Antibody	Costumer	Dilution
Rabbit anti-phospho-Akt (Ser473)	Cell Signaling #4060	1:1000
Rabbit anti-Akt	Cell Signaling #9272	1:1000
Rabbit anti-phospho-S6 (Ser240/244)	Cell Signaling #2215	1:1000
Rabbit anti-phospho-4Ebp1 (Thr37/46)	Cell Signaling #9459	1:1000
Rabbit anti-4Ebp1	Cell Signaling #9452	1:1000
Mouse anti-puromycin	Millipore MABE343	1:1000
Mouse anti-GAPDH	Abcam ab 8245	1:10000
Mouse anti-Lys48	Millipore 04-263	1:5000
Rabbit anti-Lys63	Millipore 05-1308	1:2000

Table 3: Antibodies used for Western Blot

3.7.4. BONCAT

BONCAT was performed treating 20ug of proteins with 75uM Acetylene-PEG_4-Biotin (Jena Bioscience), 5mM $CuSO_4$, 70mM Sodium Ascorbate, 2mM THPTA (Tris(3-hydroxypropyltriazolylmethyl)amine, Sigma, ref. 762342). Biotinylated proteins were then separated by electrophoresis and immunoblotted on nitrocellulose. The resulting blot was blocked in 5% nonfat dried milk and incubated overnight with HRP-Conjugated Streptavidin (1:10000) or anti-GFP antibody (1:2000) in nonfat dried milk. Chemiluminescence is detected using Immobilon *Classico* western HRP substrate. Images were acquired using the ImageQuant LAS system.

3.7.5. Myosin Heavy chain electrophoresis

EDL and soleus were homogenized in SDS-PAGE solubilization buffer (62.5mM Tris-Cl, pH6.8, 2.3% SDS, 5% 2-mercaptoethanol, 10% glycerol). The whole cell lysate was quantified using a Lowry protein assay kit (Thermo Fisher). The proteins were precipitated in cold acetone and resuspended in a buffer containing 50mM Tris pH 7.5, 150mM NaCl, 10mM MgCl2, 0.5mM DTT, 1mM EDTA, 10% glycerol, 2% SDS, 1% Triton X-100, Roche Complete Protease Inhibitor Cocktail and Roche Phospho-Stop Phosphatase Inhibitor Cocktail. The click reaction (BONCAT) was performed adding 75uM Acetylene-PEG_4-Biotin (Jena Bioscience), 5mM $CuSO_4$, 70mM Sodium Ascorbate, 2mM THPTA (Tris(3-hydroxypropyltriazolylmethyl)ami ne, Sigma, ref. 762342). The electrophoresis was performed overnight on 7% PAGE. The resulting blot was probed with HRP streptavidin to identify myosin heavy chain type 1 (slow-twitch, fatigue-resistant) from soleus muscle and type 2 (fast-twitch, fatigue-sensitive) from EDL muscle.

3.7.6. Quantification of Immunoblotting

Quantification of the signal obtained through immunoreaction was measured with ImageJ software. The signal of interested protein was normalized for levels of a housekeeping protein, representative of gel loading. BONCAT was quantified, normalizing the signal for ponceau detected proteins. For specific proteins, we normalized by GAPDH since its content did not change during experimental conditions. Results are expressed as mean±SEM.

3.8. Gene expression analysis

3.8.1. RNA extraction

According to the manufacturer's instructions, total RNA was extracted from Gastrocnemius muscle by using Trizol (Life Technologies)

3.8.2. Reverse Transcription

400 ng of total RNA was reversely transcribed to obtain cDNA using SuperScriptTM IV (Life Technologies) in the following mix:

- Random primer hexamers (50ng/µl): 1µl
- dNTPs 1mM: 1µl

The volume was brought to 13µl with RNase-free water.

Samples were denatured at 65°C for 5 minutes to avoid secondary structures of RNA. After the denaturation, samples were added to the following components:

- DTT 100mM: 1µl
- Rnase OUT (Life Technologies): 1µl
- SuperScriptTM IV (Life Technologies): 1µl
- RNase-free water: 0,5µl The reaction program was:

Step 1: 23°C for 10 minutes

Step 2: 50°C for 10 minutes

Step 3: 80°C for 10 minutes

At the end of the reaction, the volume of each sample was brought to 50µl with RNase-free water.

3.8.3. Real-Time PCR reaction

Quantitative real-time PCR was performed using SYBR Green chemistry (Applied Biosystems). SYBR Green is a fluorescent dye used as a nucleic acid stain. Indeed, it intercalates into double-strand DNA, producing a fluorescent signal. Real-time PCR products accumulate during PCR cycles, creating an amplification plot, which is the plot of fluorescence signal versus cycle number thus, allowing their detection through a real-time PCR machine. A the beginning of PCR, the minor change in fluorescent signal defines the baseline for the amplification plot.

An increase in fluorescent signal above the baseline indicates the detection of PCR products. A fixed fluorescence threshold can be set above the baseline. Ct (threshold cycle) is the fractional cycle number at which the fluorescence passes the fixed threshold. So, a lower Ct value indicates a higher amount of the sample, which can be therefore detected earlier through the PCR process.

1µl of diluted cDNAs was amplified in 10µl PCR reactions in an ABI Prism 7000 (Applied Biosystems) thermocycler, coupled with an ABI Prism 7000 Sequence Detection System (Applied Biosystems) in 384-wells plates (Micro Amp Optical, Applied Biosystems). In each well, 5µl sample mix and 5µl reaction mix were mixed.

Sample mix was prepared as follows:

- cDNA: 1µl
- RNase-free water: 4µl
- SYBR Green was added to the primer mix as follows:
- SYBR Green qPCR (Applied Biosystems): 4,8µl
- Forward/Reverse primer mix (50mM): 0,2µl The PCR cycle used for the Real-Time PCR was:

Step 1: 95° C for 15 minutes

Step 2: 95° C for 25 seconds

Step 3: 58° C for 1 minute

Step 4: go to step 2 for 40 times

3.8.4. Quantification of the PCR products

Pfaffl in 2001 described a quantification method to evaluate the differences in gene expression, by measuring the ratio between a test sample and a housekeeping gene (Pfaffl, 2001). The relative expression ratio of a target gene is calculated based on the primer efficiency (E) and the threshold cycle deviation (DCt) of an unknown sample versus a control, and expressed in comparison to a reference gene.

The mathematical model is defined with this equation:

$$\text{Ratio} = \frac{(E_{\text{target}})^{\Delta Ct}}{(E_{\text{reference}})^{\Delta Ct}}$$

The reference gene used in our real-time PCR was HPRT, which did not change under experimental conditions.

3.8.5. Primer pair design

Gene-specific primer pairs were selected with Primer Blast software (http://www.ncbi.nlm.ni h.gov/tools/primer-blast/). Primer pairs were selected in a region close to the 3'-end of the transcript and amplified fragments of 150- 250bp in length. To avoid the amplification of contaminant genomic DNA, the target sequences were chosen on distinct exons, separated by a long (more than 1000bp) intron. The melting temperature of about 58-60° C.
The sequences of the primer pairs used for Cre:
Forward: GAACGCACTGATTTCGACC
Reverse: AACATTCTCCCACCGTCAG

3.9. Statistical analysis

Generally, we minimized physiological variation by using the same age mice to reduce the standard deviation. Comparisons were made by using a two-tail Student's t-test, with $p \leq 0.05$ considered statistically significant.
For all graphs, data are represented as mean±SEM.

4. RESULTS

4.1. MetRS expression and ANL incorporation

To test whether there is both the correct expression of the MetRS and the GFP protein, we infected three-month-old MetRS animals with AAV9 containing the sequence for the Cre recombinase protein[40]. After one month, we administered ANL to animals for one week. Figure 1 shows that AAV9-infected muscle fibres express the mutated MetRS L274G, which occurs along with the GFP. Moreover, infected fibres also efficiently incorporated ANL into newly synthesized proteins, thus allowing their detection using click-immunohistochemistry reactions (FUNCAT), and showing a high correlation between GFP staining and FUNCAT.

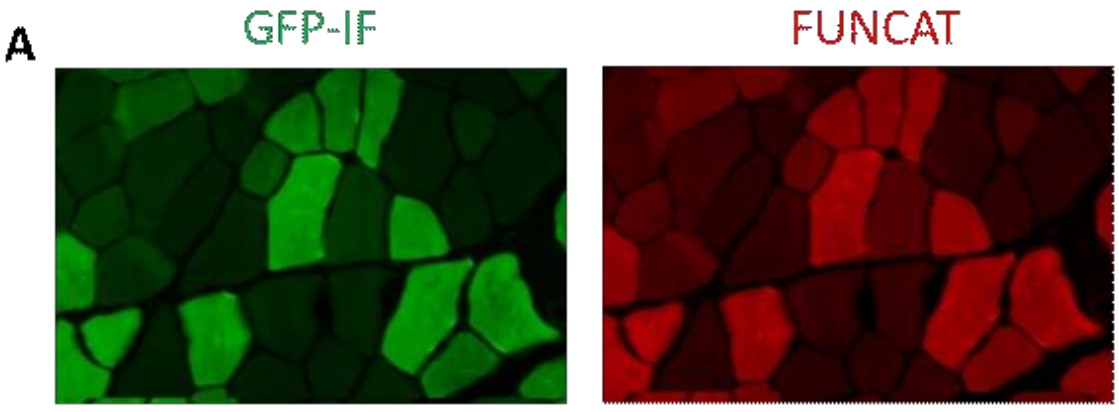

Figure 1: The correct expression of MetRS that occurs along with the GFP tag (left panel). ANL incorporation occurs only in infected fibres (right panel).

4.2. Generation of muscle-specific MetRS mouse line

To generate a skeletal muscle-specific MetRS mouse line, we crossed a Cre mouse line under the control of *mlc1f promoter*[37] with a MetRS mouse line. *Mlc1f* promoter is specific and strongly expressed starting on day ten during embryonic development[38]. The expression occurs only in adult skeletal muscle fibres and allows selective analysis of skeletal muscle proteins. Indeed, we extracted RNA samples from gastrocnemius muscle, sciatic nerve, spinal cord and aorta to confirm whether the mutant is exclusively expressed in skeletal muscle fibres. By quantitative RT-PCR for CRE recombinase and WB analysis of the GFP-tag, we

observed that the MetRS gene is expressed only in adult skeletal muscle fibres (**Figure 2**).

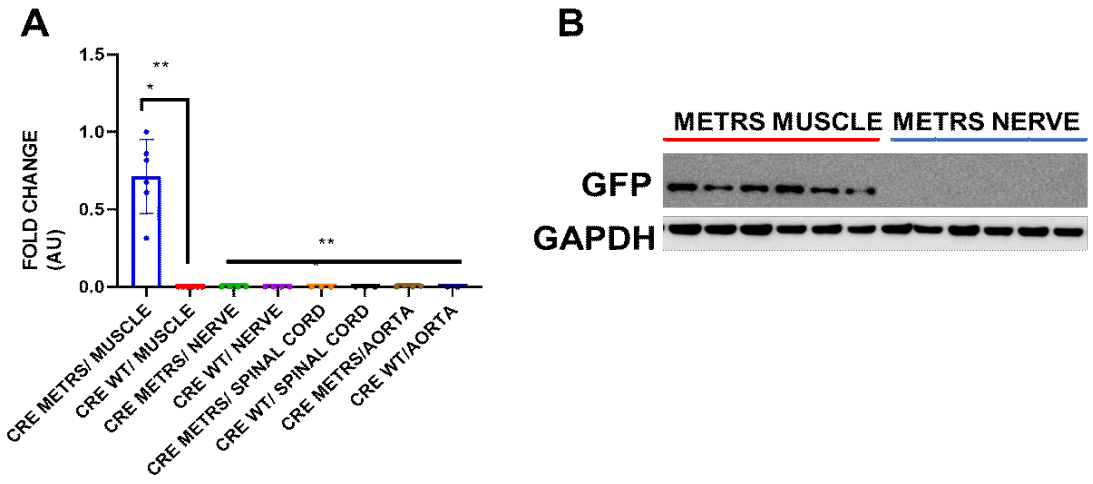

Figure 2: Validation of skeletal muscle-specific MetRS. A) CRE mRNA expression levels analyzed by RT-PCR in muscles of MetRS knock-in and control mice. n=4 mice each group***p≤0.001. **B)** Representative WB shows no GFP expression in nerve tissue.

4.3. ANL incorporation is efficient in all skeletal muscles examined

To better understand the incorporation's uncanonical amino acid, we administered ANL to two different groups of animals. Three-month-old homozygote and heterozygote MetRS animals were injected intraperitoneally for one week with 90mM ANL. All muscles were collected on the eighth day, and biotinylated proteins were identified using click-western blot techniques. These experiments show that, albeit ANL incorporation occurs both in homozygous and heterozygous animals, homozygous mice have a higher content of biotinylated proteins (**Figure 4**). The different amount of identified proteins is maybe due to the fact that the amount of mutated methionyl-tRNA synthetase highly influences incorporation. Since the natural methionyl-tRNA synthetase cannot activate ANL, a higher amount of expressed mutant MetRS results in a more robust ANL incorporation into newly synthesized proteins even if the competition between the two of them remains.

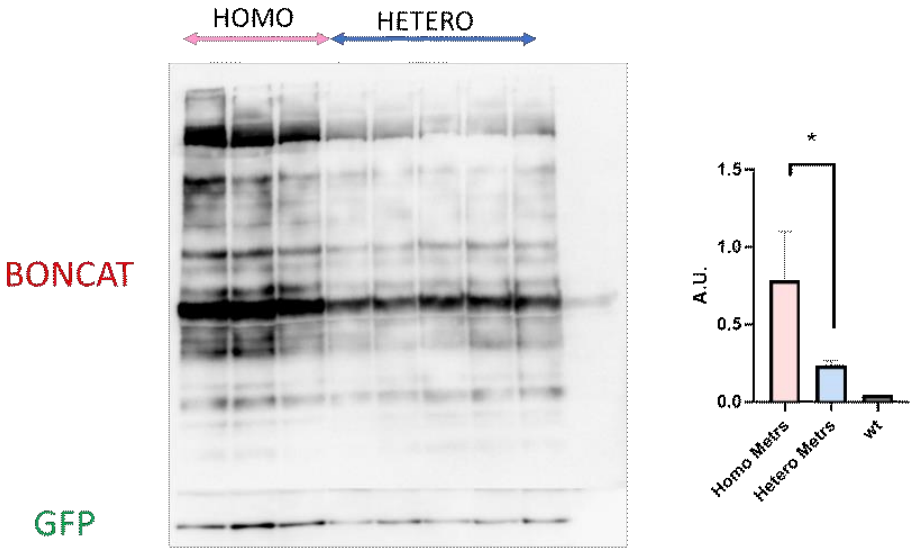

Figure 4: Homozygous animals incorporate more than heterozygous ones. *n=3* homozygous mice. *n=5* heterozygous mice.

Moreover, all skeletal muscles were collected and analyzed for ANL incorporation. *EDL, soleus, gastrocnemius, tibialis anterior* and *diaphragm* samples were labelled and identified with BONCAT. These results showed an efficient ANL incorporation in all muscles, even though slow muscles such as the *soleus* incorporate more than the predominantly fast diaphragm (**Figure 5**).

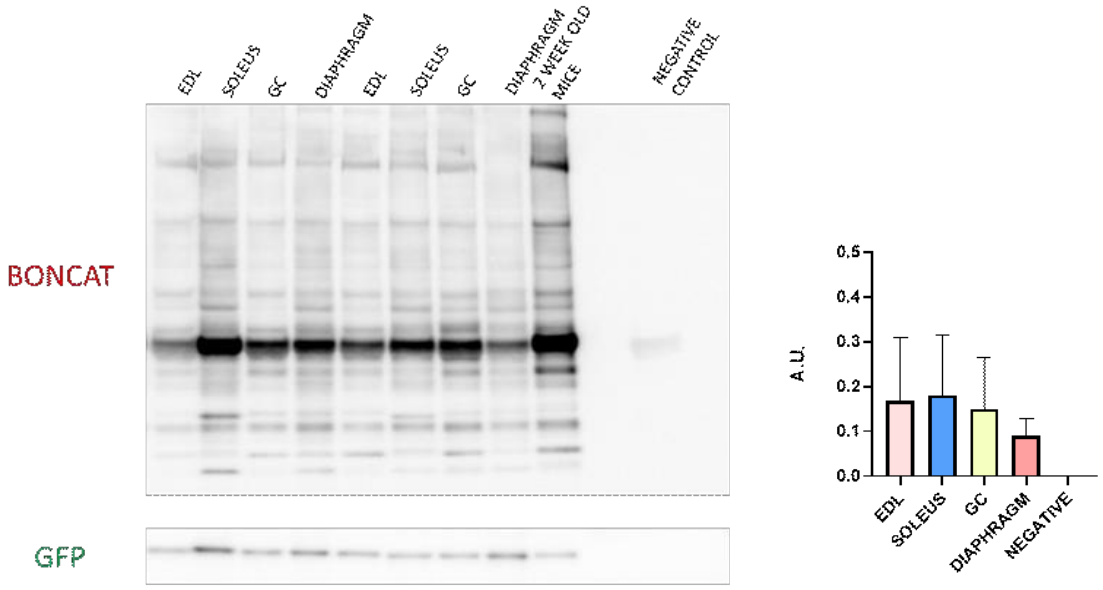

Figure 5: BONCAT reveals efficient incorporation in all skeletal muscle examined with higher levels of biotinylated proteins in slow muscles. n=4 mice each group.

The engineered methionyl-tRNA synthetase is expressed along with the native MetRS. The coexistence between the two leads to the incorporation of both methionine and azidonorleucine.

The previous chapter proved that higher mutant MetRS in homozygous mice results in more robust labelling. Next, we labelled animals with both ANL intraperitoneal injections and ANL supplied water to see if dosage and labelling time directly influence the labelling.

Dosage quantifications were not possible administering ANL in drinking water due to variability in the single animal's water intake. To test this correlation, we choose to administer ANL through intraperitoneal injections. Two groups of three-month-old animals were treated with single pulses of 2 and 4 mg of ANL. Muscles were collected 24 hours after the injection. L13G mutant MetRS maintains the ability to activate methionine. However, this activation occurs with a 270-fold lower specificity[41] and a higher dosage of azidonorleucine leads to a higher ANL incorporation **(Figure 6)**.

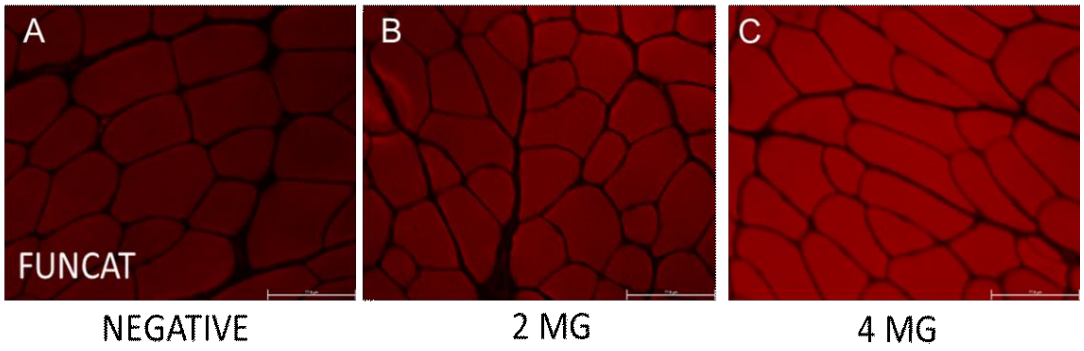

Figure 6: Representative images of FUNCAT (red) performed on cryosections of *gastrocnemius* muscles. Intraperitoneal injections of 2 **(B)** and 4 **(C)** mg of ANL proved dosage-dependent labelling. n=3 mice each group.

Since there are no data on skeletal muscle ANL bioavailability reported in the literature, we administered single ANL pulses to control the amount of time required to have effective incorporation in muscle proteins. We performed this experiment during the dark phase because the protein synthesis rate increases during the night following food intake[41]. We administered ANL to animals and sacrificed them after 1, 3, 5 and 24 hours. We observed a time-dependent ANL incorporation into muscle proteins. After three hours, some ANL-containing polypeptides were

already detectable. The following hours resulted in more substantial incorporation reaching the highest levels after 24 hours. **(Figure 7).**

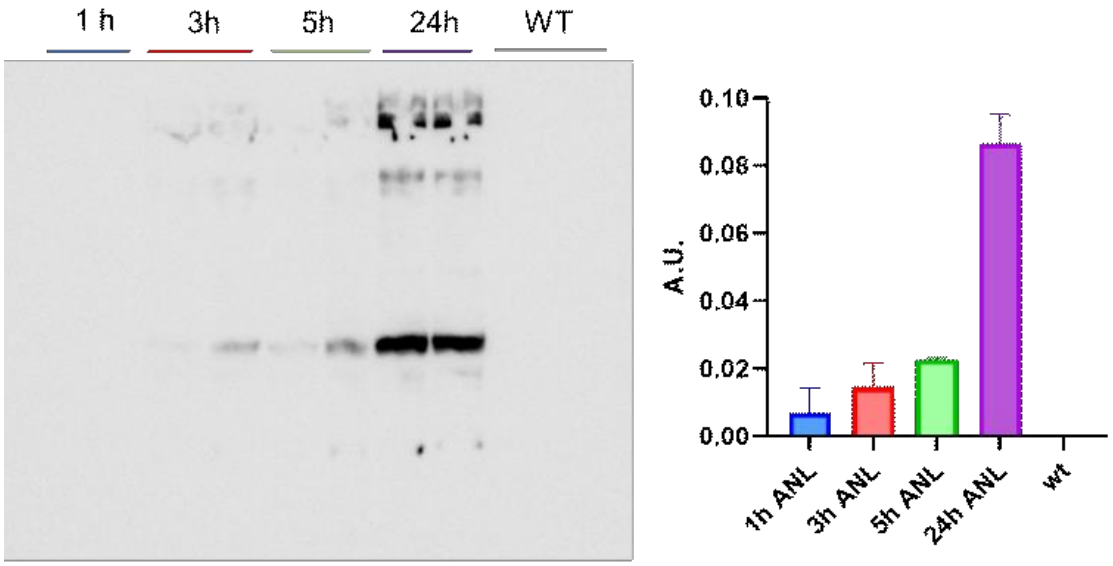

Figure 7: Representative WB of ANL incorporation following a single pulse (n=2 mice/group).

ANL i.p injections allow to monitor protein synthesis in a dose-controlled manner. Even though these experiments were ideal for detecting the time ANL takes to reach the muscle intracellular pool and be incorporated into proteins, the number of detected polypeptides was low. 90 mM ANL concentration used for the i.p. injections is the highest concentration without toxic effects on animals. Thus, we changed the administration route to increase ANL concentration in the amino acids cellular pool.

We added ANL to animals drinking water to have continuous labelling during the day. This new route allowed to have a higher amount of labelled proteins with no evident toxicity **(Figure 8)**.

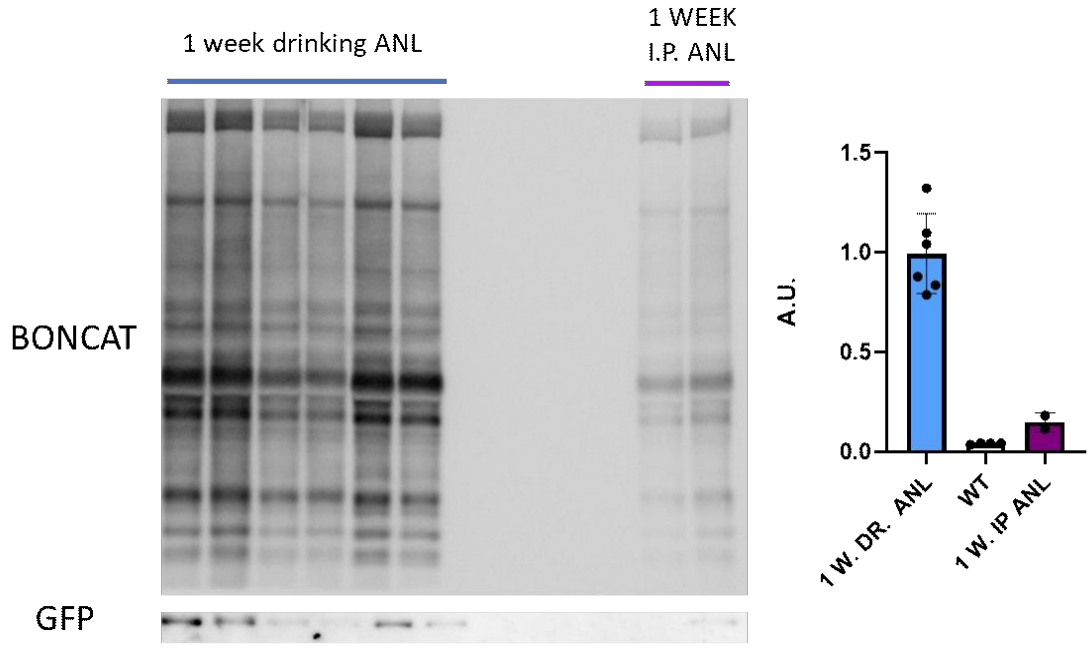

Figure 8: ANL administered through drinking water (first five lanes) results in higher labelling than i.p. injections (last two lanes).

We then checked how many days are necessary for solid labelling by administering to animals ANL for 3, 5 and 7 days in drinking water. BONCAT technique performed on muscles proved increased labelling over time, and a higher amount of labelled proteins was detected after seven days. Moreover, low variability between all the treated animals within a group suggested that water intake is similar between littermates **(Figure 9)**.

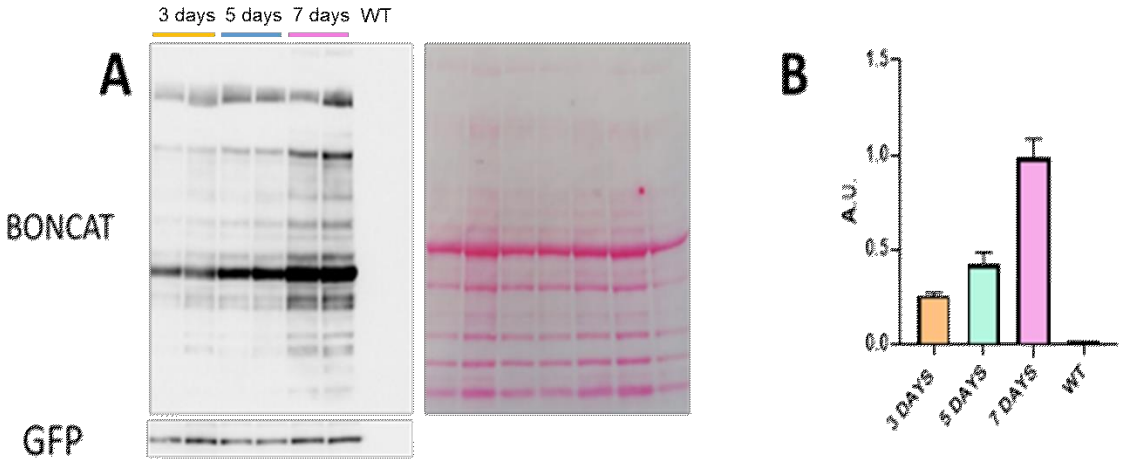

Figure 9: Representative WB of MetRS samples treated with ANL for three, five and seven days. *n=3* mice each group. The labelling increases over time, resulting in more biotinylated proteins after seven days than three and five days.

4.4. Long time ANL labelling does not affect muscle histology or force

Previous studies involving the use of radioactive tracers measured the turnover of specific proteins. ^{3}H-leucine injections were indeed used to measure myofibrillar proteins synthesis rate. These studies were fundamental to understand that myofibrillar protein such as actin and myosin account for almost 60% of the total skeletal muscle proteins[42] and different stimuli highly influence their turnover. Moreover, experiments based on amino acid isotopes revealed also the slow turnover rate of these proteins. Both actin and the different myosin chain isoforms have half-lives that expand from days up to weeks[43]. The importance of these proteins in muscle plasticity and their slow turnover rates is the reason why a longer labelling time is required. For this purpose, we increased ANL labelling from 1 week to 3 weeks. We divided animals into three groups that drank ANL supplied in drinking water for one, two and three weeks. The water intake was measured every other day, revealing a constant water intake. In addition, they consumed about 4ml of water/day, which is similar to the daily intake of control animals[44]. Bodyweight, lean mass and fat mass were also analyzed using an EchoMRI-100 system. No macroscopic changes in mice behaviour, weight and lean mass suggested the absence of ANL toxicity during the treatment.

However, incorporating ANL into newly synthesized proteins can be toxic at a cellular level, causing misfolding problems. To assess the absence of intracellular toxicity, hindlimb muscles were collected and analyzed. Again, histological stainings such as hematoxylin-eosin, PAS and SDH staining suggested that ANL incorporation did not compromise the physiological role of labelled proteins **(Figure 10)**.

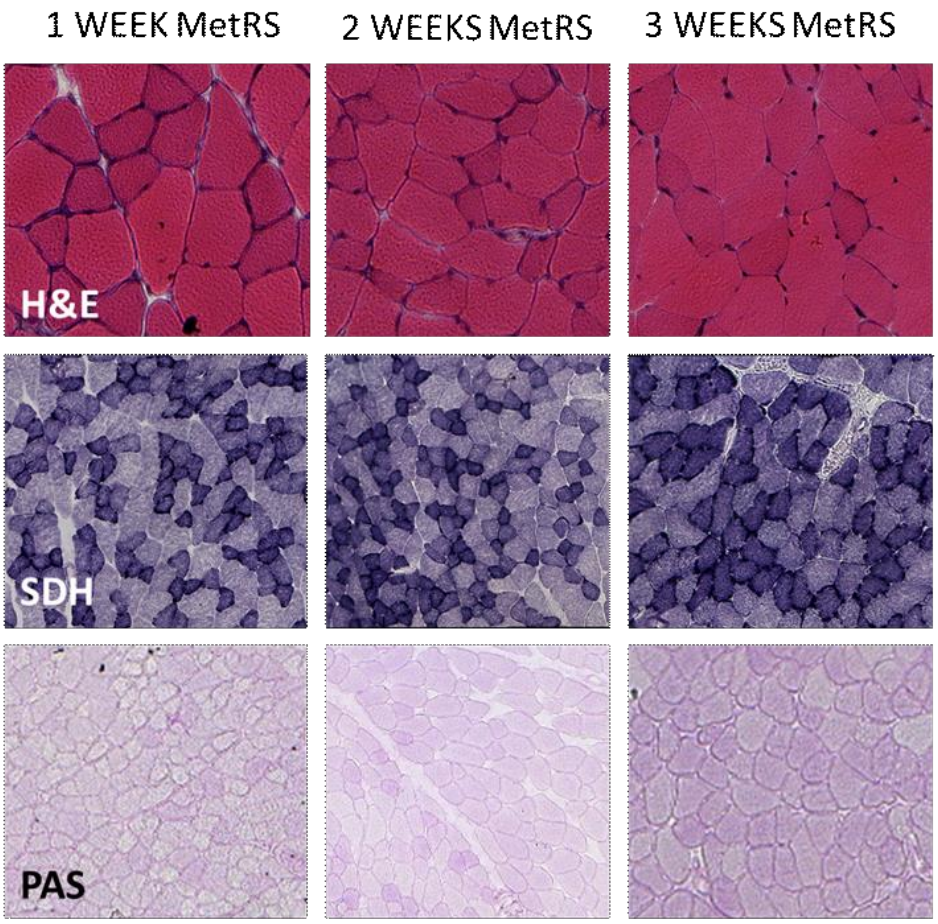

Figure 10: Histological analysis confirmed the absence of ANL-containing proteins toxicity

These results were also confirmed by *in vivo* force production of gastrocnemius muscles[45]. Both absolute and normalized force were unaffected by ANL incorporation **(Figure 11)**.

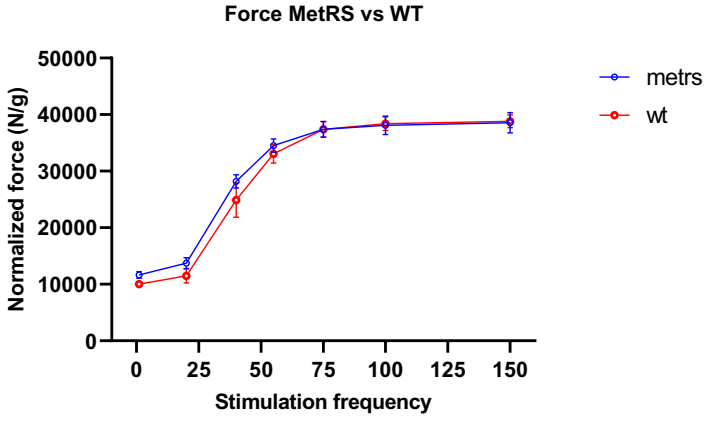

Figure 11: Muscle force production was analyzed to assess muscle proteins functionality. N=5 mice for the control group and n=5 mice for ANL-treated mice.

The absence of myopathic features indicates the functionality of newly synthesized proteins containing ANL residues instead of methionine. We next identified and visualized these proteins with BONCAT (**Figure 12 A**) and FUNCAT techniques (**Figure 12 B**). No differences were found between these three labelling timings.

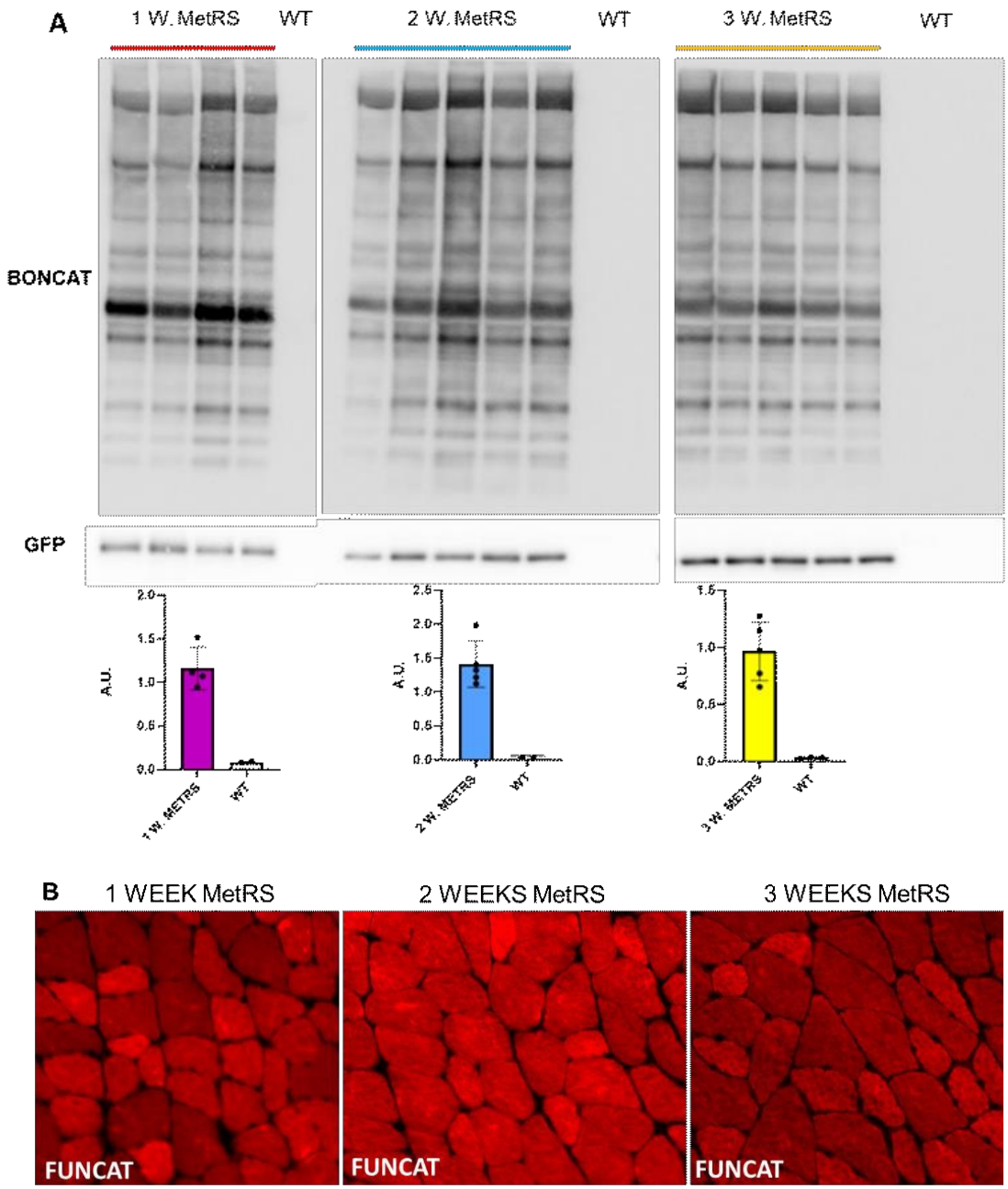

Figure 12: Both BONCAT**(A)** and FUNCAT (in red) **(B)** proved efficient labelling throughout the treatment. N=5 mice each animals group.

4.5. MetRS-AKT transgenic mice as hypertrophy model

Different stimuli such as muscle contraction, electrical inputs, nutrients and hormones can increase muscle mass. This condition, also called hypertrophy, is determined by increased protein synthesis in existing fibres without the formation of new fibres. Our laboratory has already demonstrated that constitutive activation of AKT leads to muscle hypertrophy, improving force production and muscle metabolism[12]. To determine the changes in protein synthesis in this model, we generated Akt-MetRS mice. For both transgenes, the expression was under the control of the Mlc1f promoter. In this way, it is possible to mimic a hypertrophic stimulus specifically in skeletal muscle fibres and obtain a resulting labelled proteome of these animals. At a basal level, AKT is bound to an estrogen receptor domain which marks it for degradation. Still, tamoxifen injections lead to AKT activation, S6 phosphorylation, ribosome biogenesis, tRNA synthesis and transcription factor activation[11].

For these experiments, MetRS and MetRS-Akt animals were treated for 1 and 3 weeks with 1 mg of tamoxifen. 30 mM ANL was administered in drinking water during the treatment time. Lean and fat mass were quantified and normalized by body weight (**Figure 13 A**). From these results, 1-week treatment was sufficient to cause a slight decrease in fat mass along with an increased lean mass even though higher muscle hypertrophy is obtained after three weeks. At the end of the treatment, muscles were collected and analyzed. Histological analysis revealed no myopathic signs suggesting physiological muscle growth (**Figure13 B**).

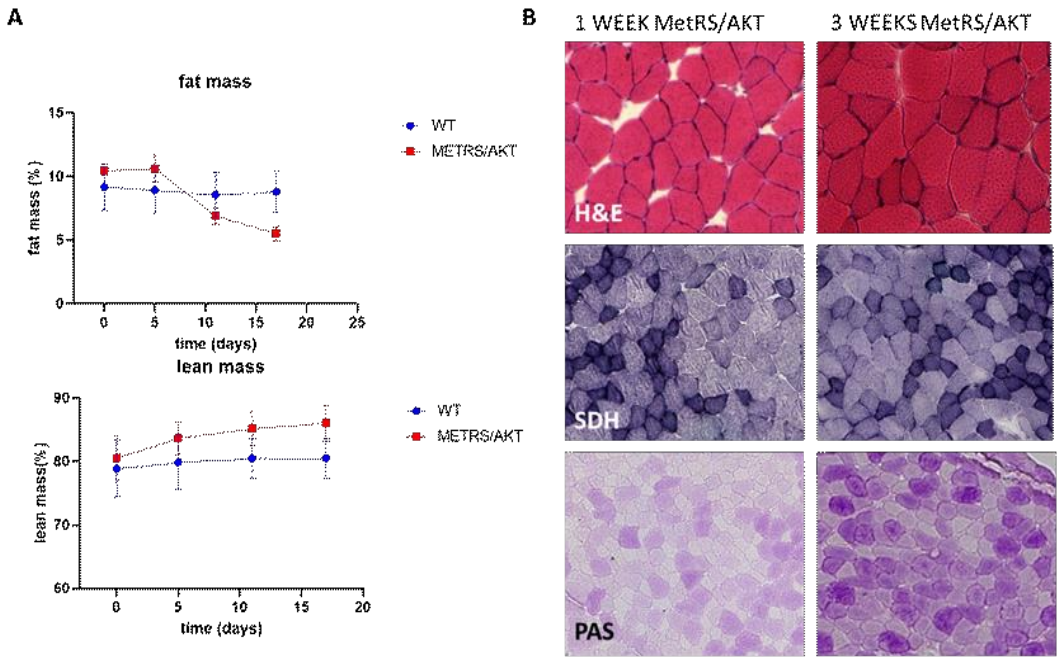

Figure 13: AKT activation increases lean mass and decreases fat mass (A) with no alteration in muscle histology (B). n=5 animals for fat and lean mass analysis.

AKT is a hypertrophy mouse model where muscle mass increase is independent of satellite cell activation[12]. The increased muscle force can be explained as increased myofibrillar functionality due to increased protein synthesis. To test this theory, we tried to understand whether AKT overexpression leads to increased myosin heavy chain labelling, thus to a higher turnover of these proteins. Hence, MetRS and MetRS-AKT animals were labelled for three weeks with ANL, and, during this time, animals received i.p injections of tamoxifen to promote muscle hypertrophy. Gastrocnemius and TA muscles were used for labelling analysis, while EDL and soleus, respectively composed of fast and slow fibres, were used for myosin electrophoresis experiments. Labelling analysis revealed no significant differences in chemiluminescent and fluorescent intensity between the two experimental groups (**Figure 14**).

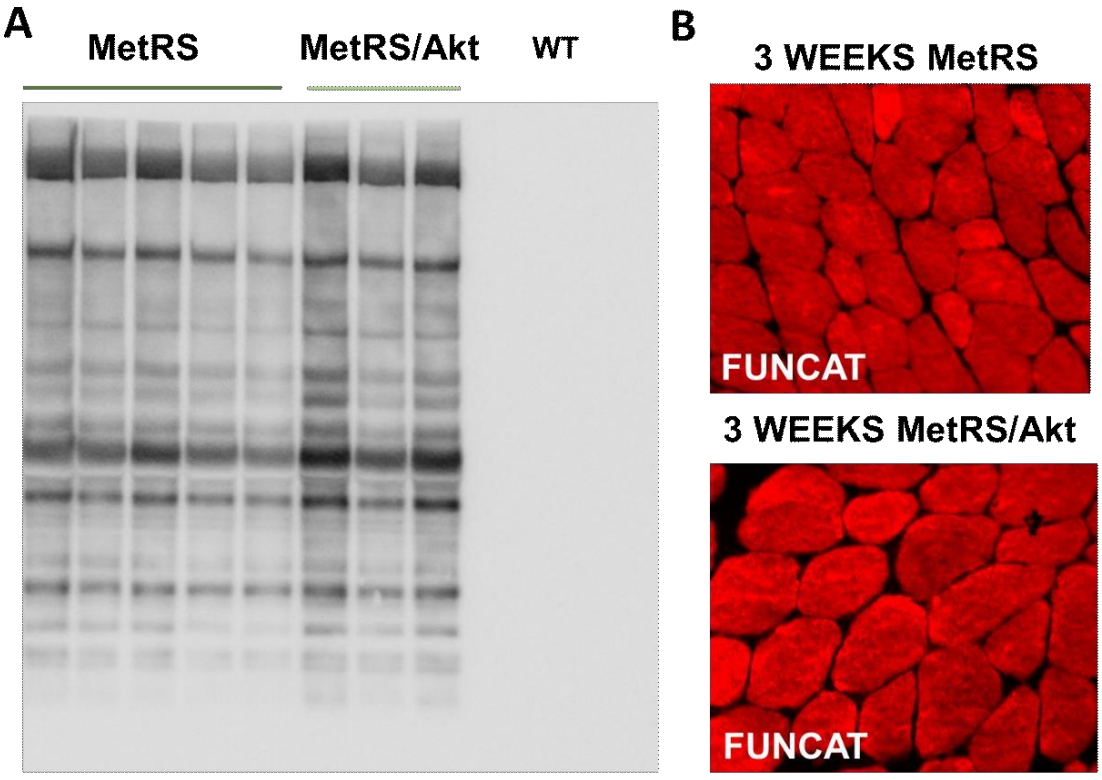

Figure 14: A) BONCAT analysis in MetRS and MetRS/AKT animals revealed no significant differences in protein labelling. **B)** FUNCAT (in red) confirmed WB results. N=5 mice each group.

Both weights of GC muscles and total lean mass observed with MRI analysis increased, suggesting a difference in protein content between MetRS and MetRS-AKT animals. Since no significant change in the whole cell lysate WB analysis was observed, we controlled the labelling of myofibrillar proteins with myosin electrophoresis. We lysed EDL and soleus muscles in a SDS buffer that extracts myofibrillar proteins. After protein quantification, we performed a 24-hours SDS page to separate myosins heavy chain from all other proteins.

The experiment illustrated in the figure below (**Figure 15**) shows two important aspects of muscle hypertrophy. First of all, myosin labelling increases in MetRS/AKT animals compared to MetRS mice, confirming an increased myofibrillar protein synthesis during AKT-mediated hypertrophy. Secondly, EDL muscle, mainly composed of fast fibres (2B and 2X fibres), has lower labelling than slow soleus muscle. These results suggest that the two tissues have different protein synthesis rates in both hypertrophic and control conditions,

confirming previous results obtained with SUnSET tecniques[45].

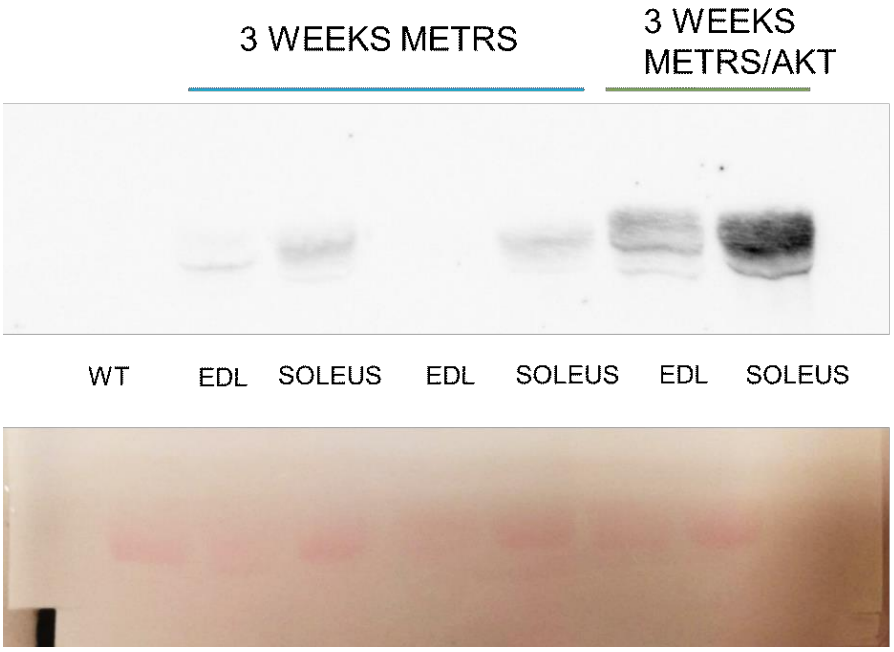

Figure 15: WB analysis of myosin heavy chain electrophoresis

4.6. Proteomics analysis of MetRS and MetRS-AKT animals

Protein labelling with ANL introduces a modified amino acid with molecular weight slightly different from the natural methionine. Azidonorleucine weights 23 Dalton more than its natural analogue, and its incorporation can be used for highly sensitive protein identification via mass spectrometry techniques. Cell-type-specific ANL incorporation allows for tissue-specific proteome analysis in a complex protein mixture. Our collaborators, supervised by Prof. Marcus Krüger (CECAD Institute of Cologne), provided mass spectrometry analysis of quadriceps samples of MetRS and MetRS-AKT animals labelled for one, two and three weeks. These preliminary results suggested that higher labelling time allows for better peptide identification in physiological conditions, even though no changes in the overall number of enriched proteins are observed **(Figure16)**.

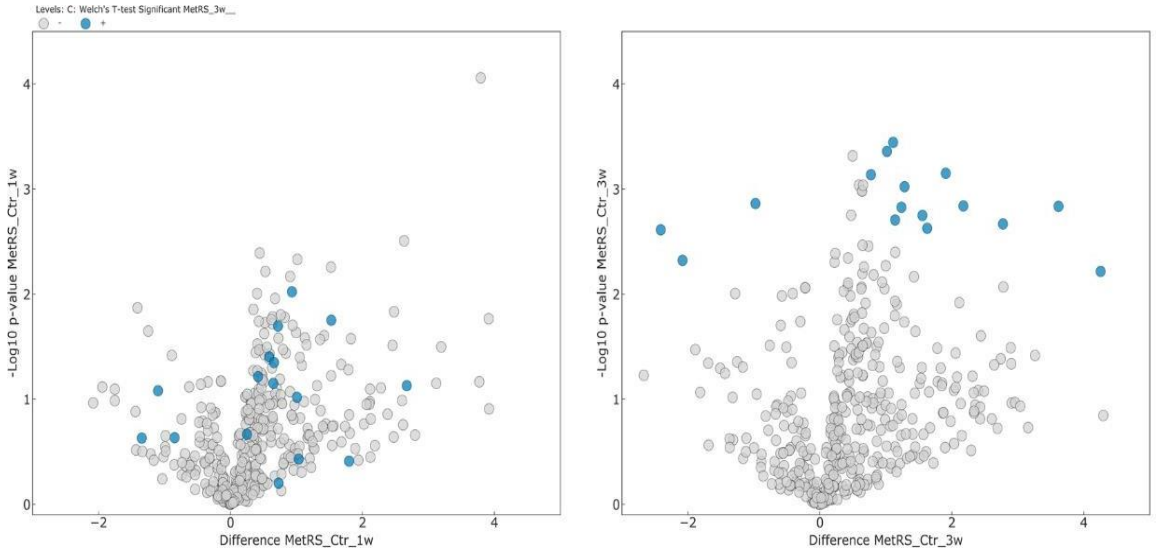

Figure 16: Three-weeks MetRS samples were enriched more efficiently thanone-week MetRS samples.

The following experiments compared the amount of enriched proteins between MetRS and MetRS–AKT animals. We observed, in particular, overexpression of ribosomal proteins such as Rpl5, Rpl26, Rps11, Rps9, suggesting increased ribosome biogenesis in response to increased protein synthesis. Moreover, a higher expression of mitochondrial proteins such as Aifm1, Ndufc2, Etfb was justified by the higher energy production required in growth processes. Besides identifying structural proteins such as actin, we noticed the presence of a protein of endoplasmic reticulum Hspb1, which plays an important role in protein folding and quality control. Along with markers of increased protein synthesis, we also observed an increased expression in Uba1, the ubiquitin-like modifier-activating enzyme 1 involved in the first step of ubiquitination and UPS degradation.

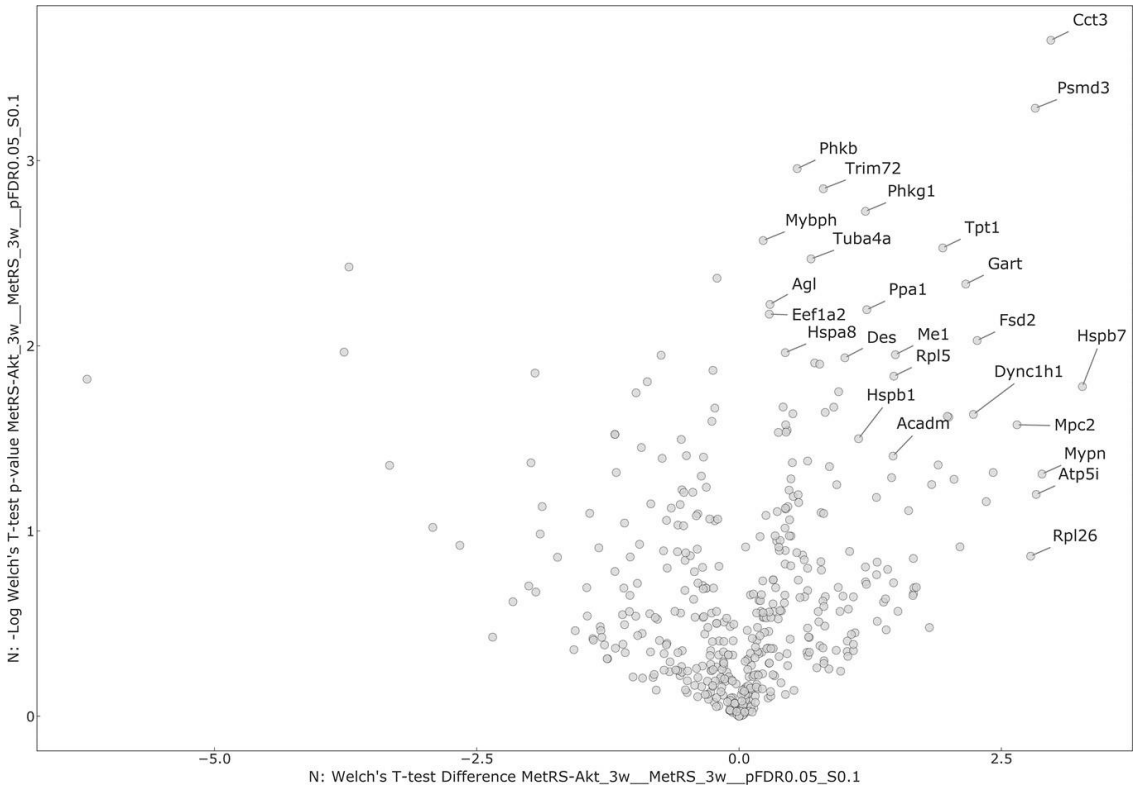

Figure 17: Enriched proteins in three weeks MetRS and MetRS-AKT samples.

4.7. Localization of ANL-containing proteins

One of the most significant drawbacks of SUnSET is the lack of localization of the newly synthesized proteins. After the translation, each polypeptide must move in the cell compartment of interest guided by specific sequences[46].

Puromycin, however, blocks protein synthesis. Besides the toxicity implied in the ribosome blockage, there is an accumulation in the cytoplasm of incomplete peptides that cannot reach their target. It is possible, using MetRS, to localize precisely a newly-synthesized protein of interest. On the other hand, the synthesis of ANL-containing proteins does not interfere with the biological function of the polypeptide. It is normally translated, moved into specific cellular compartments and can be localized coupling click reaction to a proximity ligation assay[47]. Briefly, click reaction couples a biotin-alkyne molecule to the ANL azido group. Then, different antibodies raised in two different species targeting biotin and the protein of interest (POI) are recognized by two secondary antibodies carrying oligonucleotides. The close proximity of biotin and the protein of interest results in an oligomerization reaction[48] that can be visualized as puncta.

We applied this technique to localize dystrophin and actin because of their abundance in skeletal muscle and because they were identified in mass spectrometry analysis. The other reason behind the choice of these two proteins was the localization. Actin is the component of thin filaments, and it is mostly localized in the cytoplasm. Dystrophin, differently, is a cohesive protein. It links the muscle fibre cytoskeleton to the extracellular matrix, and it is localized on the surface membrane of striated muscle[49].

We performed FUNCAT-PLA on both MetRS and MetRS/AKT samples localizing the two proteins of interest. When dystrophin was considered, puncta increased proportionally with the time labelling and the hypertrophic stimulus (**Figure 16 A**). On the other hand, Actin PLA signals increased significantly during more extended labelling, even if it was not influenced by the hypertrophic stimulus (**Figure 16 B**). As expected, dystrophin PLA signals were primarily present on the plasma membrane. The ones present in the cytoplasm were attributed to dystrophin proteins synthesized by ribosomes close to the myofibrillar apparatus rather than sarcolemmal ribosomes.

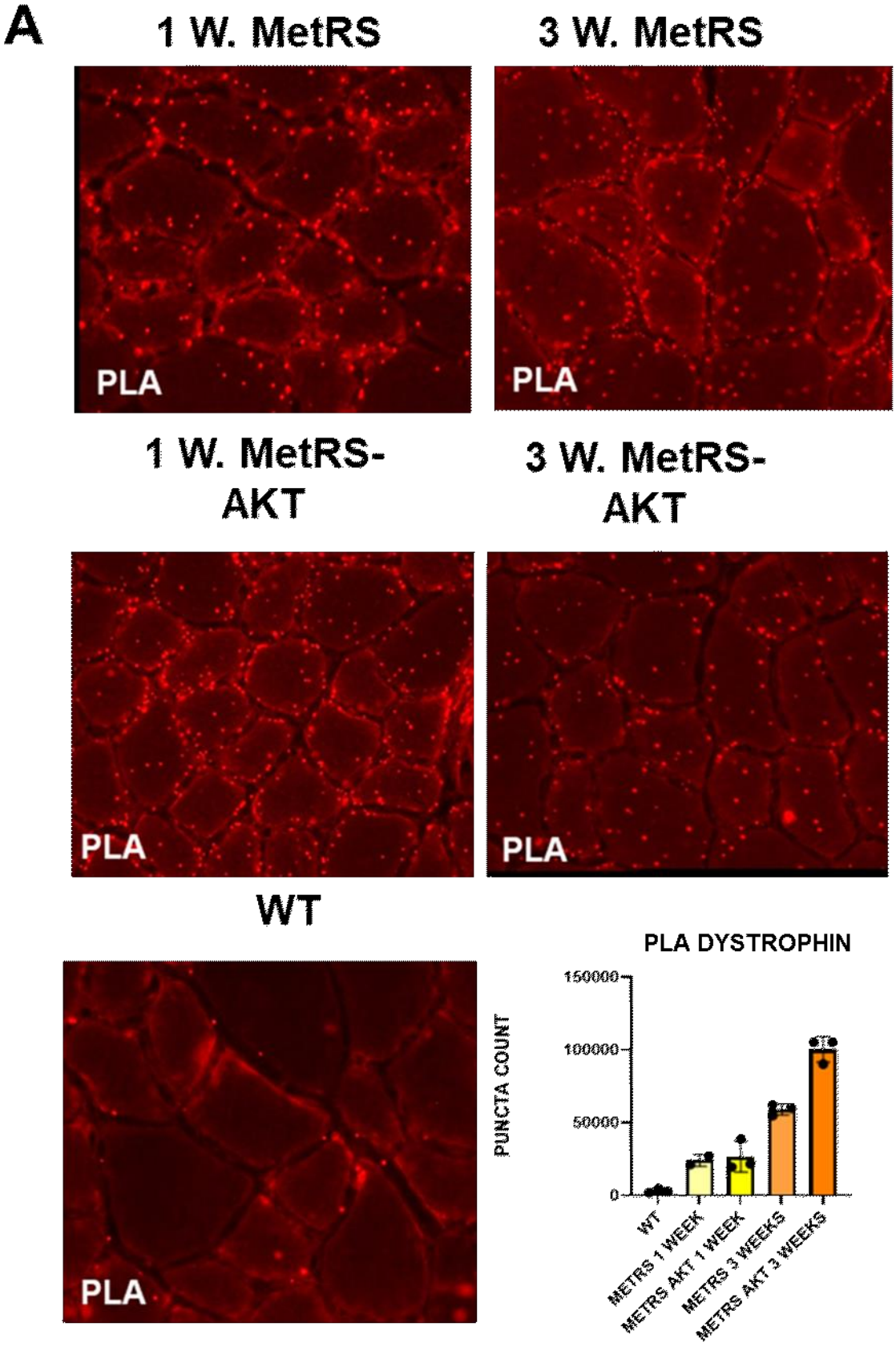
A
1 W. MetRS
3 W. MetRS
PLA
PLA
1 W. MetRS-AKT
3 W. MetRS-AKT
PLA
PLA
WT
PLA
PLA DYSTROPHIN
PUNCTA COUNT
150000
100000
50000
0
WT
METRS 1 WEEK
METRS AKT 1 WEEK
METRS 3 WEEKS
METRS AKT 3 WEEKS

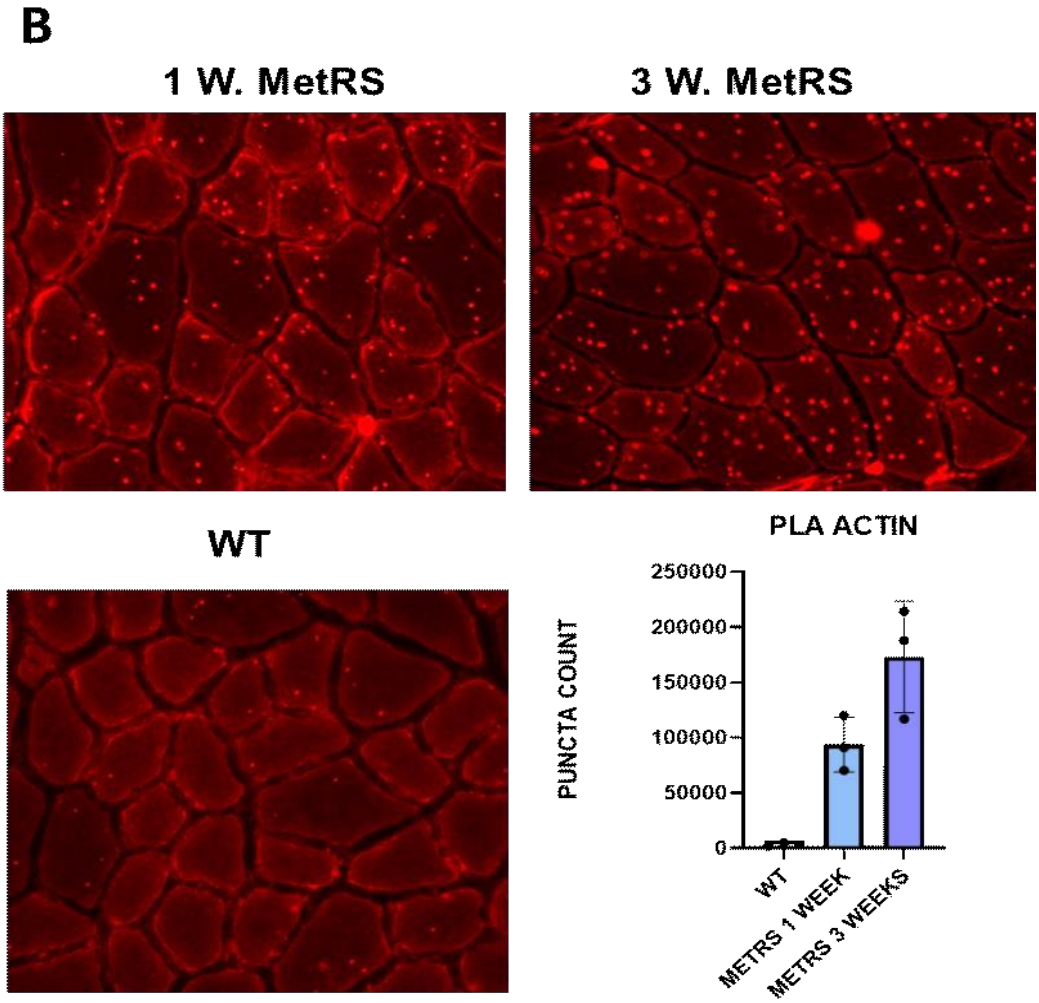

Figure 16: FUNCAT-PLA (red puncta) with dystrophin as POI proved the sarcoplasmic localization of dystrophin **(A)** FUNCAT-PLA with actin as POI **(B)** showed its cytoplasmatic localization. N=3 mice for each experiment.

4.8. Overload hypertrophy leads to increased labelling of muscle fibres near the myotendinous junction

Another hypertrophic model widely used is the synergist ablation. This model consists in overloading the EDL muscle by ablating its major synergist, i.e. the tibialis anterior. Previous studies attributed the increased myofiber CSA and myonuclear number[49] to a higher protein synthesis rate. These results were confirmed by both higher levels of puromycin-containing peptides and increased radioactivity (when radioactive isotopes were used as tracers). However, the rapid increase in muscle mass is caused by oedema, so we used tibialis anterior

tenotomy to limit inflammation. Since our lab already demonstrated that TA tenotomy increases protein synthesis rate using SUnSET[49], we wanted to test the efficacy of the MetRS labelling on this model. We performed tenotomy of the TA tendon of MetRS animals, and 24 hours after the chirurgical operation, EDL was almost 30% bigger than the controlateral muscle[50]. One day after the operation, we labelled with i.p. injections of 2 mg/day of ANL for three days and, after, mice were sacrificed for muscle collection. EDL and TA muscles were fixed in PFA and clicked in a whole-mount preparation (**Figure 17**).

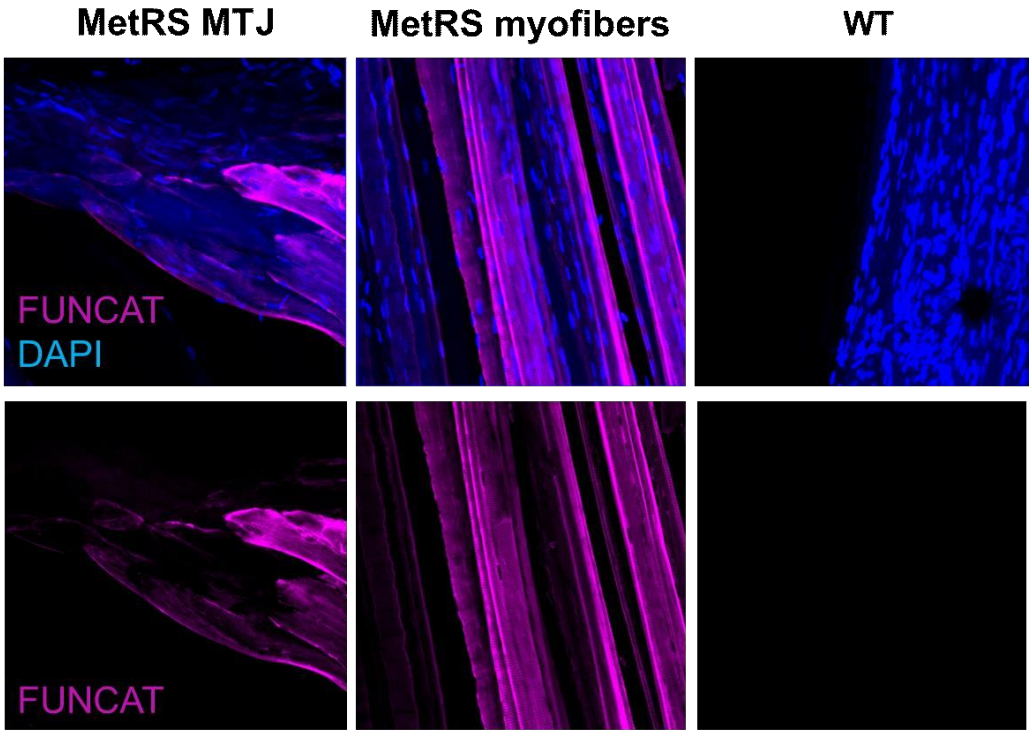

Figure 17: FUNCAT (magenta) performed in a whole-mount preparation proved an increased protein synthesis near the myotendinous junction. DAPI staining of both tendon and myofibers nuclei (blue). N=3 ANL- treated animals.

The resulting analysis shows no significant difference in the IF levels between overloaded and control leg. However, the protein synthesis rate seems to be higher close to the myotendinous junction when compared to the myofiber centre, suggesting a correlation between mechanotransduction and protein synthesis rate (**Figure 17**).

Mechanotransduction pathways, implicated in the transduction of mechanical signals, regulate cell growth processes via Yes-Associated Protein (YAP) and

Hippo signalling network[49]. YAP overexpression promotes indeed hypertrophy[50] in a mTORC1-independent fashion. To test this theory, we checked for YAP expression during overload. We performed anti-YAP staining on whole-mount EDLs of overloaded animals. We found that YAP strongly localises in the nuclei near the myotendinous junction rather than along the myofiber. (**Figure 18**).

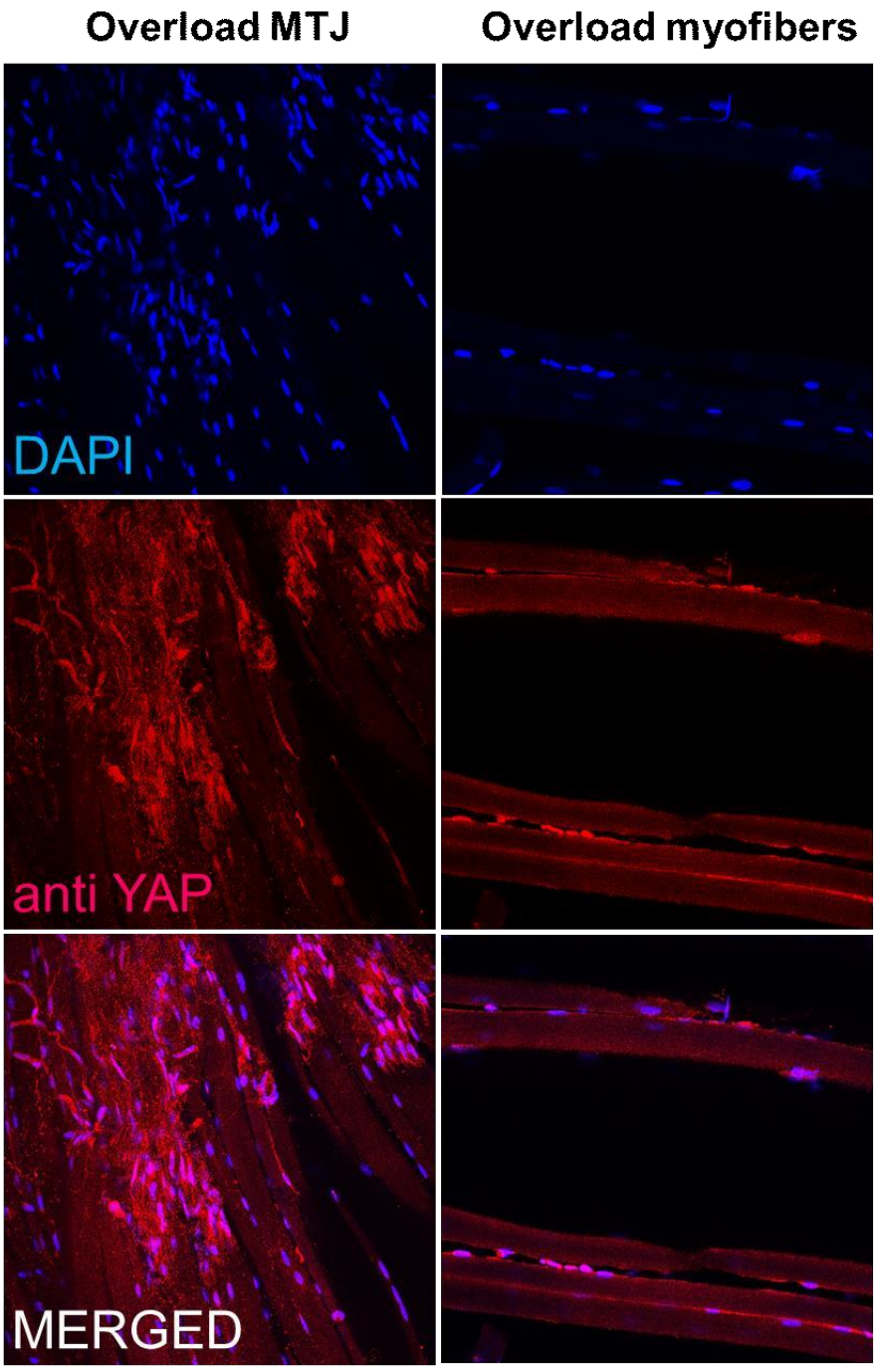

Figure 18: YAP nuclear localization in overload muscle hypertrophy. Anti-YAP staining (red) shows a nuclear localization (DAPI blue) at the myotendinous junction.

4.9. Protein synthesis in different fibre types

Skeletal muscle fibres are classified according to many parameters, including their metabolism (glycolytic or oxidative) and MHC isoforms, besides EDL, mainly composed of fast 2A and 2X fibres and soleus composed of slow 1 and 2A fibers, all other muscles, including gastrocnemius and tibialis anterior, present mixed fibre populations. Here we wanted to visualize on cryosections the different labelling of fast and slow fibres. To do so, we labelled MetRS animals with ANL for one week. After that, we collected hindlimb muscles and performed FUNCAT and anti-myosin staining on serial gastrocnemius cryosections. We chose this muscle because of its high heterogenicity, including 1, 2A, 2B and 2X fibres (**Figure 19**).

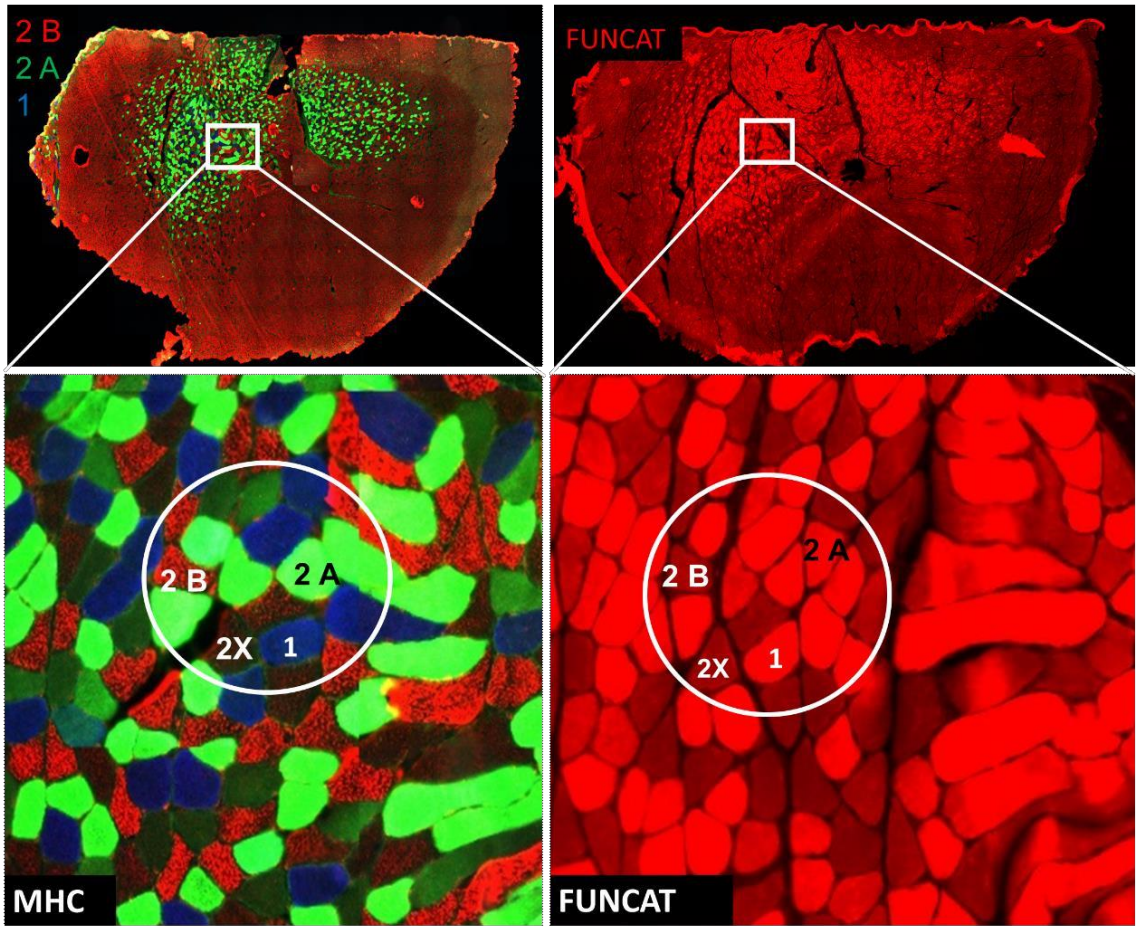

Figure 19: FUNCAT (in red) and anti-myosin staining (2A in green, 2B in red, 2X in black, 1 in blue) on serial cryosections proved a correlation between protein synthesis and fibre type.

Physiological perturbations such as food deprivation and disuse alter protein synthesis in a fibre type-dependent manner. SUnSET experiments already proved the existence of a correlation between fibre-type and protein synthesis rate[51] in both starving and denervation conditions. The problem with these techniques was related to poor sensitivity in labelling visualization. ANL labelling overcomes this drawback, proving a different labelling rate even in the absence of perturbations. Animals in physiological conditions seem to have higher labelling rates in oxidative slow-twitch type 1 fibres and oxidative fast-twitch type 2A fibres than in glycolytic fast-twitch type 2X and 2B fibres.

4.10. Analysis of muscle proteome in catabolic conditions: starvation

To explore fibre type-dependent labelling in the presence of atrophic stimuli, we administered ANL to mice placed on food deprivation. We divided animals into two groups composed of three animals each. One group has fasted for 24 hours and the other one for 48 hours. Fed control groups were labelled for the same amount of time as fasted mice. 30 mM ANL was administered to both groups in drinking water. During the treatment, animals water intake was similar, suggesting similar protein labelling. Starved animals lost 10% of body weight after 24 hours and 45% after 48 hours. Moreover, weight loss was proportional to muscle loss.
All animals were sacrificed in the morning, muscle tissues were collected, and labelled proteins were identified using BONCAT techniques. The amount of labelled proteins decreased in both starved groups (**Figure 20**).

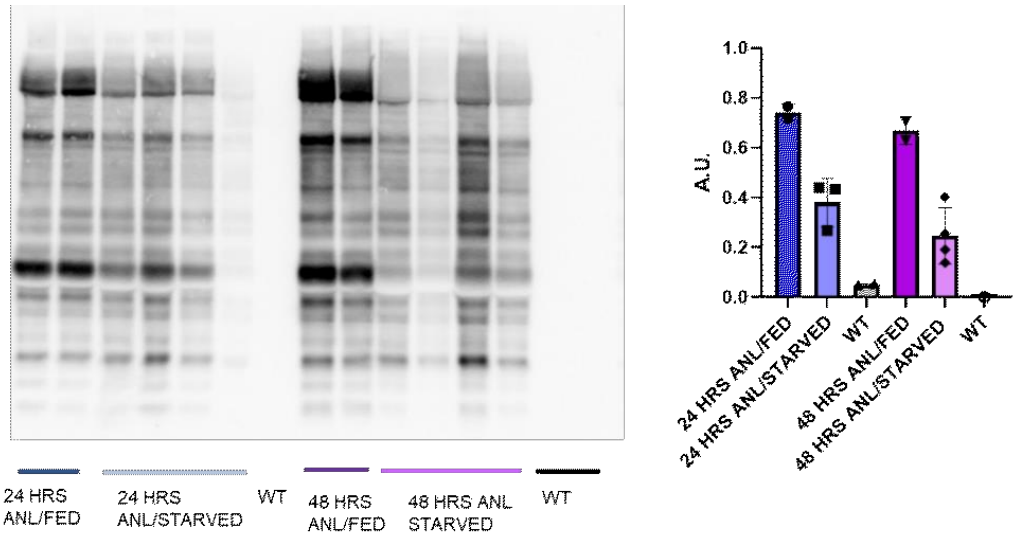

Figure 20: BONCAT experiments show how protein labelling decreases in starving conditions.

Moreover, we observed a proportional decrease in biotinylated proteins. After 24 hours, labelled proteins decreased by 50%, while 48 hours starvation caused a further decrease of 25%. Even though BONCAT is instrumental in identifying the total amount of proteins, it is difficult to understand which fibres undergo atrophy first. Immunofluorescence analysis overcame this problem showing a different fluorescence intensity in muscle fibres in response to starvation **(Figure 21).**

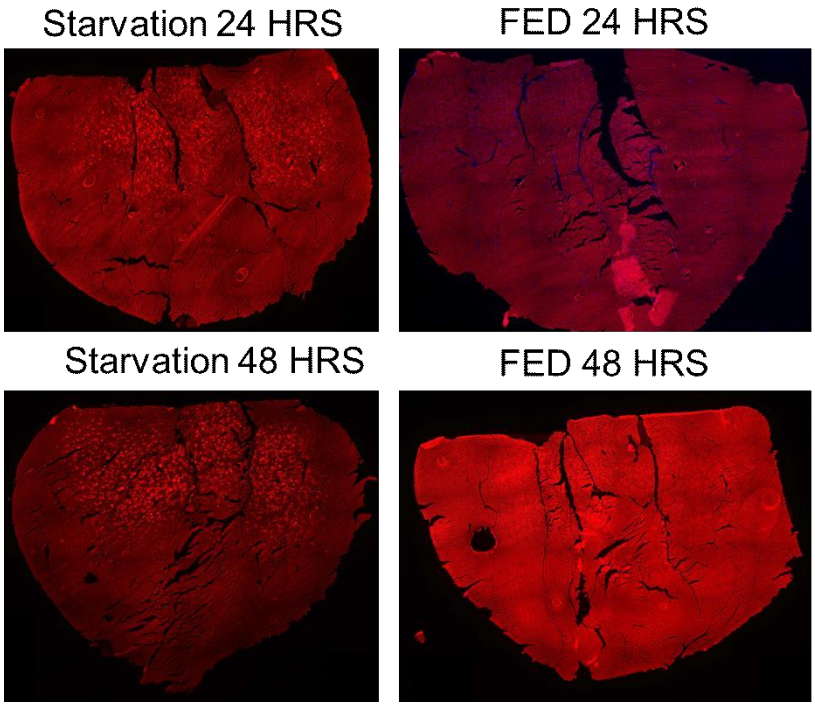

Figure 21: FUNCAT (red) of 24- and 48-hours starvation proved the labelling decreases differently across the muscle.

To answer whether protein labelling changes in a fibre type-specific manner, we combined FUNCAT with anti-myosin staining on serial cryosections **(Figure 22)**. The figure below shows that I (blue) and 2A fibres (green) are less influenced by nutrient deprivation than 2B (red) and 2X (black) fibres.

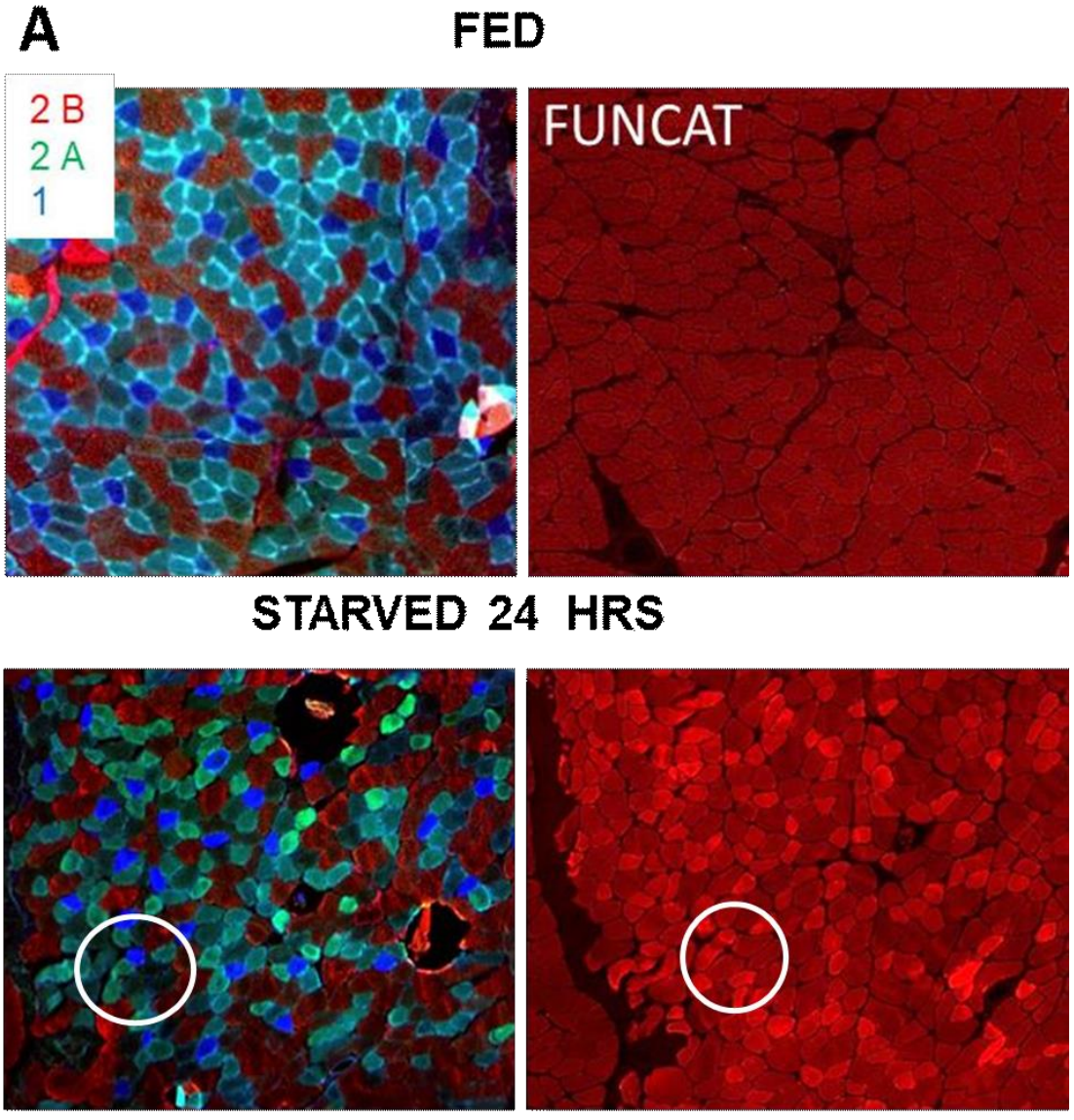

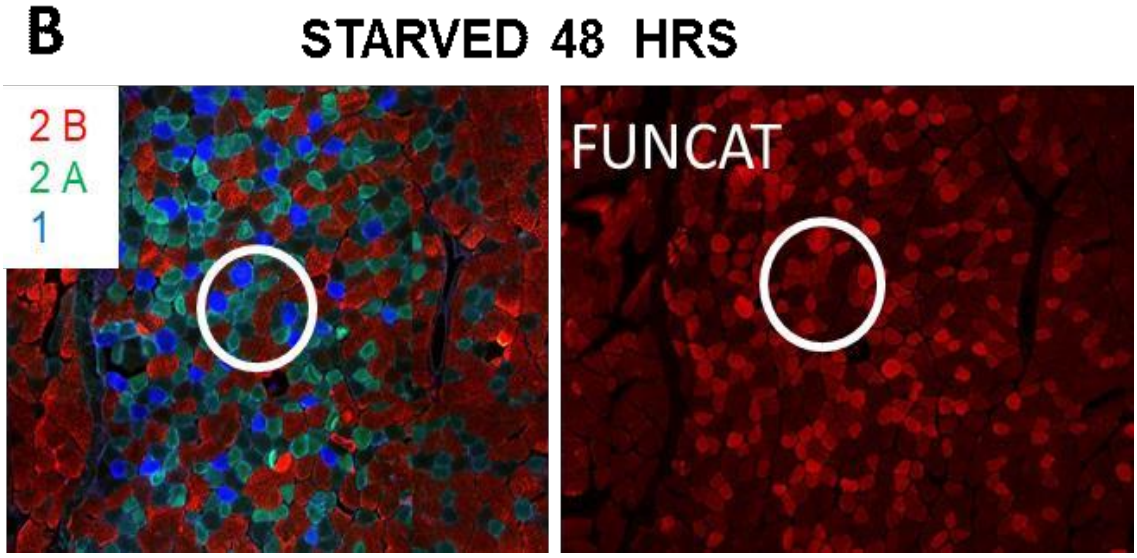

Figure 22: FUNCAT (in red) and anti-myosin staining (2A in green, 2B in red, 2X in black, 1 in blue) on serial cryosections correlate with a decreased fibre type-specific protein labelling A) 24 hrs labelling and B) 48 hrs labelling (red) and anti-MHC staining (2A green, 2B red, 1 blue)

4.11. Analysis of muscle proteome in catabolic conditions: chemical denervation

Muscle atrophy mirrors the skeletal muscle ability to change in response to external stimuli. Atrophying stimuli can be related to nutrient availability and electrical inputs coming from the peripheral nervous system. The particular type of atrophy caused by impairments in muscle contractility due to denervation is called neurogenic atrophy[52]. This situation alters the balance between protein synthesis and degradation, leading to loss of muscle mass and reduced quality of life[53]. During acute denervation, myofibers shrink and become angulate and acute denervation markers such as NCAM increase in the cytoplasm of muscle fibres.

These sets of experiments aim to reveal what happens to muscle proteins in response to chemical denervation induced by botulinum neurotoxin injections. The toxin cleaves the synaptosomal associated protein of 25 kDa (SNAP-25), preventing the fusion of acetylcholine synaptic vesicles with nerve terminals leading to reversible denervation and muscle atrophy[54]. Importantly, this treatment does not

lead to degeneration of motor neurons, leaving NMJ anatomically intact. When locally injected, BoNT is a very neurospecific, potent and reversible drug[55] that causes adaptive changes involving both axon terminals and innervated myofibers. Axon nerve sprouts[58] to reinnervate the muscle, and on the other hand, the muscle responds with fibre grouping and a fast to slow transition[56], **(Figure 23)**.

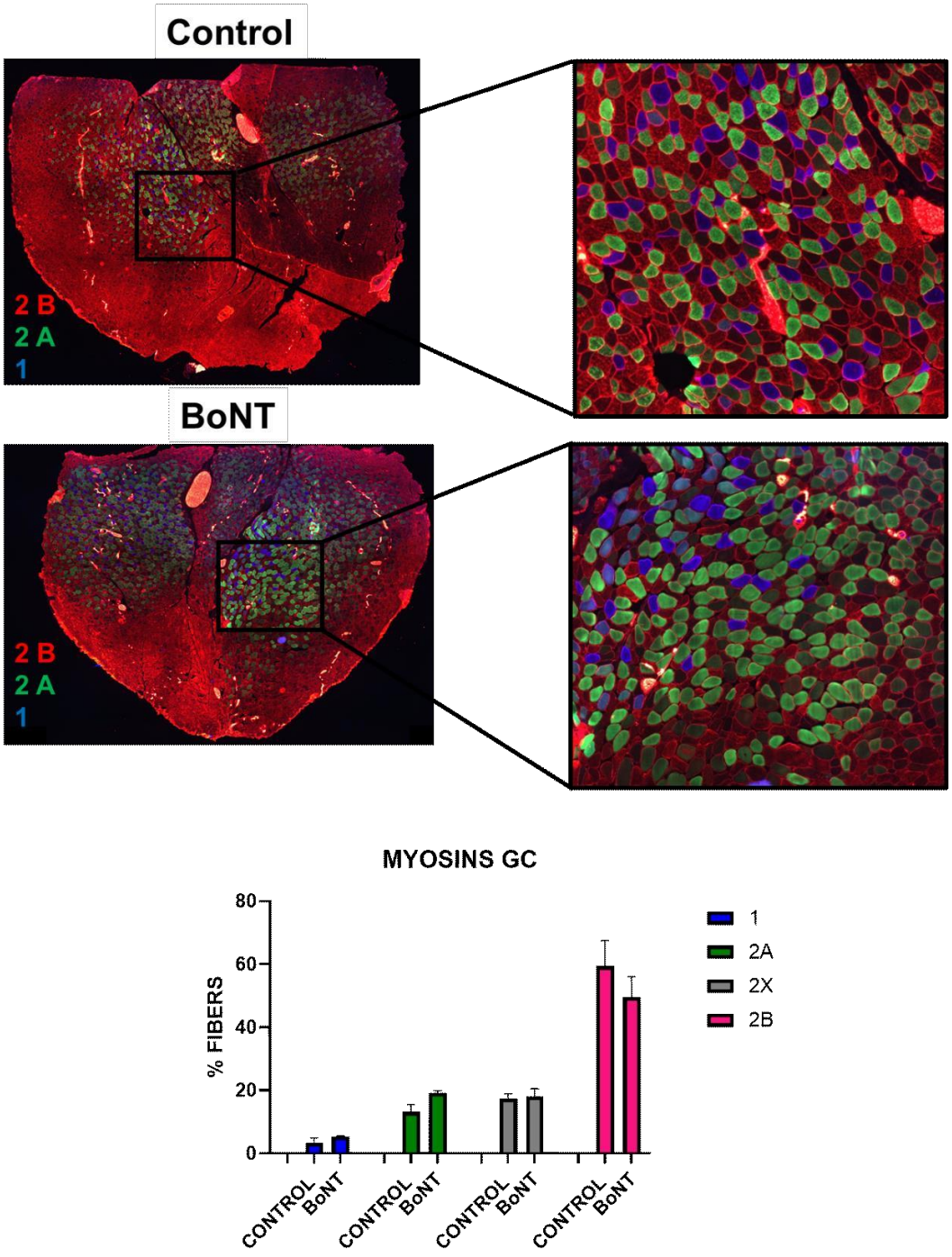

Figure 23: Fiber type transition from fast to slow in BoNT injected muscles. MHC staining show 2A (green), 2B (red), 2X (black), 1 (blue).

We treated animals with BoNT and promoted protein labelling at two different time points. Both groups of animals were injected intramuscularly with 0,2 pg/g of botulinum neurotoxin. The neurotoxin transported with high specificity into nerve terminals induces chemical denervation, and we observed the complete blockage of the injected leg after one day. The day after the injections, the first group of animals were labelled with ANL for one week. At the end of the treatment, we performed both BONCAT and FUNCAT on collected muscles. At this time point, we observed a robust decrease in protein labelling in BoNT muscles compared to control **(Figure 24)**.

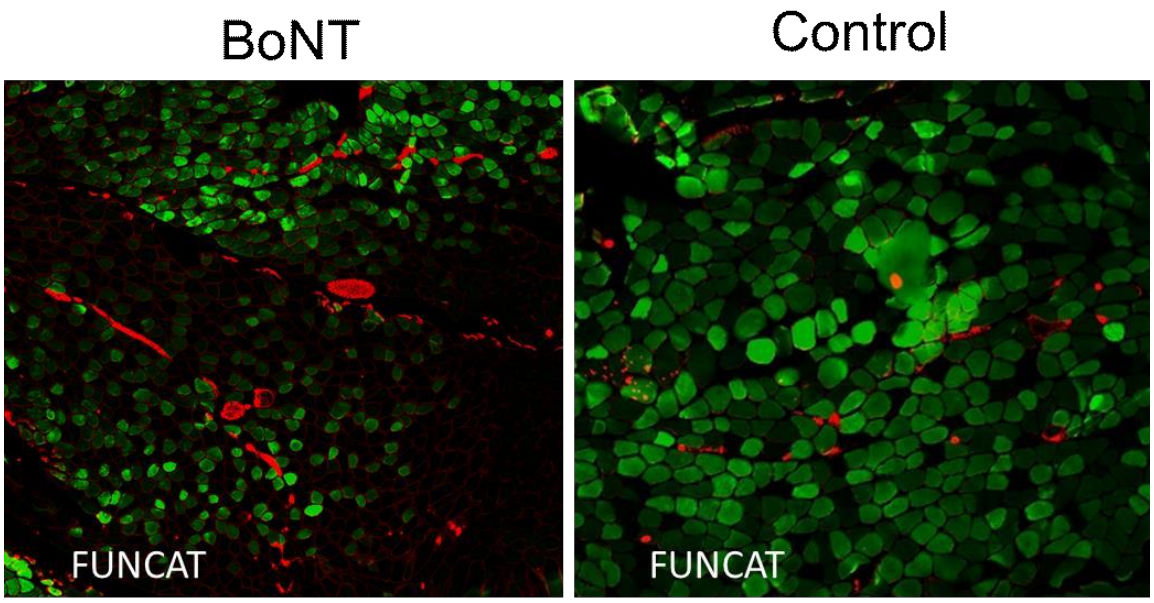

Figure 24: Protein labelling observed with FUNCAT (green) resulted significantly decrease in BoNT muscles. *n=4* animals used for the control group and *n=5* BoNT injected animals.

We used Neural Cell Adhesion Molecule (NCAM) staining on both Tibialis Anterior and Gastrocnemius muscles to answer whether unlabeled fibres were denervated. NCAM is a widely used marker of denervation. In wild-type animals, it is localized at the NMJ while, in denervated animals, it is inside the cytoplasm. We observed an increased proportion of cytoplasmic NCAM, confirming the current denervation. Moreover, the absence of P-S6 positive fibres, protein downstream mTORC1, indicates decreased levels of mTORC1- mediated protein synthesis **(Figure 25)**.

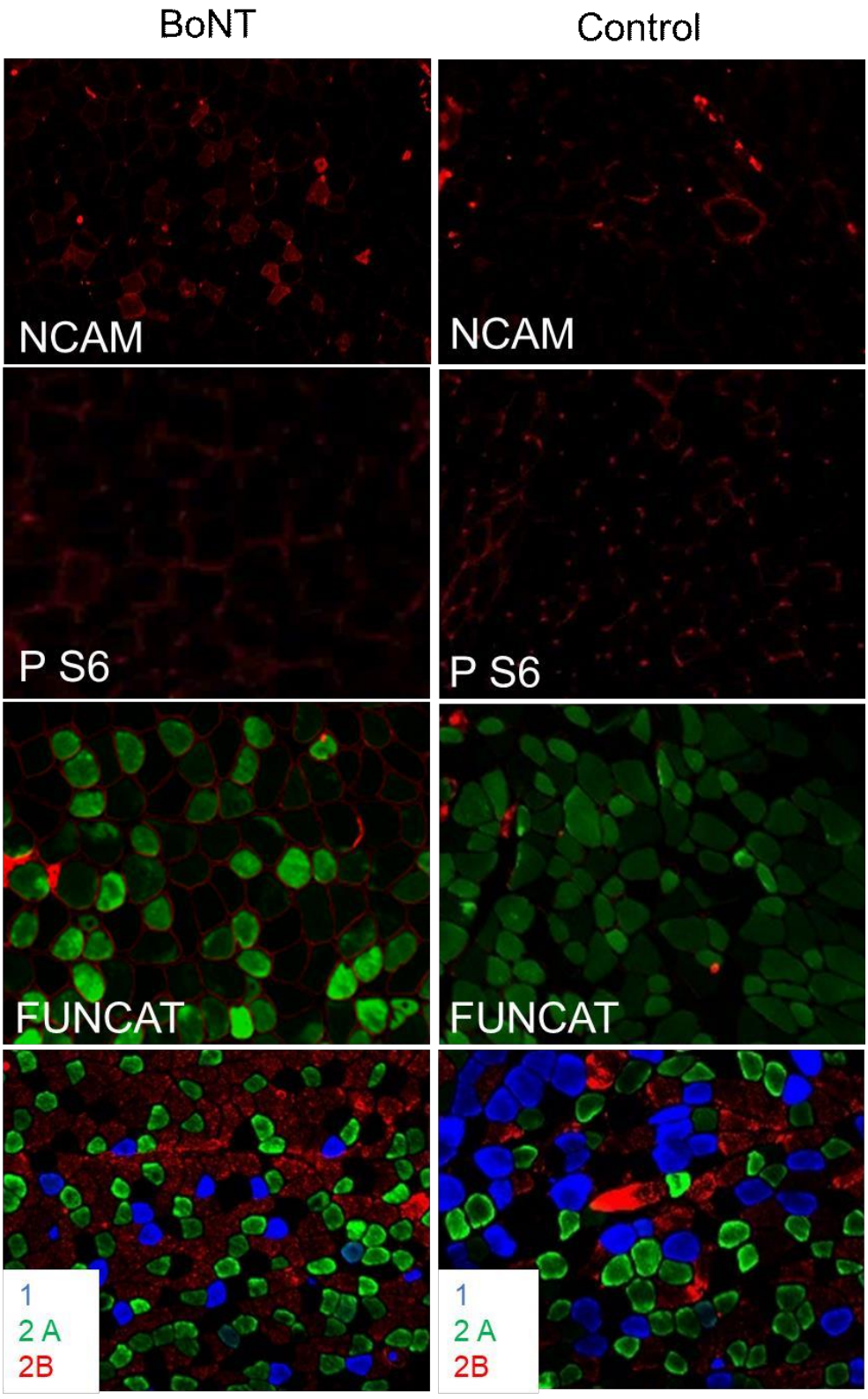

Figure 25: NCAM, PS6, FUNCAT and anti-myosin stainings performed on serial muscle cryosections confirmed the denervation and the absence of protein synthesis mTORC1-mediated.

Previous studies proved that sprouting onset occurs the third week after denervation. To see how muscles protein are regulated in this circumstance, we labelled MetRS animals starting at day 14 after chemodenervation until day 21. Three weeks-labelling of denervated animals was remarkably different from the previous experiment even though ANL was administered for the same amount of time **(Figure 26).**

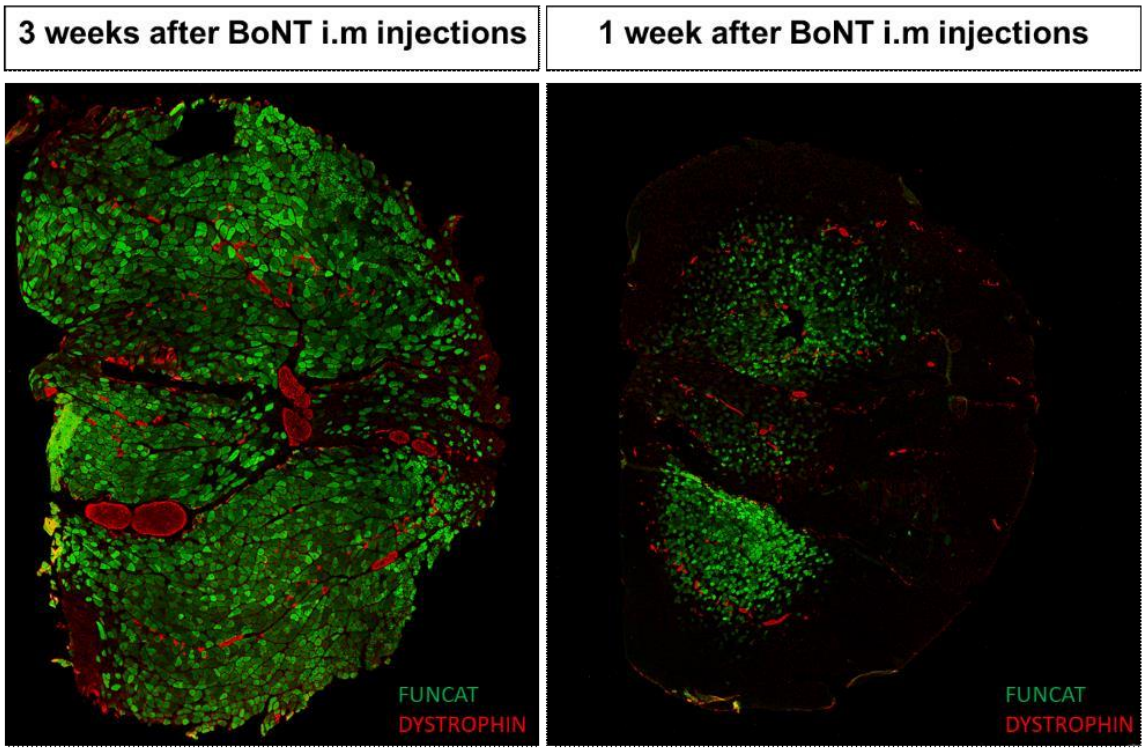

Figure 26: 1-week ANL labelling (in green) is entirely different between 1-week chemodenervated animals and three-weeks chemodenervated ones. n=3 mice for both control and chemodenervation conditions.

The fibre grouping was reduced, and the correlation between labelling and fibre type disappeared. Comparing myosin staining with FUNCAT to find a correlation between increased protein synthesis and fibre-type was challenging since fast-twitch fibres are also efficiently labelled. Moreover, the absence of NCAM-positive fibres indicated no occurring denervation. At the same time, P-S6 positive fibres showed an increased protein synthesis mTORC1-mediated. To confirm the last IHC result, we performed WB analysis on downstream effectors of mTORC1, and indeed, we identified increased phosphorylation of P-AKT, P-S6, P4E-BP1, suggesting mTORC1 pathway activation. **(Figure 27).**

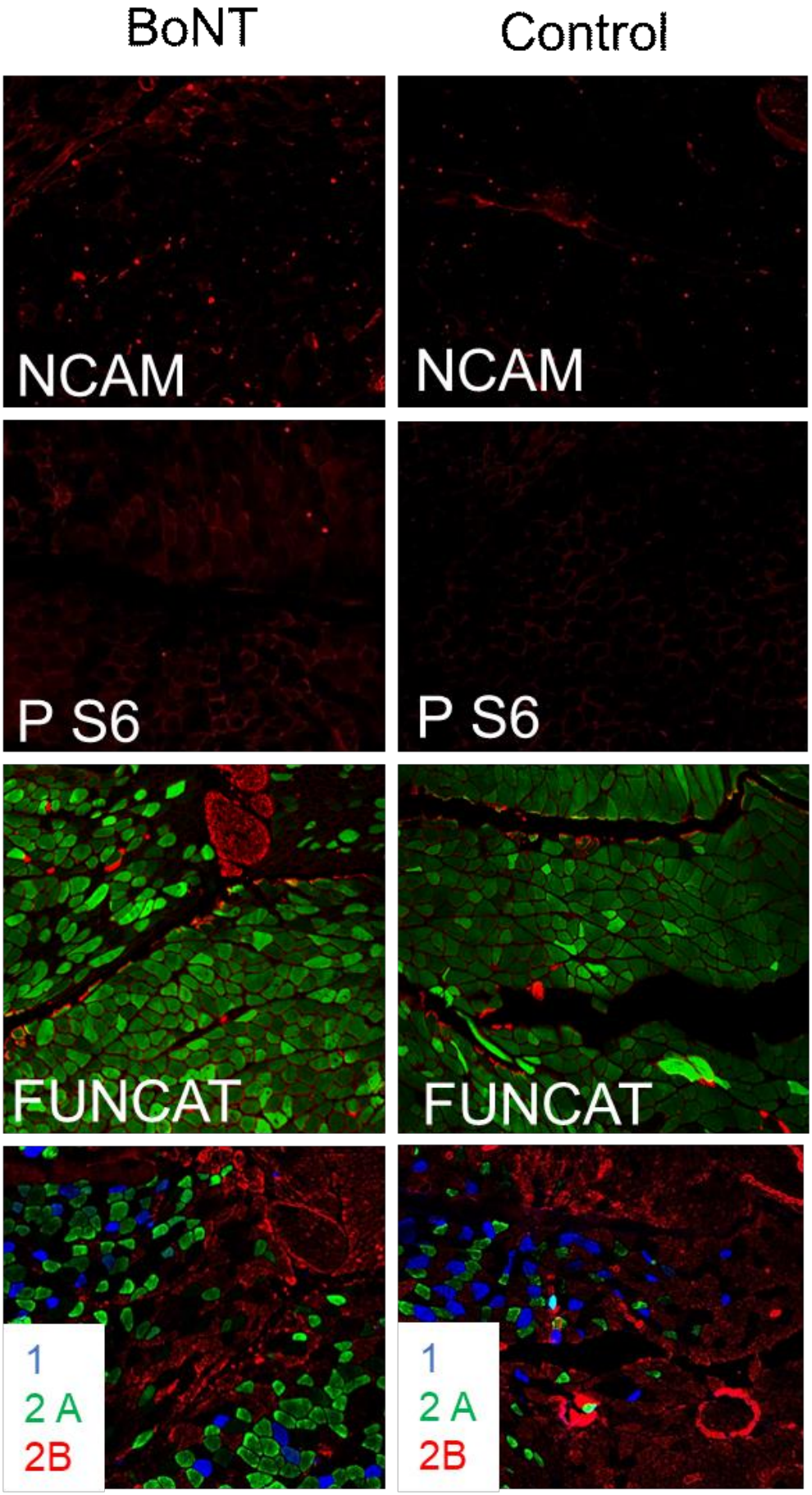
BoNT
Control
NCAM
NCAM
P S6
P S6
FUNCAT
FUNCAT
1
2 A
2B
1
2 A
2B

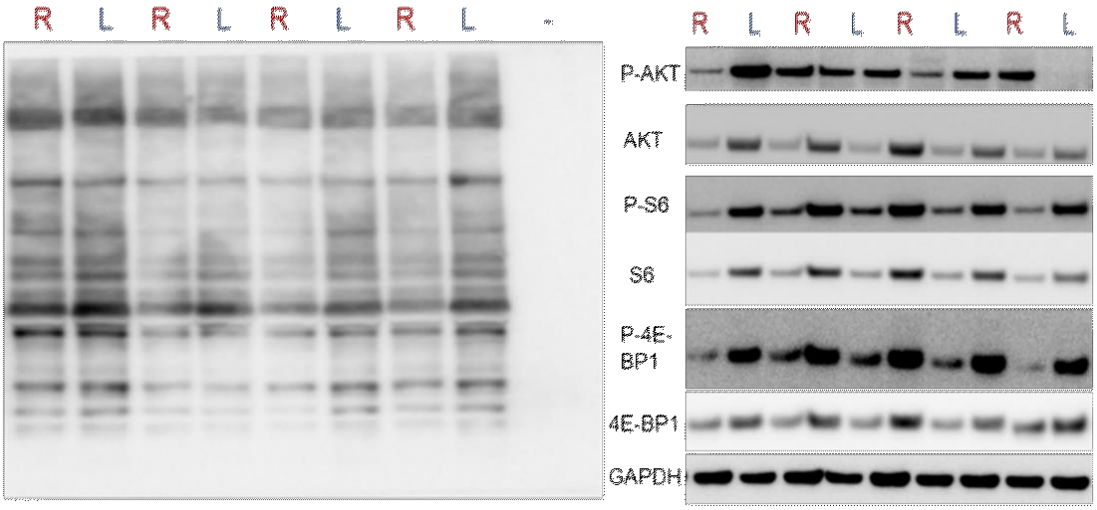

Figure 27: mTORC1 mediates proteins synthesis in reinnervated muscles confirmed with both IHC and WB. First panel: FUNCAT (green), myosins (2A in green, 2B in red, 2X in black, 1 in blue), P-S6 (in red), NCAM (red). In the second panel: Click-WB (left) and WB for Akt-mTORC1 pathway (right) R=control leg, L=BoNT leg.

Surprisingly fluorescence intensities quantifications revealed higher labelled proteins in BoNT fibres compared to control. These results suggest compensatory mechanisms that occur during denervation. Some fibres resist better to toxin-induced denervation and compensate the others with an increased protein synthesis rate **(Figure 28).**

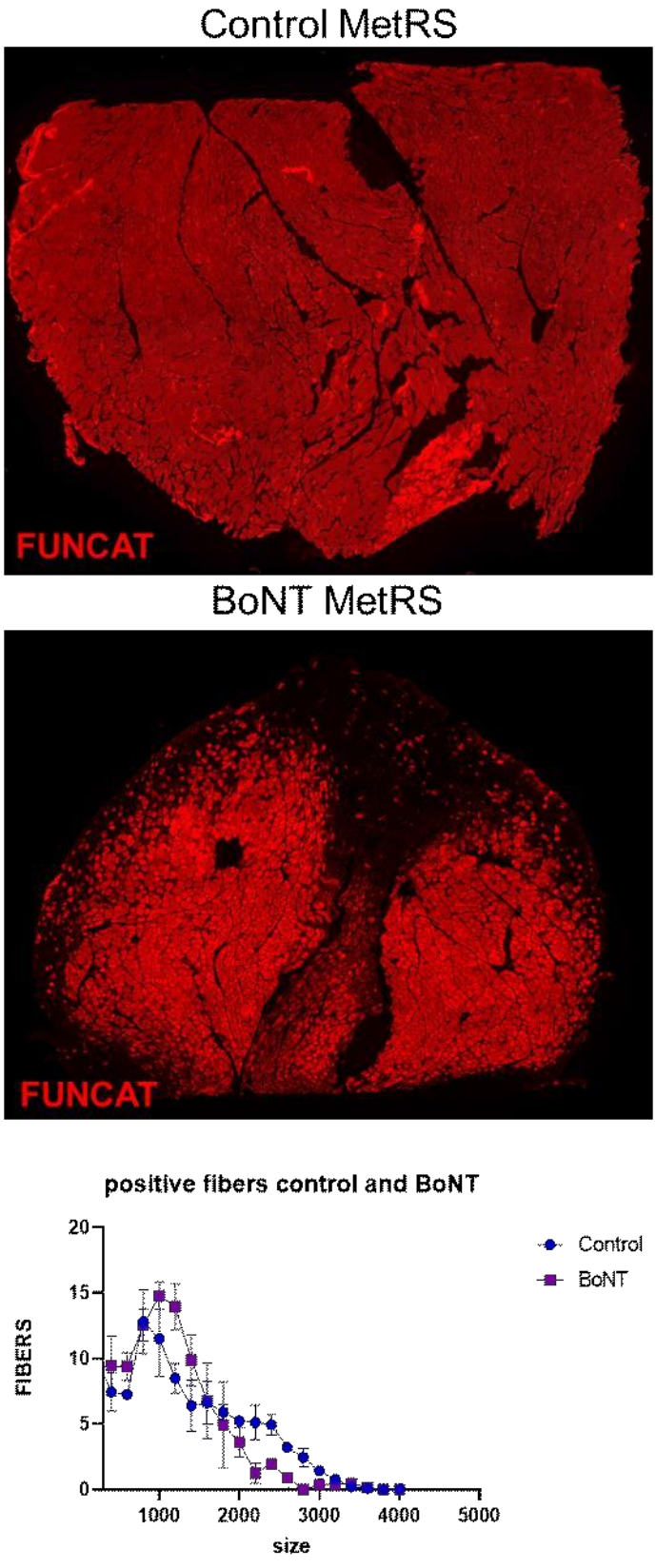

Figure 28: Fluorescence quantifications of FUNCAT (in red) reveal higher labelling of chemodenervated fibres.

4.12. Muscle-specific labelled proteins are present in sciatic nerves

Nerves show incredible plasticity and adapt to BoNT induced paralysis by increasing sprouting of new nerve terminals **(Figure 29)**[4,57]. Even if poorly understood, this ability seems to be mediated by both nerve and muscle proteins. The nerve-derived signal proteoglycan agrin and its interaction with MuSK (muscle-specific kinase) trigger postsynaptic differentiation and synaptic nuclei specialization[55]. Moreover, evidence from electric stimulation of chemo-denervated muscle suggests a strong implication of muscle-derived signalling factors in nerve sprouting, confirming muscle-nerve intercommunication and its importance in neuromuscular homeostasis[58].

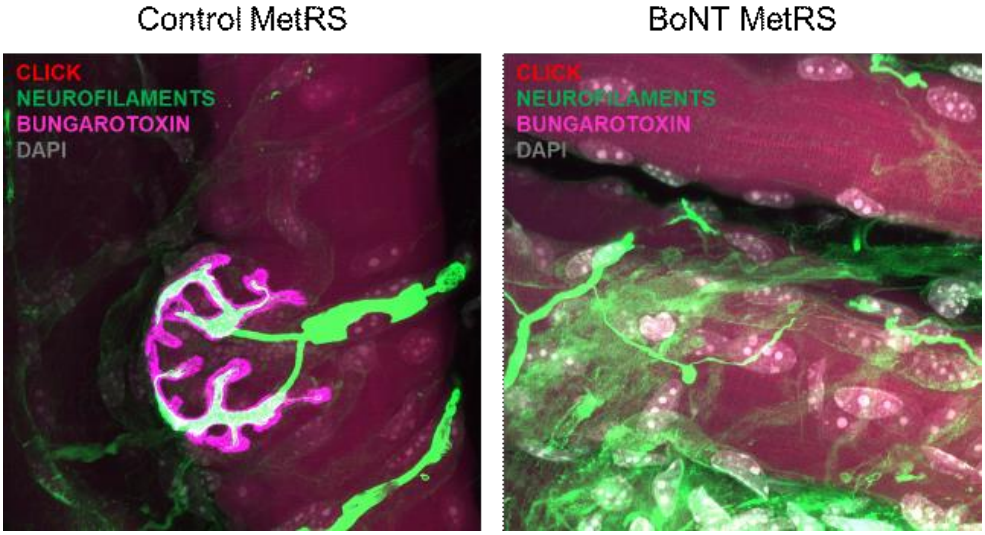

Figure 29: Sprouted nerves (in green) in Control MetRS animals and BoNT injected animals. FUNCAT (in red) shows efficient labelling in myofibers and at the NMJ level(magenta). Nuclei are stained with DAPI (in gray).

We labelled BoNT-injected animals with ANL for one week and collected animals muscles. Whole-mount preparations of soleus muscles were costained with α-bungarotoxin (a peptide extracted from *Bungarus multicinctus* venom that binds with high affinity to the α-subunit of the nicotinic acetylcholine receptor of neuromuscular junctions) and neurofilaments antibodies, proved increased sprouting in slow muscles[59].

The previous results proved that *in vivo* labelling of MetRS transgenic mice allows

for a sensitive visualization and localization of newly synthesized skeletal muscle proteins. For that reason, we wanted to test whether labelled proteins that originate within the muscle can also be found in sciatic nerves, thus demonstrating inter-tissues communication. This novel mouse model allows for such analysis because of its muscle specificity. Cre-Mlc1f promoter is indeed expressed exclusively in skeletal muscle fibres, so labelled proteins present in different tissues are synthesized within skeletal muscle and transported to other organs. We collected sciatic nerves of chemically denervated animals and performed western blot analysis and IF on these samples. The presence of ANL- incorporating peptides, revealed both with BONCAT and FUNCAT, indicates a potential role of skeletal muscle proteins in sciatic nerve tissue homeostasis.

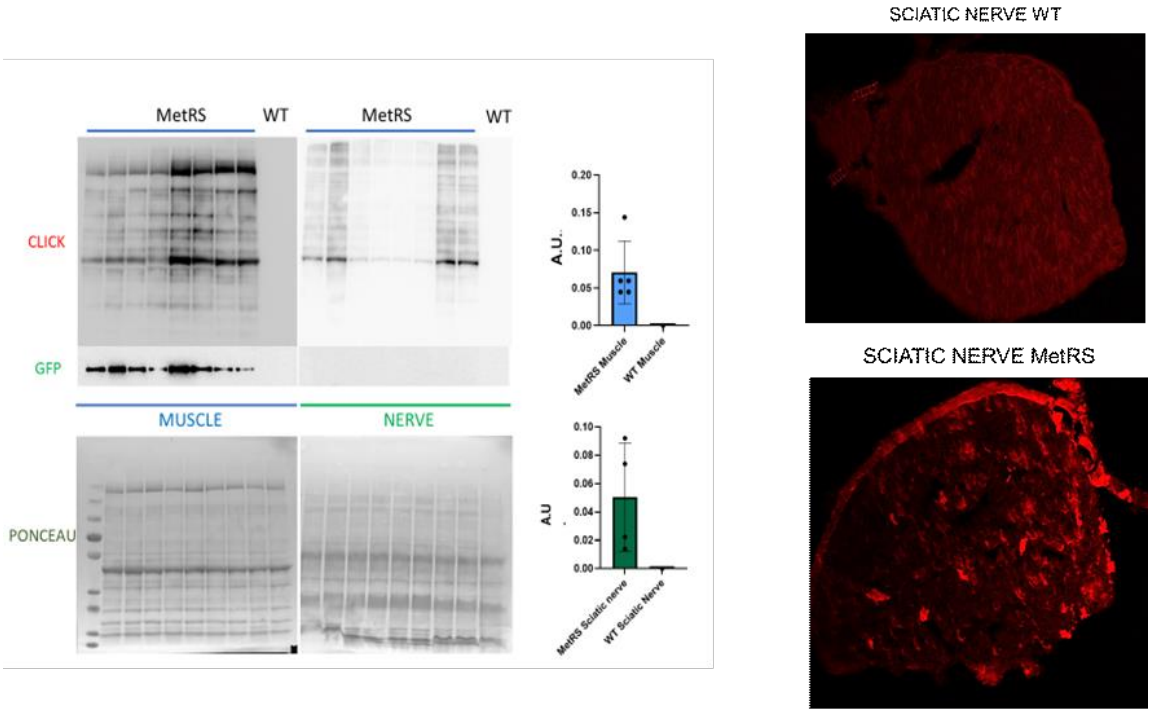

Figure 30: FUNCAT (right panel in red) and BONCAT (left panel)on MetRS muscle and nerves.

As expected, the amount of labelled proteins in nerves is far lower than in muscles. The absence of GFP in WB analysis confirms once more the correct MetRS expression only in skeletal muscle fibres **(Figure 30)**. The proteins identified in sciatic nerves are most likely muscle-synthesized proteins retrogradely transported into the nerve axons. Labelled proteins in nerves are significantly less from muscle, and GFP-WB shows no mutated MetRS expression **(Figure 31)**.

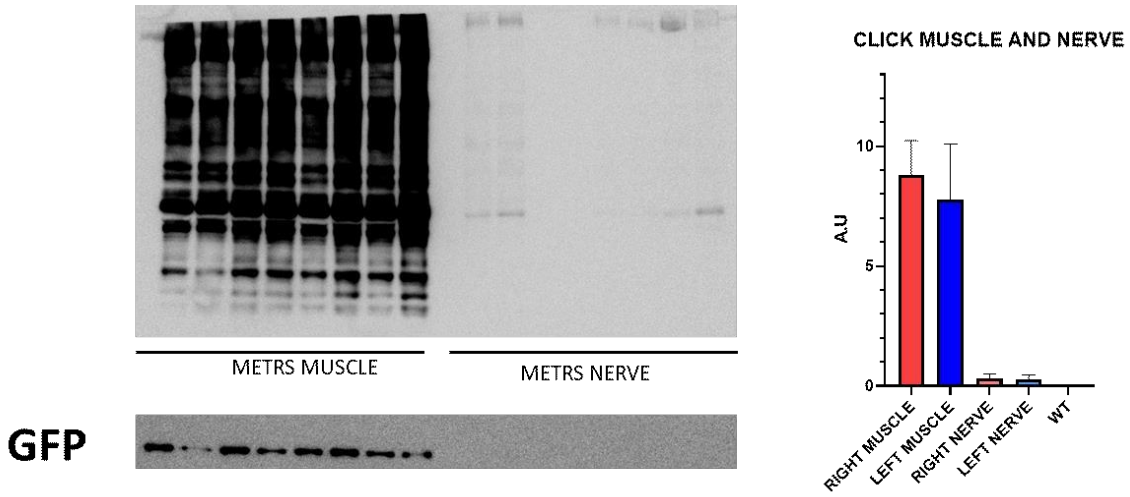

Figure 31: BONCAT of muscle (first five lanes) and nerves (last five lanes) prove muscle proteins' retrogradely transport into sciatic nerves. The absence of GFP indicates MetRS is not expressed in sciatic nerve. N=5 animals for each group.

The presence of muscle proteins influencing peripheral system development was abundantly studied. The improved survival of motoneurons in muscle-conditioned media suggested muscle-derived trophic factors in the nervous system homeostasis[58]. ANL labelling can potentially answer some of these questions and further study the muscle-nerve interaction.

4.13. Rapamycin, a mTORC1 inhibitor, decreases protein labelling

MTORC1 plays a crucial role in the regulation of adult muscle. In two different hypertrophy models, the overexpression of a constitutively active AKT and the stimulation of BMP (Bone Morphogenic Protein) pathway, the administration of rapamycin (a specific inhibitor of mTORC1) decreased protein synthesis[60]. To test whether ANL labelling decreases in response to mTORC1 inhibition, we administered rapamycin to MetRS animals. Animals were divided into two experimental groups, one treated with rapamycin and one with the vehicle as control. All animals were treated with rapamycin and ANL at the same time.

After three days of treatment, muscles were collected. Tibialis Anterior and Gastrocnemius muscles were used for WB analysis, while from FDB muscle, we obtained single fibres for FUNCAT analysis. Phosphorylation of S6, a mTORC1

downstream target, was decreased after rapamycin administration, suggesting that rapamycin treatment was effective and likely that mTORC1-mediated protein synthesis was reduced **(Figure 32)**.

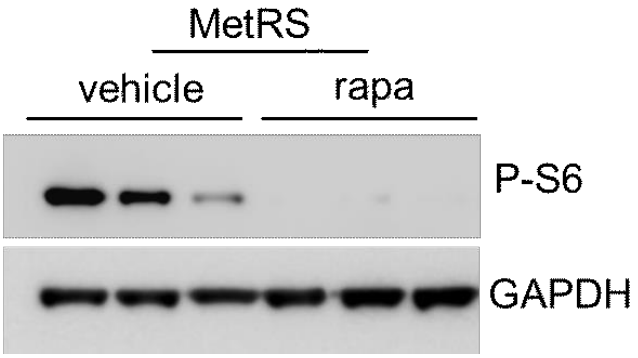

Figure 32: Rapamycin inhibits protein synthesis in a mTORC1 dependent manner. P-S6, a mTORC1 downstream target, decreased after the treatment.

Single fibres analysis of vehicle and rapa-treated animals were stained for FUNCAT and α-bungarotoxin that binds to acetylcholine receptors. The image below shows very interestingly, that three days-treatment of MetRS mice with rapamycin partially decreased the signal of labelled proteins at the NMJ level **(Figure 33)**.

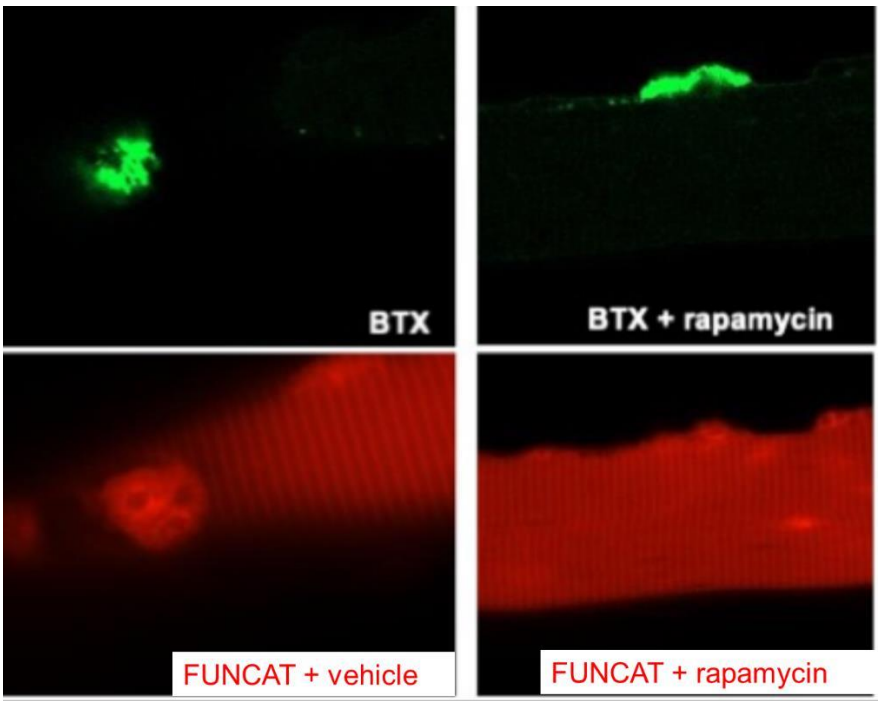

Figure 33: The amount of labelled proteins in the NMJ decreases when rapamycin is administered to animals. FUNCAT (in red) and α-bungarotoxin (in green). Left panel: FUNCAT in vehicle-treated animals. Right panel FUNCAT on rapamycin-treated animals.

4.14. Analysis of labelled proteins in HSA-Cre-MetRS Raptor ko mice

Rapamycin is known to be a partial inhibitor of mTORC1. Moreover, treatment of adult mice with rapamycin leads to a prolonged lifespan and improved mice performance. On the other hand, we have found that genetic inhibition of mTORC1 through deletion of Raptor, a scaffold protein of mTORC1, only in skeletal muscle does not affect muscle morphology and performance in the short period. However, a more extended deletion period results in muscle myopathy, with central nuclei, fibre damage and weakness. Unexpectedly, Raptor ko muscles display NMJ fragmentation and motor neuron endplate degeneration[61]. The fact that deletion of a gene in skeletal muscle has an effect at the pre-synaptic level prompted us to assume that either Raptor can have a crucial role in the synthesis of crucial proteins for NMJ integrity and motor neuron stability or muscle can secrete specific factors that can influence the motor terminal in a mTORC1-dependent manner. To understand the role of muscle mTORC1 in NMJ stability, we took advantage of the MetRS mouse. To determine if muscle proteome is altered in response to Raptor deletion, we have generated HSA-Cre-MetRS-Raptor ko mice by crossing inducible muscle-specific Raptor ko mice with MetRS animals. Mice were treated for three weeks with tamoxifen-containing chow, and one month from the beginning of the treatment, mice were sacrificed, and muscles were collected. We choose this experimental approach because we have previously observed that Raptor is absent at this timepoint, both at mRNA and at protein levels[61]. Western blot **(Figure 34)** showed that the amount of labelled proteins is similar in MetRS and MetRS-Raptor ko mice at a basal stage. Indeed, at this time point, we did not observe any histological and functional alteration.

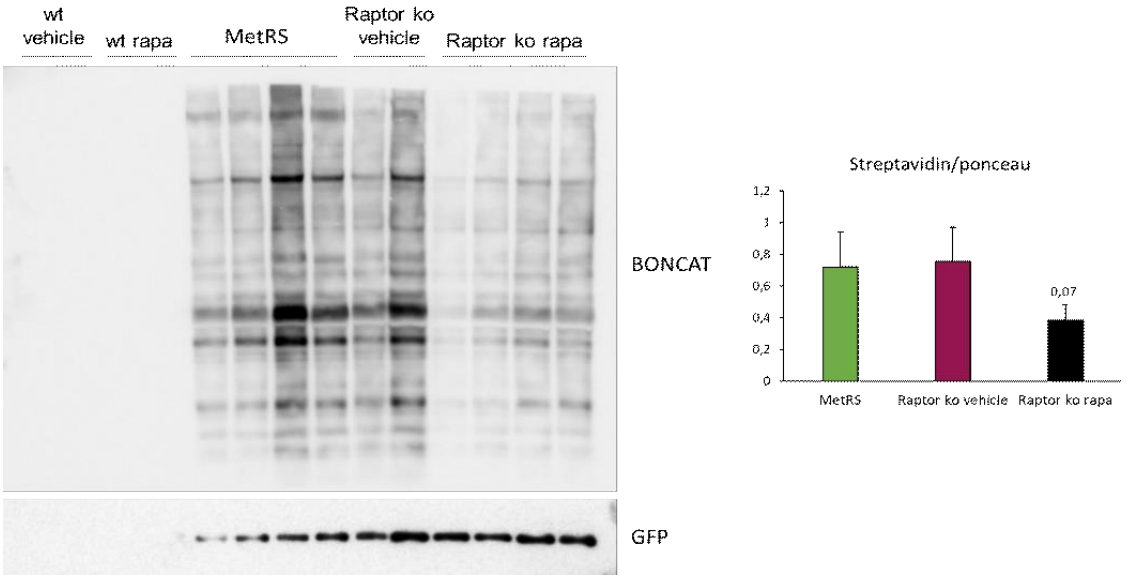

Figure 34: Rapamycin decreases protein labelling in RAPTOR KO animals

The absence of alteration is due to the little mTORC1 left that is still sufficient for maintaining proper muscle homeostasis. When we treated Raptor mice with rapamycin to stronger inhibit mTORC1, we started to observe the appearance of myopathic features, similarly to long-term ko animals where Raptor is further decreased compared to one-month treatment[63]. When we treated MetRS Raptor ko mice with rapamycin, the amount of labelled proteins was strongly reduced compared to vehicle-treated MetRS-Raptor ko. Moreover, in this case, the decrease of ANL-labelled proteins occurred in a fibre-type-dependent manner, with type 2B and 2X being the most affected **(Figure 35).**

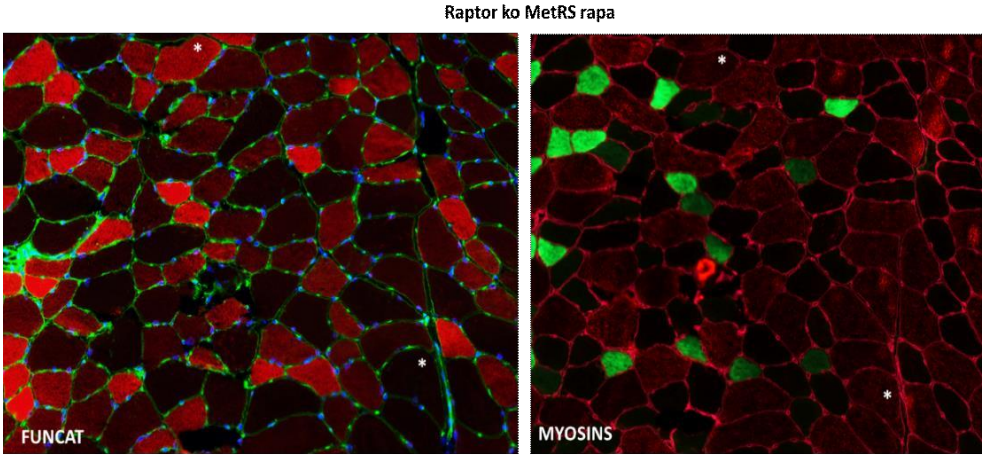

Figure 35: FUNCAT in the left panel (red) shows a fibre type-dependent labelling. 2A fibres (green) and 2X fibres (black).

4.15. Analysis of muscle proteome in pathological conditions: Duchenne muscular dystrophy

The sensibility of the technique allows many applications, especially on pathological conditions where the muscle is affected. We crossed Cre-MetRS mice with a MDX mouse model for Duchenne muscular dystrophy (DMD) to see how protein synthesis can change in pathological conditions. The mutation in *MDX* mice is a nonsense point mutation that prevents full-length dystrophin expression[62]. Dystrophin absence, as observed in Figure 36 causes distinct phases in the disease progression. In the first two weeks, no myopathic signs are observed. Between 3 and 6 weeks, muscle fibres undergo necrosis and regeneration, and some of them become hypertrophic. *MDX* muscles are highly heterogeneous with necrotic fibres, revertant central nucleated fibres and fibrotic infiltrating tissue. Histological analyses of *MDX* mice show muscle fibres variability in response to dystrophin absence **(Figure 37).**

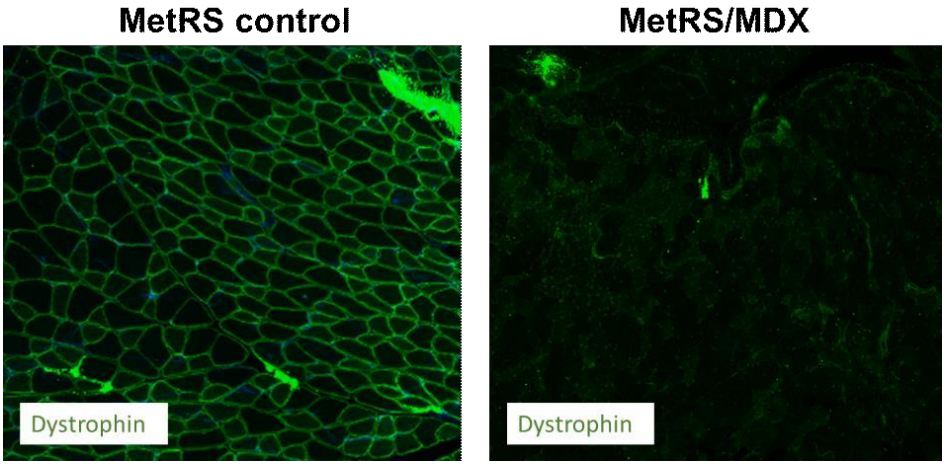

Figure 36: Dystrophin (green) of MetRS animals (left panel) and MetRS/MDX muscles (right panel).

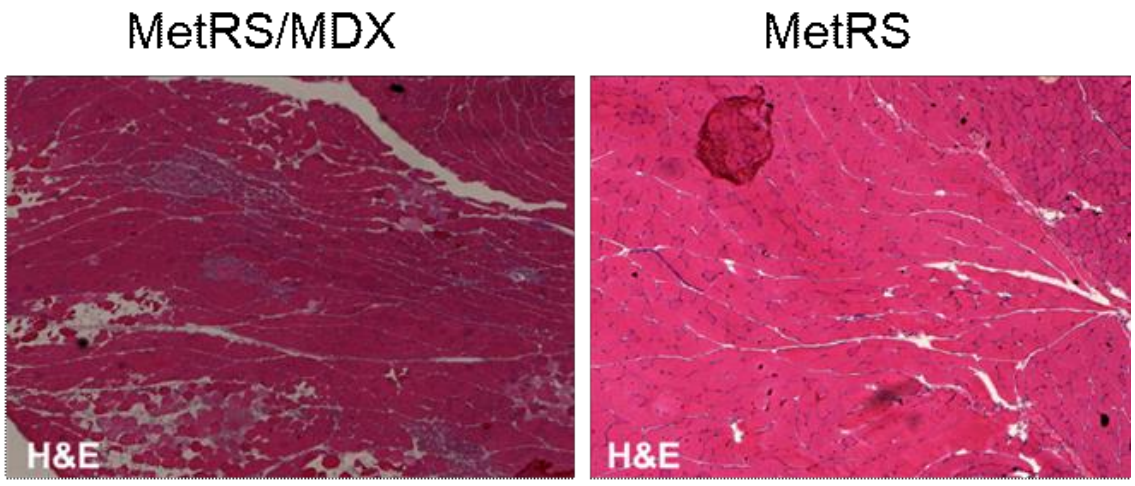

Figure 37: H&E staining of MetRS (right panel) and MetRS/MDX (left panel) muscles.

To monitor how fibres labelling changed in DMD, we administered 30mM ANL to six-months-old MetRS/MDX animals for one week. After muscle collection, we performed FUNCAT and visualized in detail protein labelling **(Figure 38).** The figure below shows MetRS healthy fibres presenting homogenous labelling. On the other hand, MetRS/MDX muscles presented larger hypertrophic fibres with higher fluorescence intensity and black regions identified as fibrotic tissue deposition.

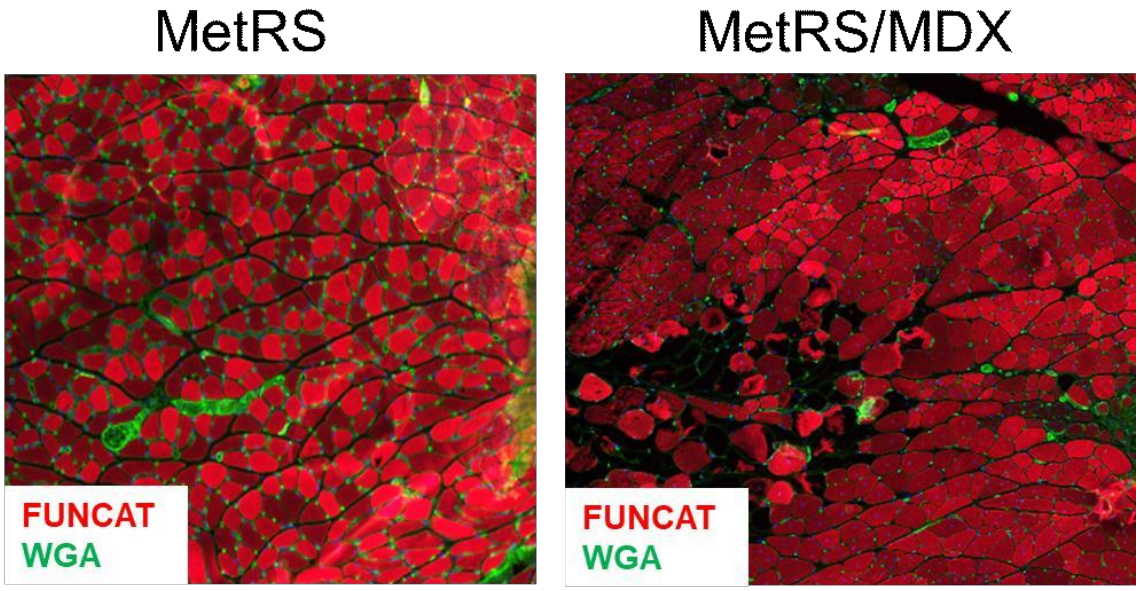

Figure 38: FUNCAT (red) on MetRS (left panel) and MetRS/MDX (right panel).

Revertant fibres can be observed in MDX mice in response to muscle precursor cells proliferation. To control the correlation between regenerating fibres and

protein labelling, we combined FUNCAT with BF-G6. BF-G6 antibody recognizes embryonic myosin, and it can be used as a marker of regeneration[62]. The constant fibre damage results in skeletal muscle regeneration and, thus, in the appearance of G6-positive fibres. Unexpectedly, in our case, revertant fibres presented a decreased protein labelling. Mlc1f promoter is expressed in early stages of mice embryonic life; however, there is the possibility that revertant fibres may not have yet a proper MetRS expression. In addition, it has been reported that DMD fibres may have an increased protein turnover[63] lowering the amount of incorporated ANL. **(Figure 39)**.

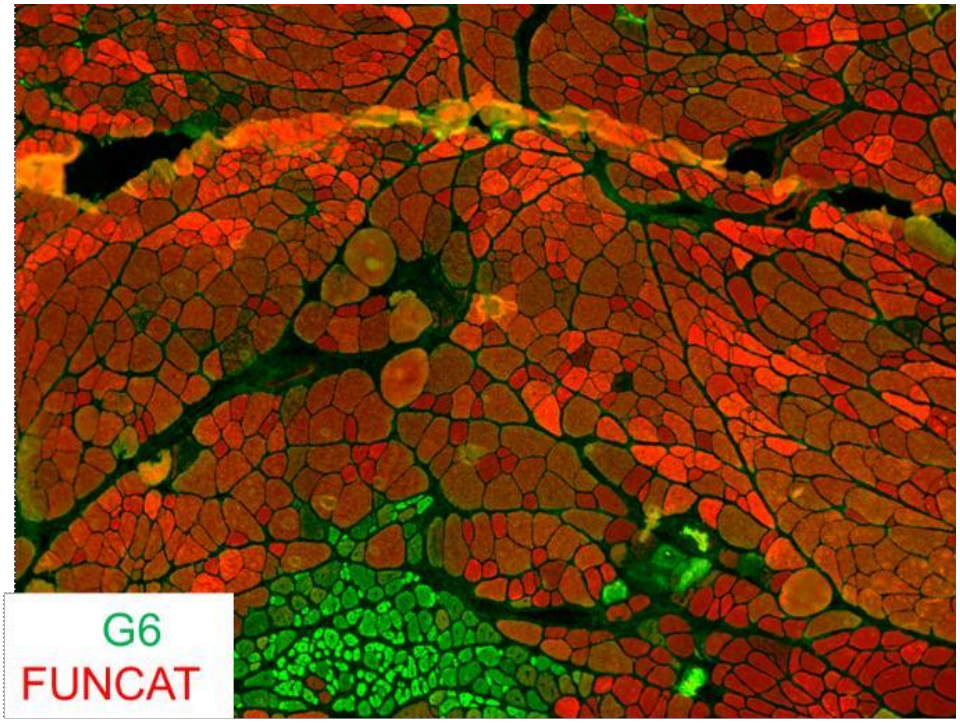

Figure 39: FUNCAT (red) indicating protein labelling. G6 for embryonic myosin (green).

4.16. Analysis of muscle proteome in pathological conditions: cancer cachexia

Cancer cachexia is a multi-organ syndrome that is characterized by a substantial loss in body weight. It occurs in 50-80% of cancer patients due to drastic muscle and adipose tissue loss. As cancer cachexia leads to a decrease in physical performance and quality of life and is associated with poor survival (accounting for more than 20% of cancer deaths), it is of major clinical relevance. Furthermore,

cachectic patients show lower response rates to chemotherapy and reduced tolerance to anticancer treatment[64].

Mlc1f-MetRS mouse line was back-crossed into a Balb/C background to generate a model to use C26 colon carcinoma cells to induce cachexia. Two-month-old mice were injected subcutaneously with 5*10^5 C26 colon carcinoma cells[65]. Control and C26 tumour-bearing animals were given ANL in the drinking water when they started losing body weight (day 11) and were sacrificed when they lost 20% of their initial body weight. Importantly, C26-injected MetRS mice lose body weight at the same rate as tumour-bearing wild-type animals while administering ANL. **(Figure 40)**.

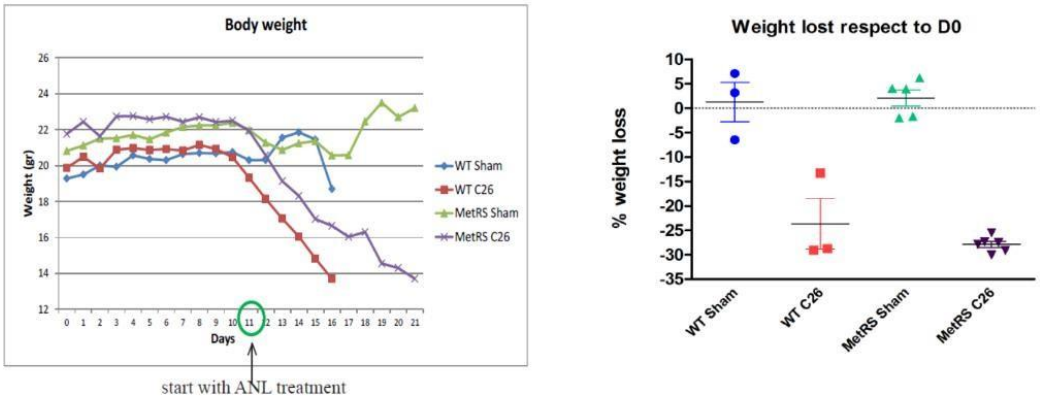

Figure 40: Weight loss in cachectic animals

Preliminary western blot analyses showed labelled proteins in skeletal muscle during the cachectic phase are significantly less than in sham control animals **(Figure 41).**

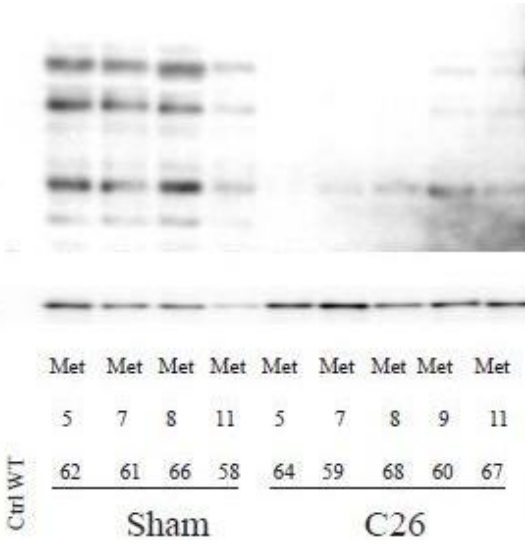

Figure 41: Representative BONCAT of cachectic animals.

Interestingly, through click-immunohistochemistry, we found that the decrease in the amount of labelled proteins during cachexia occurred only in specific myofibers, suggesting that cancer cachexia leads to a decrease in protein synthesis rate in a fibre type-dependent manner **(Figure 42).**

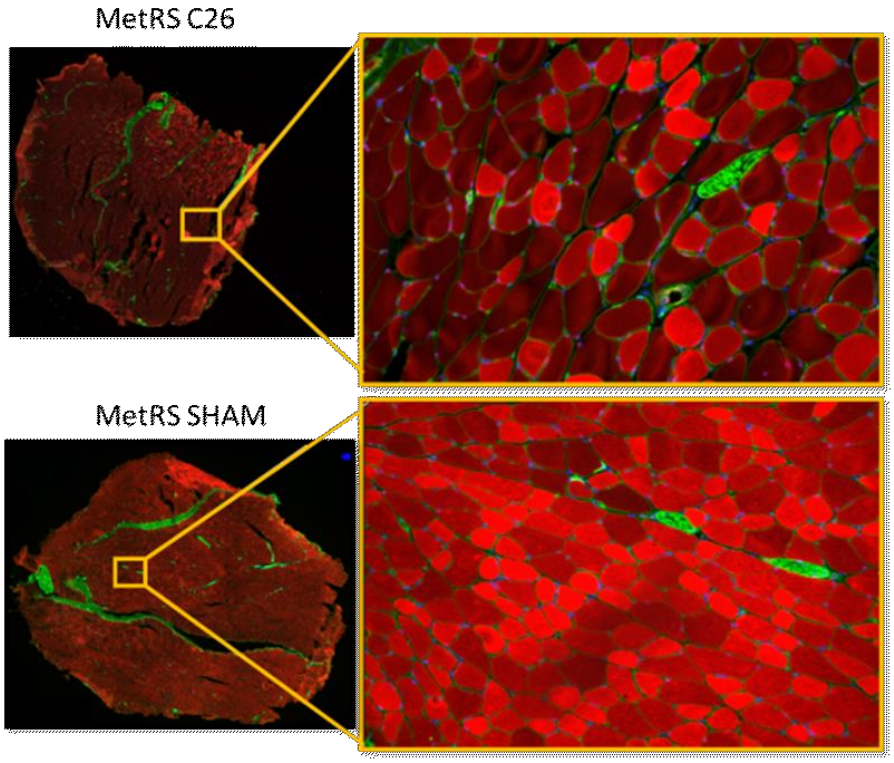

Figure 42: FUNCAT (red) in cachectic mice (upper panel) proved a fibre type-dependent reduction in protein labelling compared to sham (lower panel).

5. DISCUSSION

Anabolic and catabolic stimuli finely regulate muscle mass which largely contributes to whole-body homeostasis. Effective tools to monitor protein synthesis in skeletal muscle are necessary to answer questions regarding protein homeostasis in physiological and pathological conditions. For this purpose, we successfully generated a muscle-specific mutated MetRS that allowed ANL incorporation into nascent polypeptides instead of methionine. Muscle-specific labelled proteins were identified using BONCAT and visualized with FUNCAT. Unlike SUnSET and SILAC techniques that exploit the natural translational apparatus of the cell[66],[67] , this new tool requires a mutated aminoacyl-tRNA synthetase. Mutated methionyl-tRNA synthetase activates specifically ANL that is incorporated into proteins instead of methionine. Complete proteins weigh more than biological peptides; however, they are correctly folded and functional.

BONCAT allows us to identify newly-synthesized polypeptides, which are full-length differently from truncated proteins obtained from ribosome blockage (Puromycin)[68]. First experiments were meant to determine the amount of labelled proteins detected specifically in skeletal muscle tissue. Keeping in mind that the competition between the mutated and natural methionyl-tRNA makes methionine incorporation four times faster than azidonorleucine[34], we analyzed labelled proteins when ANL was administered either through intraperitoneal injections or supplied in drinking water. Using single pulses of ANL, we observed that the uncanonical amino acid is incorporated in a concentration-dependent manner with a robust detection 24 hours after the first ANL injection. Unlikely SUnSET that allows the identification of proteins synthesized in 30 minutes, ANL labelling is more suitable for extended labelling. A steady-state between the azidonorleucine and methionine pool can be achieved with more prolonged ANL administration, allowing a partial substitution of methionine residues by azidonorleucine[69] into newly synthesized proteins. A complete substitution would only be possible removing methionine from the animal's diet; however, this results in a non-physiological condition[70],[71].

Methionine is an essential amino acid involved in many biological pathways. Besides its importance in protein translation, it is the precursor for Cysteine and GSH biosynthesis. Methionine-deficient diet induces, indeed, steatohepatitis and

oxidative stress damage[71]. Moreover, it participates in the biosynthesis of S-adenosyl-methionine (SAM), creatine and phosphatidylcholine metabolism that again play an essential role in nonalcoholic steatohepatitis (NASH) and non-alcoholic liver cirrhosis[71]. Moreover, wild-type tissues cannot incorporate ANL, and reduced protein synthesis in response to methionine absence occurs.

Another point to consider is the difference between mitochondrial and cellular methionyl-tRNA synthetase. Mammalian mitochondrial DNA encodes for 22 tRNAs conjugated to their specific amino acids by mitochondrial tRNA synthetases. Since ANL cannot be charged on the mitochondrial tRNA synthetase, the lack of methionine is responsible for decreased mitochondrial protein synthesis. Mitochondria protein synthesis impairment is correlated with translational defects in complexes I, III, IV, ATP synthase and complex V. It leads to decreased oxygen consumption, reduced galactose oxidation and enhanced lactate production[72]. MELAS syndrome, in particular, is associated with protein synthesis and mitochondria chain respiratory defects. It is a mitochondrial myopathy characterized by lactic acidosis, muscle weakness and mobility impairments[73]. When methionine is removed from mice diet, both systemic and muscle-specific toxicity occurs. We concluded that the best way to analyze muscle proteome through uncanonical amino acids administration is to increase ANL concentration and labelling time with an oral administration route. From the bioavailability point of view, ANL incorporation is similar to SILAC labelling. The uncanonical amino acid enters the cell using LAT1 transporters[74], and it does not react with intracellular metabolites. Since it is, however, bulkier than the methionine thioether group, it could interfere with protein turnover. Previous studies showed that incorporating uncanonical amino acids such as AHA and HPG does not interfere with the proper folding, localization, and functionality of the proteins[75]. We confirmed those results, administering to animals, up to three weeks, ANL supplied in drinking water. We analyzed treated animals' muscle histology and force production and observed no interference with the protein functionality.

Our group has already demonstrated that EDL overload and AKT activation increase protein synthesis (puromycin) and RNA content[76]. In particular, the constitutive expression of AKT transgenic animals induces muscle hypertrophy and improved force production[45] suggesting that increased muscle mass and strength correspond to functional hypertrophy. We crossed MetRS transgenic animals with AKT mice to monitor protein synthesis in hypertrophic animals. Unexpectedly, the comparison between MetRS and MetRS-AKT animals showed, both with FUNCAT and BONCAT techniques, no significant increase in total labelled proteins. However, when myofibrillar proteins content was analyzed, a higher amount of labelled myosin heavy chain isoforms was observed. Previous studies based on oxide deuterium administration[77] suggested that the increased cross-sectional area of fibres may be due to increased myofibrillar proteins. There are, however, gaps in the literature on whether hypertrophy-induced myofibril protein accretion occurs via enlargement of preexisting myofibrils or through myofibrillogenesis[78]. The results we obtained so far cannot answer this question because both mechanisms can determine the increased myofibrillar labelling we observed. Further proteomic analysis combined with proximity ligation assays may help us understand better what happens during AKT-induced hypertrophy.

The AKT hypertrophy model induces protein synthesis in a mTORC1- dependent manner. P-S6 phosphorylation results in increased ribosome biogenesis and protein synthesis[79]. Different stimuli, however, promote protein synthesis via mTORC1-independent pathways. Goodman et al. demonstrated that mechanical overload models are characterized by an increased YAP nuclear localization that increases the expression of c-Myc, a potent activator of ribosome biogenesis[80] and protein synthesis. Independent studies showed an interaction between YAP protein and TEAD transcription factors in the regulation of skeletal muscle mass[81]. We induced EDL mechanical overload in MetRS animals and analyzed labelled proteins. Unexpectedly, the analysis of overload EDL showed an increased protein labelling at the myotendinous junction. Moreover, it was accompanied by YAP-nuclear localization, confirming a correlation between increased protein synthesis at the MTJ and YAP/TAZ mechanotransduction-induced pathway and, thus, suggesting increased mechanical signalling at the MTJ.

Muscle atrophy changes the balance between muscle protein synthesis and

degradation, causing a net loss of organelles and cytoplasm[9]. The use of radioactive isotopes showed that starvation-induced atrophy results in an overall loss of muscle proteins[9]. On the other hand, puromycin labelling proved that protein loss occurs at higher rates in fast fibres compared to slow ones. In our experiments, one-day fasted animals had a reduction in protein labelling of 50%. 48-hours-fasted animals had a further reduction of about 25%. FUNCAT analysis of skeletal muscle cryosections proved with high resolution slow skeletal muscle fibres ability to resist to starvation. We observed that labelling reduction mainly occurs in fast 2B fibres, while the more oxidative 2A fibres maintain the same fluorescence intensity as the control ones. The important loss in fast skeletal muscle fast fibres can be explained by analyzing the functionality and contractile activity of these fibres. Nutrient deprivation occurs primarily in less frequently used fibres than in slow fibres responsible for a prolonged duration of contraction[82,83].

Fractional protein synthesis rates, measured using radioactive amino acidic tracers, reported a net loss of skeletal muscle amino acids during starvation. According to our reduced labelling, protein synthesis decreased more in EDL than in the slow soleus muscle. Moreover, EDL muscle presented a higher expression of MuRF1 and atrogin-1, suggesting a higher protein degradation [84]. Under the control of FOXO3a, the two ubiquitin ligases induce muscle catabolism and amino acid production via UPS. PGC-1a (peroxisome proliferator-activated receptor γ (PPARγ) coactivator 1), a mitochondrial and oxidative metabolism regulator, protects muscle against fasting-induced atrophy[83]. Higher levels of PGC1a are correlated with genes involved in protein synthesis, such as E1Fa2 and ribosomal proteins. In addition to a decreased protein synthesis, 2B fibres had lower levels of PGC1a, making them more sensitive to starvation-induced atrophy. Our results make it difficult to understand whether reduced protein labelling is correlated with increased protein degradation or reduced protein synthesis. Decreases in RNA content of starved animals suggest that the two events occur simultaneously[85].

The further proteomic analysis will be required to understand better the fibre-type resistance to starvation. However, our results were also confirmed in another model of nutrient deprivation which is cancer cachexia. Cancer cachexia is characterized by anorexia, with a drastic loss of muscle and adipose tissue. To study the cachectic muscle proteome, we back-crossed Mlc1f CRE-MetRS animals into a Balb/C background and analysed muscle proteins changing in response to

cancer cachexia. We found that protein labelling is reduced in tumour-bearing mice, with the fast type 2B and 2X fibres being the most affected. Most importantly, the cell-type specificity of the labelling will be used to identify cachexia biomarkers implicated in muscle wasting[86]. Moreover, using this novel tool to monitor protein synthesis, we will understand how muscle wasting occurs in response to tumour growth.

The second atrophic stimuli we monitored was the chemical denervation using botulinum neurotoxin injection. BoNT drugs are potent and neurospecific toxins that cleave SNAP-25 protein, preventing acetylcholine vesicles fusion with the presynaptic membrane and neurotransmitter release. Besides its potency, the drug induces a reversible muscle contractility impairment[87]. After three weeks, indeed, the concomitant nerves sprouting and *de novo* SNAP-25 synthesis results in muscle reinnervation[88]. The two experiments we performed proved skeletal muscle plasticity in dependence upon muscle innervation. One week after BoNT injection, there was a significant decrease in protein labelling. Immunofluorescence analysis of NCAM and P-S6 proved denervation influences protein synthesis in a mTORC1-dependent manner. Literature studies based on low rRNA content and the upregulation of E3-ligases MuRF1 and MAFbx[89] suggest a shift in the protein synthesis/protein degradation balance toward protein degradation. After three weeks, however, axonal terminal sprouting reverts this situation. Markers of denervation disappear, and mTORC1 activation leads to increased muscle growth and, thus, to increased protein labelling. Surprisingly, we observed a fast-to-slow MHC composition shift not directly correlated to protein labelling. These results suggest that even though the sprouting occurs mainly in slow muscles[89], this adaptive event is not directly linked to a specific fibre type. The neuronal growth is most likely governed by the synthesis of pre-and post-synaptic proteins that influence the homeostasis of the synaptic structure. The improved survival of motoneurons in muscle-conditioned media suggests implications of muscle-derived trophic factors in the nervous system homeostasis[90]. Proteins implicated in axon regeneration such as BDNF, NT3, NT4 produced in response to treadmill training alleviate the symptoms of spinal cord injury[91]. Following these findings, we analyzed sciatic nerves of MetRS labelled animals after BoNT injection. The presence of labelled muscle proteins in this tissue confirmed the retrogradely

transport from muscle to nerve in response to chemical denervation.

During embryonic muscle development, motoneurons and muscle cells develop independently; however, their communication is fundamental in NMJ formation. Exosomes are endocytic small-membrane vesicles very important in intercellular communication[92]. Today proofs that exosomes mediate synaptic development are lacking; however, they seem to be involved in the transport of synaptotagmin 4, a membrane-trafficking protein essential in retrograde signals from muscle to nerve[93]. How muscle proteins can be transported from muscles to nerve requires more investigation. We found that rapamycin administration decreases the amount of labelled proteins at the NMJ and that muscle-specific deletion of Raptor induces NMJ fragmentation and motor endplate degeneration. These results suggest that muscle proteins synthesized at the NMJ level could be excreted in the synaptic cleft and retrogradely transported into axon endplates.

Muscle-specific tools to monitor protein synthesis in vivo are strongly required for two important reasons. First, it allows monitoring skeletal muscle plasticity in a fibre type-specific manner, independent of all associated structures. Secondly, it allows the identification of myokines and pathological biomarkers linked to muscle wasting. About the last point, we crossed a Cre-MetRS mouse line with a MDX mouse model for *Duchenne muscular dystrophy* (*DMD).* Preliminary results of this mouse model allowed us to visualize in more detail protein synthesis rates in different fibres, changing as a consequence of muscle fibre damage and regeneration. As muscle damage increases, the CK activity level in serum is detected. Moreover, cross-sectional studies showed some muscle-related proteins such as lactate dehydrogenase, carbonic anhydrase 3 and myosin light chain 3 are released in the bloodstream[94,95]. As muscle mass is replaced by adipose and fibrotic tissue, the amount of muscle proteins detected decreases. And thus, the identification of novel muscle dystrophic biomarkers can be effective both to monitor disease progression and treatment effectiveness.

In synthesis, this novel tool allowed us to monitor muscle plasticity in both atrophic and hypertrophic conditions. Moreover, we determined the presence of skeletal muscle proteins into sciatic nerves as a first step in the identification of muscle-derived neurotrophins. However, this technique, very effective for the visualization

and localization of muscle proteins, has some limitations. Newly synthesized proteins can be detected only if at least one methionine is substituted with azidonorleucine[35]. Moreover, according to the literature, a really low amount of proteins does not contain methionine residues, making them invisible to detection. The last problem is using this tool to monitor protein synthesis in patients since it requires the expression of a mutated methionyl tRNA synthetase.

The last consideration regards MetRS proteomic analysis. Recent studies identified almost 600 proteins overexpressed in excitatory neurons[39]. We identified among MetRS and MetRS-AKT samples almost 400 peptides. However, in contrast with electrophoresis results, we did not find overexpressed myosins. Moreover, high background in control samples suggested that mass- spectrometry analysis has to be improved. These difficulties were primarily due to ANL modifications. Indeed, in mass spectrometry conditions, ANL can be modified in unpredictable chemical groups. This problem, combined with nonspecific enrichment at different temperatures and reaction-time/conditions, increases background. However, the identification of ribosomal and mitochondrial proteins in MetRS-AKT animals, already reported to be involved in muscle hypertrophy[96], is a cause for optimism. Overall, combining the ANL labelling method with isotopic traces can effectively overcome all of these problems

Bibliography

1. Gillies AR, Lieber RL. Structure and function of the skeletal muscle extracellular matrix. *Muscle and Nerve*. 2011;44(3):318-331. doi:10.1002/mus.22094
2. Gautel M, Djinović-Carugo K. The sarcomeric cytoskeleton: From molecules to motion. *J Exp Biol*. 2016;219(2):135-145. doi:10.1242/jeb.124941
3. Calderón JC, Bolaños P, Caputo C. The excitation-contraction coupling mechanism in skeletal muscle. *Biophys Rev*. 2014;6(1):133-160. doi:10.1007/s12551-013-0135-x
4. Punga AR, Ruegg MA. Signaling and aging at the neuromuscular synapse: Lessons learnt from neuromuscular diseases. *Curr Opin Pharmacol*. 2012;12(3):340-346. doi:10.1016/j.coph.2012.02.002
5. Fitts RH. The cross-bridge cycle and skeletal muscle fatigue. *J Appl Physiol*. 2008;104(2):551-558. doi:10.1152/japplphysiol.01200.2007
6. Walklate J, Ujfalusi Z, Geeves MA. Myosin isoforms and the mechanochemical cross-bridge cycle. *J Exp Biol*. 2016;219(2):168-174. doi:10.1242/jeb.124594
7. Schiaffino S, Reggiani C. Fiber types in Mammalian skeletal muscles. *Physiol Rev*. 2011;91(4):1447-1531. doi:10.1152/physrev.00031.2010
8. Tajsharghi H. Thick and thin filament gene mutations in striated muscle diseases. *Int J Mol Sci*. 2008;9(7):1259-1275. doi:10.3390/ijms9071259
9. Schiaffino S, Dyar KA, Ciciliot S, Blaauw B, Sandri M. Mechanisms regulating skeletal muscle growth and atrophy. *FEBS J*. 2013;280(17):4294-4314. doi:10.1111/febs.12253
10. Moss FP, Leblond CP. Satellite cells as the source of nuclei in muscles of growing rats. *Anat Rec*. 1971;170(4):421-435. doi:10.1002/ar.1091700405
11. Hill M, Wernig A, Goldspink G. Muscle satellite (stem) cell activation during local tissue injury and repair. *J Anat*. 2003;203(1):89-99. doi:10.1046/j.1469-7580.2003.00195.x
12. Sandri M. Signaling in muscle atrophy and hypertrophy. *Physiology*.

2008;23(3):160-170. doi:10.1152/physiol.00041.2007

13. Mammucari C, Milan G, Romanello V, et al. FoxO3 Controls Autophagy in Skeletal Muscle In Vivo. *Cell Metab*. 2007;6(6):458-471. doi:10.1016/j.cmet.2007.11.001
14. Amthor H, Otto A, Macharia R, McKinnell I, Patel K. Myostatin imposes reversible quiescence on embryonic muscle precursors. *Dev Dyn*. 2006;235(3):672-680. doi:10.1002/dvdy.20680
15. White RB, Biérinx AS, Gnocchi VF, Zammit PS. Dynamics of muscle fibre growth during postnatal mouse development. *BMC Dev Biol*. 2010;10. doi:10.1186/1471-213X-10-21
16. Lecker SH, Goldberg AL, Mitch WE. Protein degradation by the ubiquitin-proteasome pathway in normal and disease states. *J Am Soc Nephrol*. 2006;17(7):1807-1819. doi:10.1681/ASN.2006010083
17. Smalle J, Vierstra RD. The ubiquitin 26S proteasome proteolytic pathway. *Annu Rev Plant Biol*. 2004;55:555-590. doi:10.1146/annurev.arplant.55.031903.141801
18. Kisselev AF, Goldberg AL. Proteasome inhibitors: From research tools to drug candidates. *Chem Biol*. 2001;8(8):739-758. doi:10.1016/S1074-5521(01)00056-4
19. Cai D, Frantz JD, Tawa NE, et al. IKKβ/NF-κB activation causes severe muscle wasting in mice. *Cell*. 2004;119(2):285-298. doi:10.1016/j.cell.2004.09.027
20. Eskelinen EL, Saftig P. Autophagy: A lysosomal degradation pathway with a central role in health and disease. *Biochim Biophys Acta - Mol Cell Res*. 2009;1793(4):664-673. doi:10.1016/j.bbamcr.2008.07.014
21. Mizushima N, Yoshimori T, Ohsumi Y. The role of atg proteins in autophagosome formation. *Annu Rev Cell Dev Biol*. 2011;27:107-132. doi:10.1146/annurev-cellbio-092910-154005
22. Takahashi Y, He H, Tang Z, et al. An autophagy assay reveals the ESCRT-III component CHMP2A as a regulator of phagophore closure. *Nat Commun*. 2018;9(1). doi:10.1038/s41467-018-05254-w
23. Yim WWY, Mizushima N. Lysosome biology in autophagy. *Cell Discov*. 2020;6(1). doi:10.1038/s41421-020-0141-7
24. Wilkinson DJ, Brook MS, Smith K. Principles of stable isotope research –

with special reference to protein metabolism. *Clin Nutr Open Sci*. 2021;36:111-125. doi:10.1016/j.nutos.2021.02.005

25. Wilkinson DJ, Brook MS, Smith K, Atherton PJ. Stable isotope tracers and exercise physiology: past, present and future. *J Physiol*. 2017;595(9):2873-2882. doi:10.1113/JP272277
26. Wilkinson DJ, Hossain T, Hill DS, et al. Effects of leucine and its metabolite β-hydroxy-β-methylbutyrate on human skeletal muscle protein metabolism. *J Physiol*. 2013;591(11):2911-2923. doi:10.1113/jphysiol.2013.253203
27. Soon-Ok Chang Hong, Layman DK. Effects of leucine on in vitro protein synthesis and degradation in rat skeletal muscles. *J Nutr*. 1984;114(7):1204-1212. doi:10.1093/jn/114.7.1204
28. Zanivan S, Krueger M, Mann M. In vivo quantitative proteomics: The SILAC mouse. *Methods Mol Biol*. 2011;757(4):435-450. doi:10.1007/978-1-61779-166-6_25
29. Voytas D, Ke N. Detection and quantitation of radiolabeled proteins in gels and blots. *Curr Protoc Toxicol*. 2001;Appendix 3:1-10. doi:10.1002/0471140856.txa03ds07
30. Goodman CA, Hornberger TA. Measuring protein synthesis with SUnSET: A valid alternative to traditional techniques? *Exerc Sport Sci Rev*. 2013;41(2):107-115. doi:10.1097/JES.0b013e3182798a95
31. Aviner R. The science of puromycin: From studies of ribosome function to applications in biotechnology. *Comput Struct Biotechnol J*. 2020;18:1074-1083. doi:10.1016/j.csbj.2020.04.014
32. Hinz FI, Dieterich DC, Tirrell DA, Schuman EM. Noncanonical amino acid labeling in vivo to visualize and affinity purify newly synthesized proteins in larval zebrafish. *ACS Chem Neurosci*. 2012;3(1):40-49. doi:10.1021/cn2000876
33. Li L, Zhang Z. Development and applications of the copper-catalyzed azide-alkyne cycloaddition (CuAAC) as a bioorthogonal reaction. *Molecules*. 2016;21(10):1-22. doi:10.3390/molecules21101393
34. Ngo JT, Schuman EM, Tirrell DA. Mutant methionyl-tRNA synthetase from bacteria enables site-selective N-terminal labeling of proteins expressed in mammalian cells. *Proc Natl Acad Sci U S A*.

2013;110(13):4992-4997. doi:10.1073/pnas.1216375110

35. Mahdavi A, Hamblin GD, Jindal GA, et al. Engineered Aminoacyl-tRNA Synthetase for Cell-Selective Analysis of Mammalian Protein Synthesis. *J Am Chem Soc*. 2016;138(13):4278-4281. doi:10.1021/jacs.5b08980
36. Azizian NG, Sullivan DK, Nie L, et al. Selective labeling and identification of the tumor cell proteome of pancreatic cancer in Vivo. *bioRxiv*. Published online 2020. doi:10.1101/2020.05.25.113670
37. Ngo JT, Champion JA, Mahdavi A, et al. Cell-selective metabolic labeling of proteins. *Nat Chem Biol*. 2009;5(10):715-717. doi:10.1038/nchembio.200
38. Alvarez-castelao B, Schanzenbächer CT, Langer JD, Schuman EM. Cell-type-speci fi c metabolic labeling , detection and identi fi cation of nascent proteomes in vivo Cell-type-speci fi c metabolic labeling , detection and identi fi cation of nascent proteomes in vivo. :1-5.
39. Alvarez-Castelao B, Schanzenbächer CT, Langer JD, Schuman EM. Cell-type-specific metabolic labeling, detection and identification of nascent proteomes in vivo. *Nat Protoc*. 2019;14(2):556-575. doi:10.1038/s41596-018-0106-6
40. Baraldo M, Nogara L, Dumitras GA, et al. Raptor is critical for increasing the mitochondrial proteome and skeletal muscle force during hypertrophy. *FASEB J*. 2021;35(12):1-16. doi:10.1096/fj.202101054rr
41. Abdeljabbar DM, Klein TJ, Link AJ. An Engineered Methionyl-tRNA Synthetase Enables Azidonorleucine Incorporation in Methionine Prototrophic Bacteria. *ChemBioChem*. 2011;12(11):1699-1702. doi:10.1002/cbic.201100089
42. SKAARA T, REGENSTEIN JM. the Structure and Properties of Myofibrillar Proteins in Beef, Poultry, and Fish. *J Muscle Foods*. 1990;1(4):269-291. doi:10.1111/j.1745-4573.1990.tb00370.x
43. Lundholm K, Edstrom S, Ekman L, Karlberg I, Walker P, Scherstén T. Protein degradation in human skeletal muscle tissue: The effect of insulin, leucine, amino acids and ions. *Clin Sci*. 1981;60(3):319-326. doi:10.1042/cs0600319
44. Bachmanov AA, Reed DR, Beauchamp GK, Tordoff MG. Food intake, water intake, and drinking spout side preference of 28 mouse strains.

Behav Genet. 2002;32(6):435-443. doi:10.1023/A:1020884312053

45. Blaauw B, Canato M, Agatea L, et al. Inducible activation of Akt increases skeletal muscle mass and force without satellite cell activation. *FASEB J*. 2009;23(11):3896-3905. doi:10.1096/fj.09-131870
46. Schatz G, Dobberstein B. Common principles of protein translocation across membranes. *Science (80-)*. 1996;271(5255):1519-1526. doi:10.1126/science.271.5255.1519
47. Söderberg O, Gullberg M, Jarvius M, et al. Direct observation of individual endogenous protein complexes in situ by proximity ligation. *Nat Methods*. 2006;3(12):995-1000. doi:10.1038/nmeth947
48. Tom Dieck S, Kochen L, Hanus C, et al. Direct visualization of newly synthesized target proteins in situ. *Nat Methods*. 2015;12(5):411-414. doi:10.1038/nmeth.3319
49. Chevron MP, Girard F, Claustres M, Demaille J. Expression and subcellular localization of dystrophin in skeletal, cardiac and smooth muscles during the human development. *Neuromuscul Disord*. 1994;4(5-6):419-432. doi:10.1016/0960-8966(94)90081-7
50. Goodman CA, Dietz JM, Jacobs BL, Mcnally RM, You J, Hornberger TA. Yes-Associated Protein is up-regulated by mechanical overload and is sufficient to induce skeletal muscle hypertrophy. *FEBS Lett*. 2015;589(13):1491-1497. doi:10.1016/j.febslet.2015.04.047
51. Goodman CA, Kotecki JA, Jacobs BL, Hornberger TA. Muscle fiber type-dependent differences in the regulation of protein synthesis. *PLoS One*. 2012;7(5). doi:10.1371/journal.pone.0037890
52. Ehmsen JT, Höke A. Cellular and molecular features of neurogenic skeletal muscle atrophy. *Exp Neurol*. 2020;331(June). doi:10.1016/j.expneurol.2020.113379
53. Burns TM, Graham CD, Rose MR, Simmons Z. Quality of life and measures of quality of life in patients with neuromuscular disorders. *Muscle and Nerve*. 2012;46(1):9-25. doi:10.1002/mus.23245
54. Salari M, Sharma S, Jog MS. Botulinum toxin induced atrophy: An uncharted territory. *Toxins (Basel)*. 2018;10(8):10-12. doi:10.3390/toxins10080313
55. Pirazzini M, Rossetto O, Eleopra R, Montecucco C. Botulinum

neurotoxins: Biology, pharmacology, and toxicology. *Pharmacol Rev*. 2017;69(2):200-235. doi:10.1124/pr.116.012658

56. Meunier FA, Schiavo G, Molgó J. Botulinum neurotoxins: From paralysis to recovery of functional neuromuscular transmission. *J Physiol Paris*. 2002;96(1-2):105-113. doi:10.1016/S0928-4257(01)00086-9
57. Ma L, Pan L, Liu W, et al. Agrin Influences Botulinum Neurotoxin A-Induced Nerve Sprouting via miR-144-agrin-MuSK Signaling. *Front Cell Dev Biol*. 2020;8(January):1-9. doi:10.3389/fcell.2020.00015
58. Bennett MR, Nurcombe V. The survival and development of cholinergic neurons in skeletal muscle conditioned media. *Brain Res*. 1979;173(3):543-548. doi:10.1016/0006-8993(79)90249-X
59. Brown MC, Holland RL, Ironton R. Nodal and terminal sprouting from motor nerves in fast and slow muscles of the mouse. *J Physiol*. 1980;306(1):493-510. doi:10.1113/jphysiol.1980.sp013410
60. Bodine SC, Stitt TN, Gonzalez M, et al. Bodine_2001. 2001;3(November).
61. Baraldo M, Geremia A, Pirazzini M, et al. Skeletal muscle mTORC1 regulates neuromuscular junction stability. *J Cachexia Sarcopenia Muscle*. 2020;11(1):208-225. doi:10.1002/jcsm.12496
62. Radley-Crabb HG, Marini JC, Sosa HA, Castillo LI, Grounds MD, Fiorotto ML. Dystropathology increases energy expenditure and protein turnover in the Mdx mouse model of Duchenne muscular dystrophy. *PLoS One*. 2014;9(2). doi:10.1371/journal.pone.0089277
63. MacLennan PA, Edwards RHT. Protein turnover is elevated in muscle of mdx mice in vivo. *Biochem J*. 1990;268(3):795-797. doi:10.1042/bj2680795
64. Coletti D. Chemotherapy and Muscle Wasting. *Eur J Transl Myol*. 2018;28(2):153-157.
65. Geremia A, Sartori R, Baraldo M, et al. Activation of Akt–mTORC1 signalling reverts cancer-dependent muscle wasting. *J Cachexia Sarcopenia Muscle*. Published online 2021:1-14. doi:10.1002/jcsm.12854
66. Schmidt EK, Clavarino G, Ceppi M, Pierre P. SUnSET, a nonradioactive method to monitor protein synthesis. *Nat Methods*. 2009;6(4):275-277. doi:10.1038/nmeth.1314
67. Deng J, Erdjument-Bromage H, Neubert TA. Quantitative Comparison of

Proteomes Using SILAC. *Curr Protoc Protein Sci*. 2019;95(1):1-21. doi:10.1002/cpps.74

68. NATHANS D. Inhibition of Protein Synthesis By Puromycin. *Fed Proc*. 1964;23(1963):984-989.
69. Dieck ST, M̈Uller A, Nehring A, et al. *Metabolic Labeling with Noncanonical Amino Acids and Visualization by Chemoselective Fluorescent Tagging*. Vol 1.; 2012. doi:10.1002/0471143030.cb0711s56
70. Wortham M, He L, Gyamfi M, Copple BL, Wan YJY. The transition from fatty liver to NASH associates with SAMe depletion in db/db mice fed a methionine choline-deficient diet. *Dig Dis Sci*. 2008;53(10):2761-2774. doi:10.1007/s10620-007-0193-7
71. Mazor KM, Dong L, Mao Y, Swanda R V., Qian SB, Stipanuk MH. Effects of single amino acid deficiency on mRNA translation are markedly different for methionine versus leucine. *Sci Rep*. 2018;8(1):1-13. doi:10.1038/s41598-018-26254-2
72. Bonaldo P, Sandri M. Cellular and molecular mechanisms of muscle atrophy. *DMM Dis Model Mech*. 2013;6(1):25-39. doi:10.1242/dmm.010389
73. Venturelli M, Villa F, Ruzzante F, et al. Neuromuscular and Muscle Metabolic Functions in MELAS Before and After Resistance Training : A Case Study. 2019;10(April):1-8. doi:10.3389/fphys.2019.00503
74. Kanai Y, Segawa H, Miyamoto KI, Uchino H, Takeda E, Endou H. Expression cloning and characterization of a transporter for large neutral amino acids activated by the heavy chain of 4F2 antigen (CD98). *J Biol Chem*. 1998;273(37):23629-23632. doi:10.1074/jbc.273.37.23629
75. Dieck ST, M̈Uller A, Nehring A, et al. Metabolic labeling with noncanonical amino acids and visualization by chemoselective fluorescent tagging. *Curr Protoc Cell Biol*. 2012;1(SUPPL.56):1-29. doi:10.1002/0471143030.cb0711s56
76. Pereira MG, Dyar KA, Nogara L, et al. Comparative analysis of muscle hypertrophy models reveals divergent gene transcription profiles and points to translational regulation of muscle growth through increased mTOR signaling. *Front Physiol*. 2017;8(DEC):1-11. doi:10.3389/fphys.2017.00968

77. Sieljacks P, Wang J, Groennebaek T, et al. Six weeks of low-load blood flow restricted and high-load resistance exercise training produce similar increases in cumulative myofibrillar protein synthesis and ribosomal biogenesis in healthy males. *Front Physiol*. 2019;10(MAY). doi:10.3389/fphys.2019.00649
78. Roberts MD, Haun CT, Vann CG, Osburn SC, Young KC. Sarcoplasmic Hypertrophy in Skeletal Muscle: A Scientific “Unicorn” or Resistance Training Adaptation? *Front Physiol*. 2020;11(July):1-16. doi:10.3389/fphys.2020.00816
79. Marabita M, Baraldo M, Solagna F, et al. S6K1 Is Required for Increasing Skeletal Muscle Force during Hypertrophy. *Cell Rep*. 2016;17(2):501-513. doi:10.1016/j.celrep.2016.09.020
80. Goodman CA, Dietz JM, Jacobs BL, McNally RM, You JS, Hornberger TA. Yes-Associated Protein is up-regulated by mechanical overload and is sufficient to induce skeletal muscle hypertrophy. *FEBS Lett*. 2015;589(13):1491-1497. doi:10.1016/j.febslet.2015.04.047
81. Watt KI, Turner BJ, Hagg A, et al. The Hippo pathway effector YAP is a critical regulator of skeletal muscle fibre size. *Nat Commun*. 2015;6. doi:10.1038/ncomms7048
82. Shenkman BS. From Slow to Fast: Hypogravity-Induced Remodeling of Muscle Fiber Myosin Phenotype. *Acta Naturae*. 2016;8(4):47-59. doi:10.32607/20758251-2016-8-4-47-59
83. Sandri M, Lin J, Handschin C, et al. PGC-1α protects skeletal muscle from atrophy by suppressing FoxO3 action and atrophy-specific gene transcription. *Proc Natl Acad Sci U S A*. 2006;103(44):16260-16265. doi:10.1073/pnas.0607795103
84. Holeček M, Mičuda S. Amino acid concentrations and protein metabolism of two types of rat skeletal muscle in postprandial state and after brief starvation. *Physiol Res*. 2017;66(6):959-967. doi:10.33549/physiolres.933638
85. Ogata ES, Foung SKH, Holliday MA. The effects of starvation and refeeding on muscle protein synthesis and catabolism in the young rat. *J Nutr*. 1978;108(5):759-765. doi:10.1093/jn/108.5.759
86. Guo B, Zhang ZK, Liang C, et al. Molecular Communication from Skeletal

Muscle to Bone: A Review for Muscle-Derived Myokines Regulating Bone Metabolism. *Calcif Tissue Int*. 2017;100(2):184-192. doi:10.1007/s00223-016-0209-4

87. Rossetto O, Pirazzini M, Montecucco C. Botulinum neurotoxins: Genetic, structural and mechanistic insights. *Nat Rev Microbiol*. 2014;12(8):535-549. doi:10.1038/nrmicro3295
88. De Paiva A, Meunier FA, Molgó J, Aoki KR, Dolly JO. Functional repair of motor endplates after botulinum neurotoxin type A poisoning: Biphasic switch of synaptic activity between nerve sprouts and their parent terminals. *Proc Natl Acad Sci U S A*. 1999;96(6):3200-3205. doi:10.1073/pnas.96.6.3200
89. Glass DJ. Skeletal muscle hypertrophy and atrophy signaling pathways. *Int J Biochem Cell Biol*. 2005;37(10 SPEC. ISS.):1974-1984. doi:10.1016/j.biocel.2005.04.018
90. Funakoshi H, Belluardo N, Arenas E, et al. Muscle-derived neurotrophin-4 as an activity-dependent trophic signal for adult motor neurons. *Science (80-)*. 1995;268(5216):1495-1499. doi:10.1126/science.7770776
91. Sakuma K, Yamaguchi A. The recent understanding of the neurotrophin's role in skeletal muscle adaptation. *J Biomed Biotechnol*. 2011;2011. doi:10.1155/2011/201696
92. Johnstone RM, Adam M, Hammond JR, Orr L, Turbide C. Vesicle formation during reticulocyte maturation. Association of plasma membrane activities with released vesicles (exosomes). *J Biol Chem*. 1987;262(19):9412-9420. doi:10.1016/s0021-9258(18)48095-7
93. Michael R. Bronsert, William G. Henderson, Robert Valuck, Patrick Hosokawa and KH. 基因的改变NIH Public Access. *Bone*. 2008;23(1):1-7. doi:10.1016/j.neuron.2013.01.013.Regulation
94. Al-Khalili Szigyarto C, Spitali P. Biomarkers of Duchenne muscular dystrophy: current findings. *Degener Neurol Neuromuscul Dis*. 2018;Volume 8:1-13. doi:10.2147/dnnd.s121099
95. Hathout Y, Marathi RL, Rayavarapu S, et al. Discovery of serum protein biomarkers in the mdx mouse model and cross-species comparison to Duchenne muscular dystrophy patients. *Hum Mol Genet*.

2014;23(24):6458-6469. doi:10.1093/hmg/ddu366

96. Mesquita PHC, Vann CG, Phillips SM, et al. Skeletal Muscle Ribosome and Mitochondrial Biogenesis in Response to Different Exercise Training Modalities. *Front Physiol*. 2021;12(1). doi:10.3389/fphys.2021.725866